

**OPTICAL AND INFRARED**

**STUDIES OF ASTEROIDS**

**A Thesis Submitted for the Degree of**

**Doctor of Philosophy**

**by**

**Robert Steven McCheyne**

**Department of Astronomy**

**University of Leicester**

**1985**

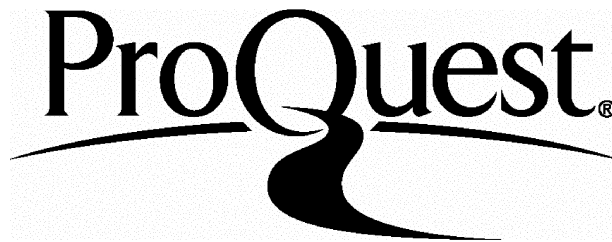
ProQuest Number: U348979

All rights reserved

INFORMATION TO ALL USERS

The quality of this reproduction is dependent upon the quality of the copy submitted.

In the unlikely event that the author did not send a complete manuscript and there are missing pages, these will be noted. Also, if material had to be removed, a note will indicate the deletion.



ProQuest U348979

Published by ProQuest LLC(2015). Copyright of the Dissertation is held by the Author.

All rights reserved.

This work is protected against unauthorized copying under Title 17, United States Code.  
Microform Edition © ProQuest LLC.

ProQuest LLC  
789 East Eisenhower Parkway  
P.O. Box 1346  
Ann Arbor, MI 48106-1346

PHILOSOPHY AND THE SCIENCES

STUDIES OF ASTROPHYSICS

A THESIS SUBMITTED TO THE FACULTY OF

PHILOSOPHY

BY

DR. J. H. COOPER

PHILOSOPHY



Thesis

Department of Astronomy

University of Leicester

1985

95480054x

## ABSTRACT

This thesis presents optical and infrared data of asteroids. The basis of the classification of asteroids by numerical taxonomy is data which are contained in the TRIAD file (Zellner, 1979). The resulting dendrograms are compared with existing classes of asteroids.

Simultaneous visible and near-infrared lightcurves of several asteroids are plotted as colour curves which, in some cases, show variations indicative of an inhomogeneous surface composition. The colour curves of 4 Vesta are explained in terms of eucrite and diogenite mineralogies. Some of these lightcurves, together with published data from previous oppositions, are used to calculate the overall shape of the asteroid and the orientation of the spin axis. These are calculated using a lightcurve amplitude-longitude relation.

Reflectance spectra in the 3 - 4 $\mu$ m region are presented, Two of which show evidence of water of hydration. These spectra highlight the importance of accurate thermal modelling. Data from IRAS is compared with the expected flux from the standard asteroid thermal model and the discrepancies examined in terms of emission from the unilluminated hemisphere.

## ACKNOWLEDGEMENTS

I am grateful for the guidance and encouragement of my supervisor, Prof. Jack Meadows and for the assistance of the other members of the group; Simon Green, Nick Eaton, Charon Birkett and John Davies. I am also indebted to Dr. Richard Jameson for the use of his simultaneous optical/infrared photometer and to Drs. Mandy Sherrington and Paul Butterworth who helped with the observations. I also thank the other members of the department, in particular, my fellow post-grads; Andy Adamson, Chris Holland, John Mardaljevic, John Fernly and John Brooker for their "stimulating conversation", witty remarks and some of the worst jokes I have ever heard. One final thank you goes to Simon for providing many amusing moments (and some new words) on the BBC micro and Nick for some serious competition.

## CONTENTS

	Page
Chapter 1: Introduction	
Introduction	1.2
Historical Review	1.4
	1.10
Chapter 2: Numerical Taxonomy and Asteroid Colours	
Introduction	2.2
Previous Classification	2.3
The Method of Numerical Taxonomy	2.8
Input Data and Results	2.13
Asteroid Colours	2.26
Discussion	2.29
	2.30
Chapter 3: Lightcurves and Colour Variations	
Introduction	3.2
Instrumentation	3.3
Acquisition and Reduction	3.9
Results	
4 Vesta	3.14
20 Massalia	3.18
29 Amphitrite	3.20
31 Euphrosyne	3.24
39 Laetitia	3.26
40 Harmonia	3.29
43 Ariadne	3.31
44 Nysa	3.33

115 Thyra	3.36
349 Dembowska	3.38
Discussion	3.41
	3.42
<b>Chapter 4: Shapes and Pole Orientations</b>	
Introduction	4.2
Amplitude-Longitude Relation	4.4
4 Vesta	4.9
20 Massalia	4.14
29 Amphitrite	4.16
31 Euphrosyne	4.20
39 Laetitia	4.20
43 Ariadne	4.24
44 Nysa	4.26
Discussion	4.30
	4.40
<b>Chapter 5: Reflection Spectra and Thermal Emission</b>	
Introduction	5.2
3 - 4 $\mu$ m Spectra	5.3
The Standard Thermal Model	5.15
IRAS Observations of 44 Nysa	5.20
Discussion	5.28
	5.29
<b>References</b>	6.1
	6.12
<b>Appendix</b>	
Lightcurves	A.2
Publications	A.12
	A.14

## **CHAPTER 1**

### **INTRODUCTION**

## INTRODUCTION

Asteroids are large lumps of rock. There are quite a lot of them. The vast majority occupy orbits between those of Mars and Jupiter. In order to understand the origin and evolution of asteroids and to interpret their composition it is essential to classify them, this is the basis of Chapter 2. Before describing the technique of numerical taxonomy previous classification schemes are reviewed. This new technique (to asteroid science) results in objects being linked together on a tree-like diagram (dendrogram), the level of the joins indicating the similarity of the asteroids. The data used in this analysis are readily available in the Tucson Revised Index of Asteroid Data (TRAID, Zellner, 1979). Finally, Chapter 2 presents the broadband colours of asteroids which have been obtained mainly as a result of observing asteroid lightcurves for the work reported in this thesis. Their relevance to classification is indicated.

Since different mineralogies can have different broadband colours, it is theoretically possible to identify asteroids with inhomogeneous surface composition by monitoring their colour over a rotation period. This has been done, but usually in the visible portion of the spectrum. Chapter 3 presents the results of studying nine asteroids at optical and near-infrared wavelengths to search for colour variations. Such variations were detected in some objects. One asteroid, which was observed at two oppositions, was

found to exhibit changes in colour on only one occasion. This is explained in terms of the orientation of its rotational axis.

The lightcurve of an asteroid contains information on the shape of the body and the direction of the rotation axis. If a sufficient number of lightcurves are available then it is possible to determine solutions for both the orientation of the rotational axis and the overall shape of the asteroid. This is the subject of Chapter 4. Brief details of the various methods which have been developed elsewhere are given, followed by an in-depth description of the method used in the chapter. The assumptions of the method are discussed. Estimates for the axial ratios of five of the asteroids from Chapter 3 are derived, as well as possible pole positions for these objects. The observed variation of the amplitude of 4 Vesta's lightcurve is explained in terms of a changing albedo across the surface of the asteroid.

The final chapter presents reflectance spectra of eleven asteroids in the 3 - 4 $\mu$ m region and suggests how they could be used to extend the current schemes of classification. The major problem in obtaining reflectance spectra at these infrared wavelengths (namely that of contamination by the thermal emission of the asteroid) is discussed and the chapter also includes a section on the standard thermal model. The effects of the rotation period, shape and the pole orientation on the nature of the thermal component of an asteroid spectrum are examined. This leads to the final data of this thesis - several observations of the

asteroid 44 Nysa by the Infrared Astronomical Satellite (IRAS). These are compared with the predicted fluxes from the standard model and the discrepancies partially explained.

The remainder of Chapter 1 is given over to a brief historical review of asteroid discoveries. All the references are listed after Chapter 5. An Appendix contains all the lightcurves which are presented in Chapter 3, but in a different format which enables information concerning the epoch of the extrema to be easily extracted. Following these are lists of published and accepted papers and of abstracts of presentations at conferences.

#### HISTORICAL REVIEW

0.4 0.7 1.0 1.6 2.8 5.2 10.0. This numerical sequence was first formulated by Titius von Wittenburg in 1766 and gives the approximate distances of the planets from the Sun in AU. The exception was 2.8 AU, since there was no known planet at this distance (Mars and Jupiter being at 1.5 and 5.2 AU, respectively). The progression is more commonly known as Bode's law, after the astronomer who stressed its importance. The possibility of the gap at 2.8 AU being important was reinforced in 1781 by Herschel's discovery of Uranus. This orbits at 19.2 AU, whereas Bode's law predicts 19.6 AU. However, it was not until January 1, 1801 that Piazzi, observing from Palermo in Sicily, first saw an object which appeared to move on subsequent nights. The orbit and ephemeris for this object were eventually determined by Gauss, and it was recovered in December 1801. This object is

now known as 1 Ceres. In the next six years, three more objects with semi-major axes of around 2.8 AU were found (2 Pallas, 3 Juno and 4 Vesta), but it was not until 1845 that 5 Astraea was discovered. Since then, the rate of discovery of asteroids has been increasing to the present rate of ~100/year.

The theory that these asteroids originated from an exploded planet was suggested very early, notably by Olbers. By 1867 sufficient asteroids had been discovered and had had their orbits calculated, that Kirkwood found a plot of the number of asteroids versus semi-major axis revealed several "gaps" (regions with very few asteroids in them) in the distribution. These Kirkwood gaps are due to perturbations in the asteroidal orbits caused by resonances with Jupiter.

In 1893 Witt of Berlin discovered the object now known as 433 Eros. This asteroid has a semi-major axis of only 1.5 AU, and thus has part of its orbit inside the orbit of Mars. Since then several "Mars crossers" have been found and asteroids which cross the orbits of Earth and even Mercury have been discovered. At present, the asteroid which has the closest approach to the Sun is 1983TB with a perihelion distance of 0.13 AU. These objects are also called Amor, Apollo or Aten asteroids depending on the exact values of their semi-major axes ( $a$ ) and perihelion distances ( $q$ ).

Amor  $1.017 < q \leq 1.3$  AU.

Apollo  $a \geq 1.0$  and  $q \leq 1.017$  AU.

Aten  $a < 1.0$  and  $Q \geq 0.983$  AU.  $Q$ =aphelion distance

Shortly after its discovery, 433 Eros was observed to exhibit light variations. These were attributed to the rotation of the asteroid with the variations being caused by its non-spherical shape. Since then, lightcurves of a large number of asteroids have been obtained and information on their rotation periods, shapes and pole positions acquired.

Around the turn of the century, interest in minor planets on the part of the astronomical community at large was waning. This was due, primarily, to the advent of spectroscopy and astrophysics. This general disinterest in asteroids, nicknamed "vermin of the skies" presumably because of their ever increasing proliferation, was to continue until the 1950's. However, important work was still carried out during the first half of the century by several dedicated workers.

In 1906 Wolf, working at Heidelberg, discovered the first of the Trojan asteroids (588 Achilles). These minor planets occupy positions  $60^\circ$  preceding, or  $60^\circ$  following, that of Jupiter at the stable Lagrangian points  $L_4$  and  $L_5$ . Hirayama discovered the existence of asteroid families (groups with similar semi-major axes and eccentricities) in 1918. Following this original work, many papers have been published on families, including their origin, generally believed to be from the fragmentation of a larger planetesimal.

Baade at Bergedorf discovered yet another asteroid with

an unusual orbit, 944 Hidalgo, in 1920. This asteroid has a perihelion in the asteroid belt but an aphelion close to Saturn's orbit, which gives it an orbit more characteristic of a periodic comet than an asteroid. As such, it is a candidate for an extinct cometary nucleus. Twelve years later Reinmuth discovered the first Apollo asteroid (1862 Apollo), but it was not recovered until 1973. This illustrates the importance and difficulty of obtaining accurate orbital elements, since the minor planet had, in effect, to be discovered twice.

The currently accepted origin of the asteroid belt was postulated by O. J. Schmidt in 1944. This theory suggests that the formation of a planet at 2.8 AU. by accretion of planetesimals was interrupted by the gravitational influence of Jupiter, resulting in the asteroid belt. At the end of the first half of the century, Kuiper initiated the first survey of asteroids. This was followed twenty years later by the more extensive Palomar-Leiden survey which searched for faint asteroids using a Schmidt telescope.

The early 1950's saw the first work on the dynamics of the asteroid region, with Opik calculating the lifetime of asteroidal orbits and Piotrowski publishing a study on the collisions between asteroids. The link between asteroids and meteorites was first proposed, soon after the discovery of 1 Ceres, by Olbers in 1803, who suggested that meteorites came from an exploded planet. In 1964 a theory which propounded the origin of meteorites as being fragments of collisions between asteroids was put forward by Anders. 1964

also saw the first calculation of the cooling rates in iron meteorites by Wood. This showed that these meteorites had originated in objects with diameters in the range 100 to 500 km. To date no direct analogue of a meteorite sample has been found among the asteroids,<sup>1</sup> but there are general similarities of spectral features between asteroids and meteorites. Indeed, the classification of asteroids has as its basis the classification scheme of meteorites. (For example, C-type asteroids are called this because of their spectral similarity to carbonaceous chondritic meteorites.)

The mass of an asteroid was not determined until 1966 by Hertz. Such calculations are difficult and use the gravitational effect of the close approach of two asteroids on the orbits of these asteroids. These effects are small and subject to large errors, so the masses cannot be calculated precisely. The accurate determination of an asteroidal mass will probably not occur until a spacecraft is sent on a mission to the asteroid belt. The total mass of the belt is estimated as  $5 \times 10^{-4}$  Earth masses with the mass of 1 Ceres accounting for 40% of this total.

1968 saw the first radar detection of an asteroid (1566 Icarus). Since then many asteroids have been detected, including the largest of the main-belt asteroids. These observations have shown that at least some asteroids have a large metal content. The exploitation of asteroids, or at

---

<sup>1</sup>. One possible exception is 4 Vesta whose visible spectra are very similar to the eucrite meteorites.

least those which have close approaches to the Earth, for their metal content is an idea which has been around for some years. Probably the best known example is that proposed by S. Herrick whereby part of 1620 Geographos is nudged into an Earth colliding orbit, which will embed it into the surface, where it can be mined for it's mineral content.

The 1970's saw a continued growth in the study of asteroids, with organised campaigns of observations conducted in 1972 (1685 Toro) and 1975 (433 Eros). Also in 1975 Bowell started a UBV photometric survey and Chapman et. al. defined the basic classification scheme using C-types, S-types, etc. The year 1976 saw the discovery, by Helin, of the first Aten asteroid and in 1977 Kowal found 2060 Chiron which orbits between Saturn and Uranus.

Today there is increasing pressure from planetary scientists for a spacecraft mission to the asteroid belt. Asteroids, together with Pluto, are the only solar system objects for which such a mission has not occurred, or been approved. The current hope is for a mission in the late 1980's or 1990's. There is a possibility of the American Galileo spacecraft making a fly-by of a convenient asteroid during it's passage through the main belt, although at the present it is only a remote possibility. The Hubble Space Telescope offers the possibility of observing asteroids with a resolution of ~25km. This would enable surface features to be identified and followed as the asteroid rotates. As well as being able to observe the shape directly, it would also be possible to determine the pointing direction of the

rotational axis.

The above historical sketch is by no means complete, but is intended to give a brief outline of the development of the study of the asteroids.

**CHAPTER 2**

**NUMERICAL TAXONOMY**

**AND**

**ASTEROID COLOURS**

## INTRODUCTION

Classification of any set of objects has as its main aim the identification of various subsets of objects within the universal group and to indicate members which are in any way unusual. It also provides a means of assessing relationships between these subsets, if such relationships exist. The quantity of asteroid data has grown considerably during the last twenty years as a result of increased instrumental sensitivity and the advent of new observational techniques. With over 2800 asteroids in known orbits, and new asteroids being discovered at a rate of approximately 150 each year, some form of classification is essential if the origin, subsequent evolution and physical properties of these objects are to be understood.

Previous classifications have been successful in identifying unusual objects (eg. 4 Vesta, 349 Dembowska) and in dividing the asteroids into different groups. The number and nature of these groups undergo revision, at intervals, while individual asteroids can migrate from one group to another on the acquisition of new data. Asteroid taxonomy is subject to the limitations which apply to virtually any classification scheme: namely, (1) incomplete data sets for some objects and (2) properties which do not have discrete values, but vary over a range of possible values.

Numerical taxonomy is a technique of classification which has not previously been applied to asteroid data sets,

but has been used extensively in other branches of science, such as microbiology. This method computes a similarity coefficient for each pair of objects and then uses this to link the individual objects together to form a dendrogram.

The next section of this chapter gives a brief resume of the various classification schemes used up until 1982. The main body of this chapter details the methods of numerical taxonomy, the data used and the results obtained. The section on colours presents the observed colours of asteroids obtained during the last three years and compares them with the results of other workers. Finally, there is a discussion of the conclusions which can be drawn from the dendrograms and infrared colours.

#### PREVIOUS CLASSIFICATION

Hapke (1971) was among the first to identify different groups in the asteroid population by plotting U-B vs. B-V colours. This enabled asteroids to be placed into four categories, called I to IV. Meanwhile, Chapman (1971) and Chapman et al. (1973) had divided over a hundred asteroids into three groups based on their visible reflectance spectra. These were called red, medium or flat, depending on the general slope of their spectrum. They also noted a correlation between slope and orbital semi-major axis, with the red spectra having smaller semi-major axes. No correlation with eccentricity, inclination, family membership or rotation period was found.

Later Zellner (1973) reported a relationship between U-V colour, albedo and the nature of an absorption feature at  $0.95\mu\text{m}$  in asteroid spectra. Zellner suggested that asteroids fall into two distinct groups. Comparison of asteroid and meteorite spectra resulted in the tentative identification of these two groups of asteroids with carbonaceous and stony meteorite samples, these groups are now called C and S-classes. Confirmation of this division was provided when Zellner et al. (1974) plotted B-V vs. polarimetric albedo ( $p_V$ ) or minimum polarization ( $P_{\text{min}}$ ).

Work by Morrison (1974) on radiometric albedos and diameters also produced these two groups, but indicated that 4 Vesta should belong to another third group, mainly because of its high albedo (0.24). McCord et al. (1970) had suggested that 4 Vesta was similar in composition to basaltic achondrite meteorites. A more elaborate scheme of classification was introduced in 1975 by McCord and Chapman who listed several visible and near infrared characteristics (such as  $R/B^1$ ,  $BEND^2$ ,  $IR^3$ ). These parameters divided the 67 asteroids in their sample into 27 groups, half of which contained only one object. They also predicted that a further

---

<sup>1</sup>  $R/B = \text{Reflectance at } 0.7\mu\text{m} / \text{Reflectance at } 0.4\mu\text{m}$ . and is a measure of the "redness" through the visible.

<sup>2</sup>  $BEND = (R_{0.56} - R_{0.4}) - (R_{0.73} - R_{0.56})$ .  $R_x$  means the reflectance at wavelength x. BEND is a measure of the curvature of the spectrum through the visible.

<sup>3</sup>  $IR = (R_{1.05} - R_{0.73})$ , and is a measure of the infrared reflectance.

40 or 50 groups existed.

Using a similar set of characteristics, Chapman et al. (1975) defined the C and S-classes more specifically. C-class asteroids have low albedos, flat spectra and large  $P_{min}$ ; while S-class asteroids have higher albedos, red spectra and small  $P_{min}$ . A new class was introduced for objects which did not fall into either of these categories, namely 'U' (for unclassifiable or unknown). Chapman et al. then proceeded to search for correlations of composition with orbital parameters and diameters. They concluded that C-classes dominate the outer regions of the asteroid belt and are the most common class amongst bodies with diameters above 40km.

It was later suggested by Zellner et al. (1975) that several of the U-class asteroids should be placed in a new group called M-class. This designation was used because the colours and spectra were suggestive of metals (nickel-iron) in the surface materials. A year later, Zellner and Gradie (1976) introduced another new class for 44 Nysa and 64 Angelina. Because their ubv colours and 0.3 to 1.1 $\mu$ m spectra were similar to those of enstatite achondrites, this group was called E-class. Zellner and Bowell (1977) showed that the unusual asteroid 349 Dembowska had similar properties to ordinary chondrites. It was later (Bowell et al., 1978) designated R-class due to its very red spectrum. This latter paper increased the number of known R-class asteroids to three, and identified several more asteroids of the E-class. The five main classes (CSMER) were precisely defined by seven parameters (see Table 2.1).

Asteroids which did not fall into these categories were again designated U-class. In all, over 500 objects were assigned to these, or to a combination of classes (eg. CMEU).

Table 2.1 Range of parameters for the main classes of asteroid.

	C	S	M	E	R
Albedo	$\leq 0.065$	0.065-0.23	0.065-0.23	$\geq 0.23$	$\geq 0.16$
$P_{min}$	1.2-2.15	0.58-0.96	0.86-1.35	$\leq 0.4$	$\leq 0.7$
R/B	1.0-1.4	1.34-2.07	1.06-1.34	0.9-1.35 <sup>a</sup>	$\geq 1.7$
BEND	0.05-0.26	0.05-0.25	$\leq 0.11$	$\leq 0.15^a$	$\geq 0.25$
DEPTH	0.95-1.0	0.8-1.0	0.9-1.0	0.9-1.0 <sup>a</sup>	$\leq 0.9$
B-V	$\geq 0.64^b$	- <sup>c</sup>	0.67-0.77	0.6-0.79	- <sup>d</sup>
U-B <sup>e</sup>	0.23-0.46 <sup>b</sup>	$\geq 0.34^c$	0.17-0.28	0.22-0.28	- <sup>d</sup>

a R/B, BEND and DEPTH have not been measured for E-class.

b Additionally,  $4.6(B-V) - 3.17 \leq (U-B) \leq (B-V) - 0.27$ . U-class allowed 0<sup>m</sup>.02 inside CSME limits when only UBV photometry is available.

c Additionally,  $B-V \geq (U-B)/7 + 0.74$ ;  $1.7(B-V) - 1.12 \leq (U-B) \leq (B-V) - 0.33$ ;  $(U-V) \leq 1.47$ . U-class allowed 0<sup>m</sup>.02 inside limits, except for last, when only UBV photometry is available.

d  $(U-V) \geq 1.47$

e U-class always allowed for  $(U-B) \leq 0.28$ , when only UBV photometry is available.

This scheme of classification was based on observational properties, and not on mineralogical

interpretation. (Broadband UVV spectral coverage cannot usually measure the basic parameters of absorption features, such as bandcentre or symmetry.) This was noted by Gaffey and McCord (1977), who proposed that asteroids should be classified according to the nature of the  $0.95\mu\text{m}$  silicate absorption feature. This led them to define about a dozen groups which were then interpreted in terms of their surface mineralogy. The following year, Chapman et al. (1978) adopted a similar method. They identified 35 spectral types, and inferred the existence of 16 different mineralogical assemblages.

Degewij and van Houten (1978) identified several asteroids as belonging to a new RD-class. These asteroids are characterised by their red spectra longward of  $0.7\mu\text{m}$  and low albedo. This group has recently been relabelled as D-class by Gradie and Tedesco (1982). Two new classes, P (for pseudo-M; like M-class, but with low albedos) and F (flat spectra, low albedo) were also introduced by Gradie and Tedesco.

Veeder et al. (1978) demonstrated that a two-colour plot involving the infrared broadband filters H and K, together with visible broadband data, could be used to distinguish between C and M-class asteroids (the C-class are bluer in V-K than the M-class, but they have similar U-B and B-V colours). More recently Veeder et al. (1982) and Veeder et al. (1983) have utilized infrared data to extend the existing classification. Notably, they have introduced A-class asteroids (after 446 Aetenes, the first identified) which have very red J-H colours.

Thus, by the early 1980s, there were two basic types of classification, that of *Bowell et al. (1978)*, which uses observational parameters and the schemes of *Gaffey and McCord (1978)* and *Chapman et al. (1978)*, which were based on a mineralogical interpretation of the observational data. As new techniques and improved sensitivity are brought to bear on asteroids, so the number of new classes proposed has increased and the older groups have been redefined or subdivided.

#### THE METHOD OF NUMERICAL TAXONOMY

Numerical taxonomy is the classification of objects by expressing their similarity to each other as a single number. This number, called the similarity coefficient, is calculated from all the parameters injected into the process. This has the advantage that no preconceived ideas on the grouping of the objects, in this case asteroids, are forced upon the results, since the calculations are carried out by computer. However, the selection of the input parameters and the subsequent interpretations are subject, to a certain extent, to the vagries of the human mind. A review of the principles of numerical taxonomy is given by *Sokal and Sneath (1963)*.

The similarity coefficients are calculated using the following equation;

$$S_{ij} = \left( \sum |x_{ik} - x_{jk}|^2 / n_{ij} \right)^{0.5} \quad (2.1)$$

where  $S_{ij}$  is the coefficient of similarity between the  $i$ th and  $j$ th asteroid;  $x_{ik}$  is the  $k$ th parameter of the  $i$ th asteroid and  $n_{ij}$  is the number of parameters for which both  $x_{ik}$  and  $x_{jk}$  exist. Thus the similarity coefficient can be considered as the mean separation of the two objects along an axis, or as a modified taxonomic distance. Thus objects which are similar are separated by short distances (small coefficients), while diverse objects are separated by large distances (large coefficients). These similarity coefficients are stored in a similarity matrix. Hence, numerical taxonomy can be considered as a multidimensional equivalent of a two-colour diagram with each parameter plotted along a separate, orthogonal axis. It should be noted that, if a parameter has a numerically large range compared with the other parameters, then it is necessary to scale the various parameters; otherwise the similarity coefficient is dominated by this parameter. This situation does not occur with the data used below. It is possible, (though generally not desirable) to weight a particular property of the asteroid by entering the data several times.

After computation of the similarity matrix, two methods were used to link the asteroids together to form the dendrogram. These methods are detailed below:

UNWEIGHTED AVERAGE LINKAGE: (Figure 2.1). The pair of asteroids, or group of asteroids, with the smallest similarity coefficient (and therefore the most similar) are found. These asteroids are then joined at this level of taxonomic distance. Thereafter, these objects are considered

Figure 2.1 Example of unweighted average linkage.

2	<u>.1</u>				
3	.25	.15			
4	.4	.6	.7		
5	.5	.3	.8	.9	
6	.6	.7	.45	.75	.3
	1	2	3	4	5

Circle:- smallest taxonomic distance ie. most similar (next join).

1 joins 2 at 0.1

3	<u>.2</u>			
4	<u>.5</u>	.7		
5	<u>.4</u>	.8	.9	
6	<u>.65</u>	.45	.75	.3
	1,2	3	4	5

Underlined:- recomputed distances from previous join.

1 joins 3 at 0.2

1 here is (1+2), calling each group by it's lowest numbered member.

4	<u>.56</u>		
5	<u>.53</u>	.9	
6	<u>.65</u>	.75	<u>.3</u>
	1,2,3	4	5

$0.56 = 0.56666\dots$

Similarities have equal weight  
 eg.  $0.56 = (0.4+0.6+0.7)/3$   
 using top matrix, or  
 $0.56 = (0.5*2+0.7*1)/3$   
 using second matrix.

5 joins 6 at 0.3

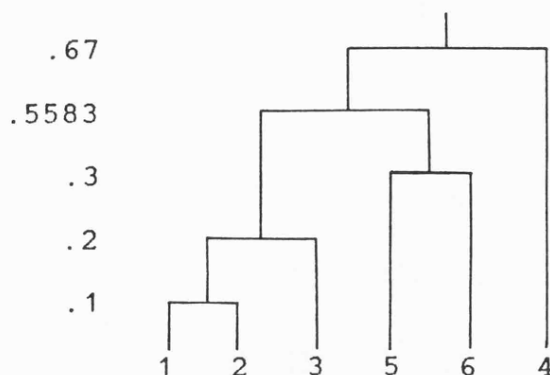
4	<u>.56</u>	
5,6	<u>.5583</u>	.825
	1,2,3	4

1 joins 5 at 0.5583

4	<u>.67</u>
	1,2,3,5,6

1 joins 4 at 0.67

RESULTING DENDROGRAM



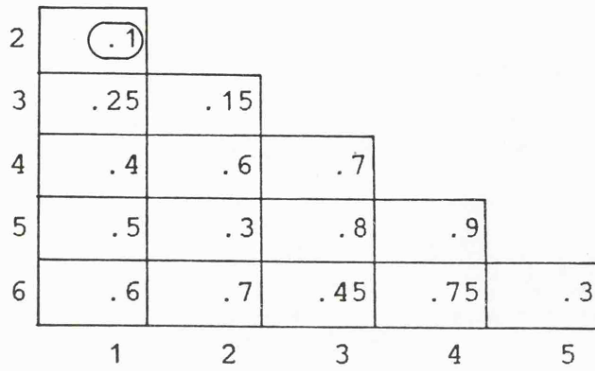
as one point in classification space situated midway between their separate positions, or weighted towards the group with the most members. The similarity matrix is then recalculated and searched for the next closest pair, or group, of asteroids.

**SINGLE LINKAGE:** (Figure 2.2). This method can best be explained by reference to Figure 2.3. Objects a and b are the two most similar, and will be linked together first. Of the two taxonomic distances a-c and b-c only the smallest (a-c) will be retained in the matrix (as the distance (ab)-c), while for d the distance ab-d will be set to the smallest of a-d and b-d (ie. b-d). The distance c-d remains unchanged at this stage. After these modifications, the new similarity matrix is searched for the next closest pair.

For each method, the similarity matrix diminishes by one row and column for each link which is made, and finally contains only one element for the last connection which will be at the highest level on the dendrogram. Figures 2.1 and 2.2 show both of the methods operating on the same initial similarity matrix. It was found for asteroid data that unweighted average linkage gave the best results, ie. with individual objects linked at low taxonomic distances while groups of asteroids were joined at relatively large distances. Single linkage tended to separate one object at a time and produced very little structure in the dendrogram.

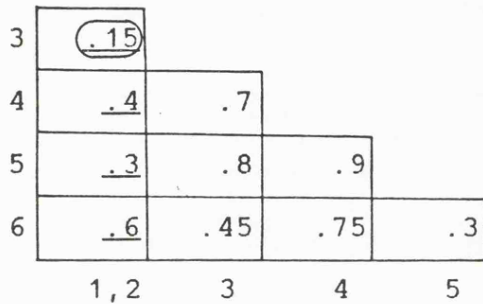
The maximum benefit is achieved from numerical taxonomy when the number of parameters entered for each taxonomic unit

Figure 2.2 Example of single linkage.

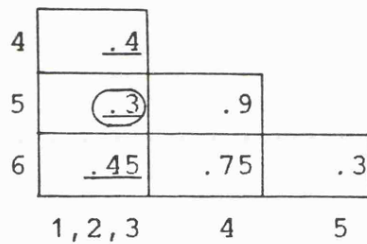


Circle:- smallest taxonomic distance ie. most similar (next join).

1 joins 2 at 0.1

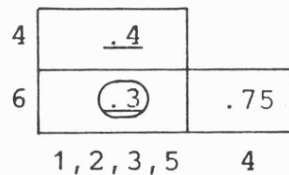


1 joins 3 at 0.15

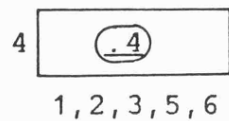


1 joins 5 at 0.3

Note:- ties with 5 joining 6, arbitrary which one to do first, but no difference to final clustering. In weighted average linkage there is liable to be a difference.

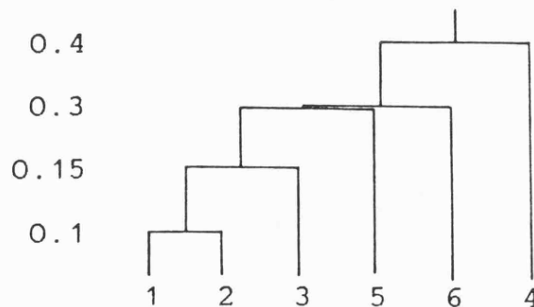


1 joins 6 at 0.3



1 joins 4 at 0.4

RESULTING DENDROGRAM





were used.

The first data set consisted solely of the 0.3 $\mu$ m - 1.1 $\mu$ m reflectance spectra of all 277 asteroids in the file. The asteroid's spectrum is expressed relative to its value at 0.56 $\mu$ m, this has the consequence of removing the effect of differing albedo between asteroids. Thus all asteroids have unity as the value of their spectrum at this wavelength. Each spectrum contained a spread of between 13 and 24 points over a possible 26 wavelengths; hence no spectrum was complete. The effect of these missing points will be discussed below.

Both unweighted average and single linkage were used on this set of data. The latter method proved to be the least satisfactory because the asteroids tended to be placed individually, or at most in small groups. This was also true for other data sets mentioned below: hence, discussion of the results will be limited to those obtained with an unweighted average linkage.

The dendrogram resulting from the unweighted average linkage splits the asteroids into two large groups plus eight objects which can be considered as "stragglers" to the main groups. Inspection of the large groups shows that one group is dominated by S-class asteroids, while the other is mainly C-classes. Strictly, the division is into those with sloping spectra (S-like, as distinct from S-class) and those with flat spectra (C-like).

The S-like region contains 118 asteroids of which 88

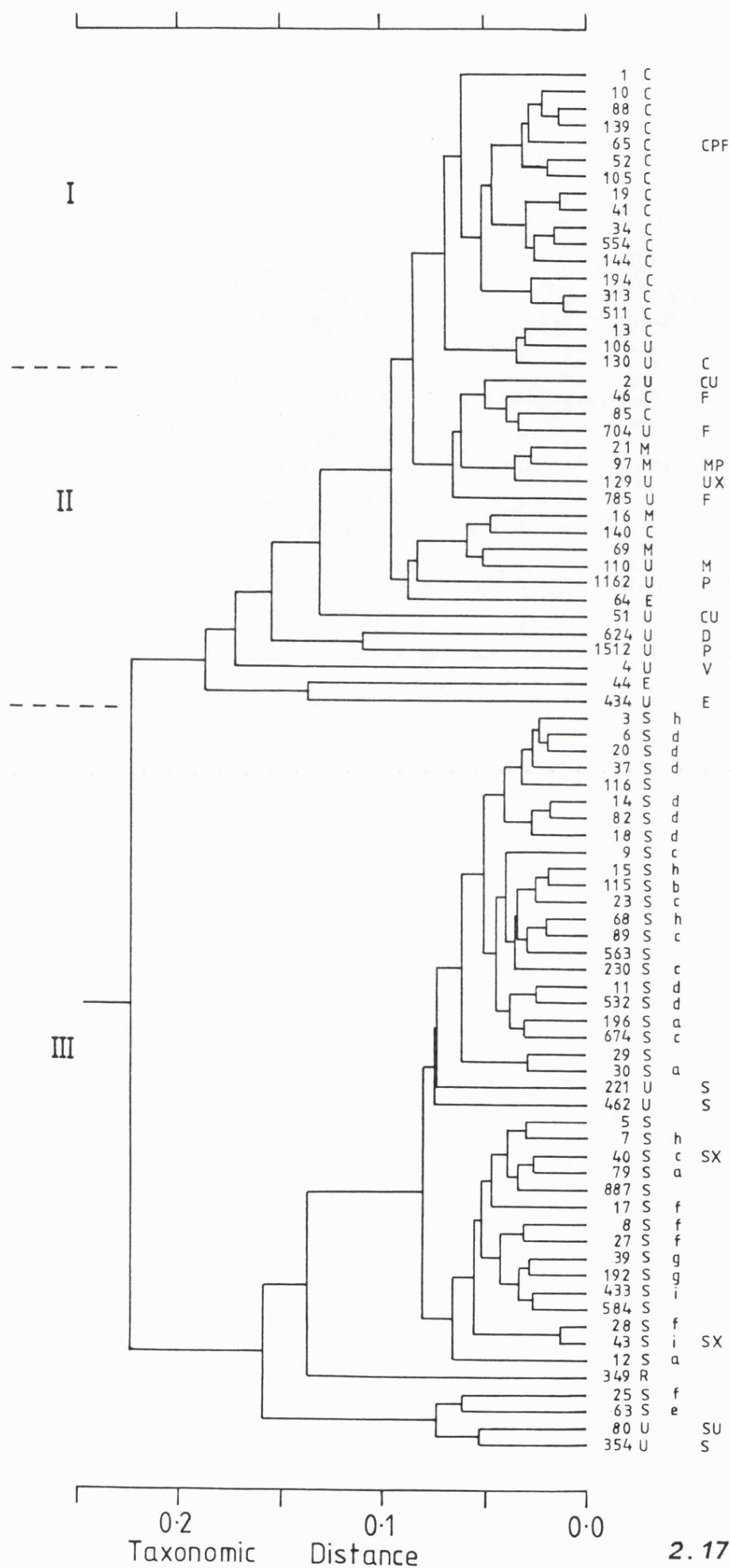
are S-classes, 2 C-classes, 2 MEU's, 4 R's and 22 U-classes. With the exception of some U-classes all the non-S-classes are linked into the group at high levels, while the majority of S-classes are connected together at lower levels (taxonomic distances of  $<0.1$ ). Recently, the asteroids have been reclassified in the light of new information. Of the S-like asteroids, one S-class has changed to RD, while three have become SX. In the other direction, one R-class and four of the U-class have changed to S-class, with three other U-class becoming SU or SX. Another eight objects, not S-class, changed to new classes which have been introduced recently (A,D,P). It is also worth mentioning that the U-class asteroids which became S-class were those most strongly connected to the S-class in the first place. Neither of the C-class asteroids, 1199 Geldonia and 365 Corduba, have changed their classification.

Turning to the 151 asteroids in the C-like region, less than half (seventy three) are, in fact, C-class, 32 are U-class, 9 M's, 2 E's, 6 S's and 29 others (CMEU,EU, etc.). In this region, the different classes are more intermingled than in the S-like region, but most of the C-classes tend to separate out from the rest at lower taxonomic distances (higher similarity). Most of the changes due to the reclassification were amongst objects in the smaller groups (M,E,CMEU etc.) which changed mainly to the new (and also small) groups of F,P,EMP, etc. None of the six S-classes in this region changed their class. The stragglers consisted of 5 U-classes and one each of C,S and R-classes.

A subset of the spectral reflectance data was used to establish the effect of the missing data points. This subset consisted of only twelve wavelength points chosen such that the number of missing data points was a minimum. These points covered the the range 0.4 to 0.8 $\mu$ m. In total, six asteroids each had one point missing. The resulting dendrogram is, in general terms, the same as with the complete set of data, but with the asteroids joining at slightly lower taxonomic distances (partly due to the fewer number of points).

The S-like region has the majority of actual S-classes joining at the lowest levels of the region. The region has gained three C-classes to make a total of five. It also acquired one each of M, CMEU and CEU-classes. All of these additions came from the asteroids of the C-like region which connected at the highest levels within that region. The number of S-classes in the C-like region dropped from five to three. The C-classes do not separate from the mixture of other classes, present in the region, as strongly as in the full data set. This is also true of the S-classes in the S-like region. Comparing the two dendrograms at the lower levels of taxonomic distance reveals that none of the detailed structure survives and that virtually all of the individual asteroids have moved relative to each other. Thus it appears that missing points do not affect the general structure of the dendrogram, but that they can influence the position of individual objects, particularly those which are closer to the major divisions of the dendrogram.

Figure 2.4 Dendrogram of 82 asteroids analysed by the parameters; U-B, B-V, R/B, BEND, DEPTH and albedo. Roman numerals indicate regions discussed in the text. The right hand columns are; asteroid number, TRIAD classification, Feierberg et al. (1982) sub-classification of S-class asteroids and recent reclassification when different from TRIAD.



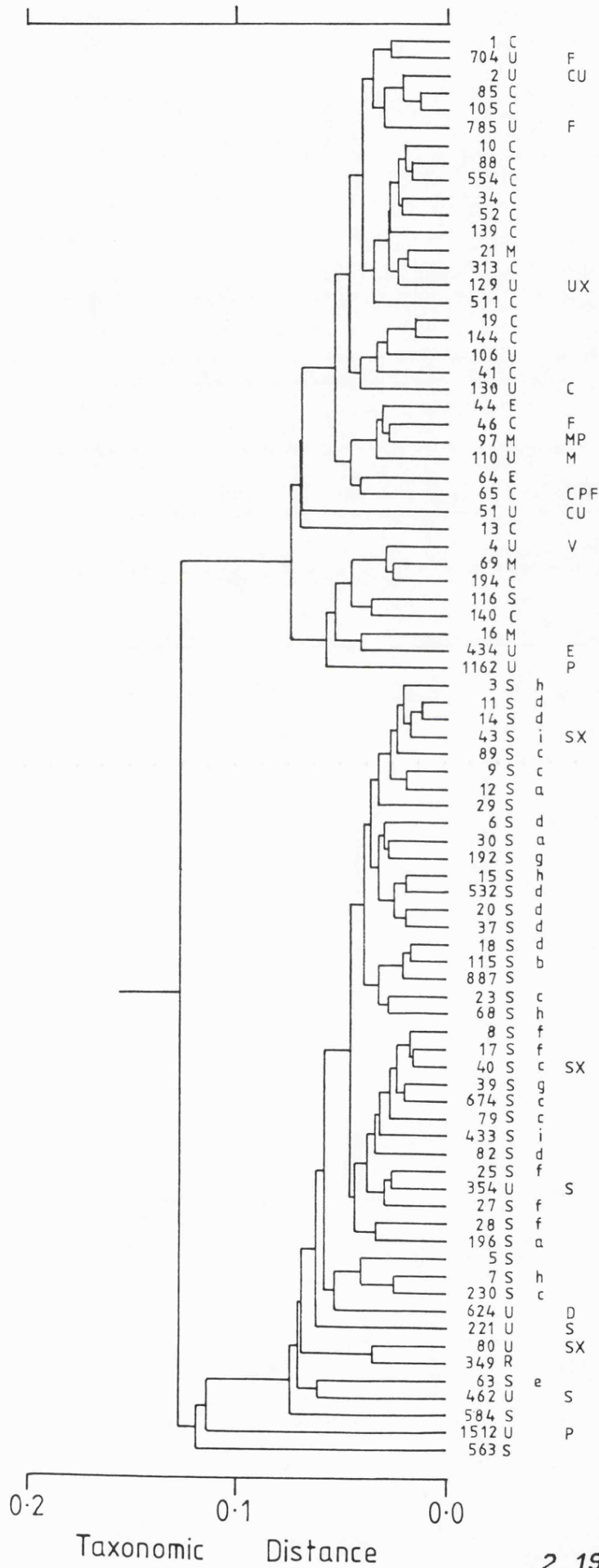
Until recently, when JHK colours have become available (Veeder et al., 1982 and references therein), asteroid classification was based on seven parameters: albedo, U-B, B-V, R/B, BEND, DEPTH<sup>4</sup> and  $P_{min}$ . The TRIAD files (Gehrels, 1979) contained 82 asteroids which had all of the first six parameters, only 60 of these also had a value of  $P_{min}$  given. These asteroids formed the basis of the second data set to which numerical taxonomy was applied. The albedo used was an average of the polarimetric and radiometric albedos, when both were available.

Figure 2.4 shows the resulting dendrogram, for the set of 82 asteroids, which clearly splits into two groups; again one is mostly S-class and the other mainly C-class. However, there are no stragglers as with the previous set of data. Also this division occurs at a larger taxonomic distance than previously, but the linkages within these two regions take place at similar levels to the earlier data set. This indicates that although the relationship between members of, for example, the S-like region, is the same for both sets of data, the two major regions have become appreciably dissimilar. This conclusion is verified by Figure 2.5 which shows the same 82 asteroids, but analysed by their relative reflectance spectra (using the same twelve wavelength points as above, there were no missing points in this data set). Regions I and II contain asteroids with flat spectra and region III those with sloping or red spectra.

---

<sup>4</sup> DEPTH= the reflectance at the bottom of an infrared adsorption feature divided by the highest reflectance on the short-wavelength side of the band.

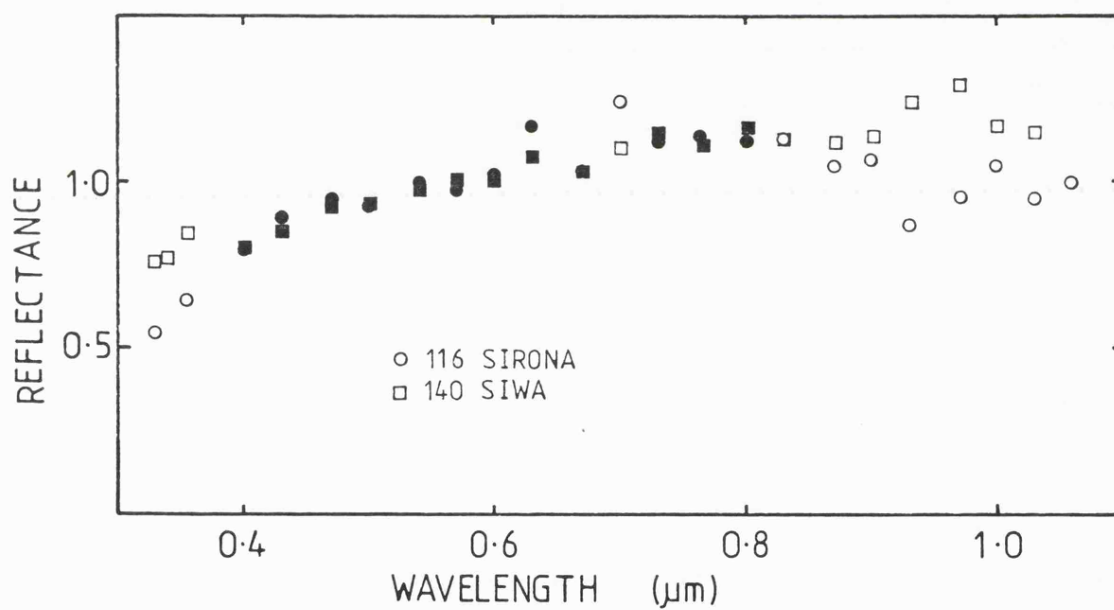
Figure 2.5 Dendrogram of 82 asteroids analysed by their relative reflectance spectra (using 12 wavelength points; 0.4, 0.43, 0.47, 0.5, 0.54, 0.57, 0.6, 0.63, 0.73, 0.765 and 0.8 $\mu$ m).



As with the first two dendrograms, the ordering of the asteroids changes from Figure 2.4 to Figure 2.5. The largest change between the two dendrograms, on the level of single asteroids, is the migration of asteroid 116 Sirona from its seemingly well-entrenched position in the S-like region in Figure 2.4 to the C-like region in Figure 2.5. A possible explanation is found by returning to the first two dendrograms discussed, which used the full spectra and the twelve wavelength subset. In the dendrogram based on the complete spectra, asteroid 116 is in the S-like region, as expected, and the asteroid 140, to which it is linked in Figure 2.5, is in the C-like region, again as expected since it is a C-class. However, when numerical taxonomy is applied to the shortened spectra, both of these asteroids move into the opposite region. This suggests that the two asteroids have similar spectra when restricted to the twelve wavelength points. This is confirmed visually in Figure 2.6, which shows the two complete spectra for these asteroids.

Returning to Figure 2.4 it can be seen that region I contains the vast majority of C-class asteroids, which are linked at low levels, while region II contains the assortment of smaller classes (with the exception 349 Dembowska, which is R-class) joining at higher levels in the dendrogram. Of the two U-classes in region I, one (130) has been reclassified, on the basis of new data, as C-class; also one of the C-classes in the region (65) has been reclassified as CPF. The majority of the asteroids in region II underwent class changes due to the reclassification, most of these changes being to the new taxonomic classes D,P and F. These

Figure 2.6 Relative reflectance spectra of 116 Sirona and 140 Siwa. Solid symbols show the subset of 12 wavelength points used in Figure 2.5.



new classes generally only contain a few asteroids and most have been introduced with the advent of infrared data (Gradie and Tedesco, 1982) which was not included in the numerical analysis. All of the S-class asteroids are contained in region III, together with four U-class asteroids (all reclassified as S-class) and the R-class object, 349 Dembowska.

Before investigating the effect of the introduction of minimum polarization into the data, it is worth considering region III of Figure 2.4 in more detail. Feierberg et al. (1982) divided 45 S-class asteroids into nine subgroups (a-i) based on eight parameters R/B, U-B, B-V, BEND, DEPTH, IR (infrared slope) together with the band centre and bandwidth of the 0.95 $\mu$ m absorption feature present in the spectra of most S-class asteroids. The authors interpret the different subgroups in terms of pyroxene and olivine mineralogy, together with iron, magnesium and other elements. Of these 45 asteroids, 33 are also among the S-classes in Figures 2.4 and 2.5 (identified by the lower case letters a-i).

Examination of region III in Figure 2.4 shows that the correlation is poor between the clustering at low levels and the subgroups proposed by Feierberg et al. (1982). However, there is a tendency for the f-group to be at the bottom of region III, while asteroids of group d are near the top of the region. The situation regarding a-i groups in Figure 2.5 is similar to the previous diagram except that the f-group asteroids have moved up slightly to occupy the central part of region III. This loose agreement between numerical

taxonomy and the subgroups of Feierberg et al. (1982) is not surprising since they state that "the [a-i] groupings should be thought of as a division of a continuum of spectra rather than as an identification of well-defined groups".

The next step in the analysis of asteroid data by numerical taxonomy was to introduce minimum polarization ( $P_{min}$ ) into the data set. In order to maintain a complete set of data it was necessary to reduce the number of asteroids in the sample to 60.

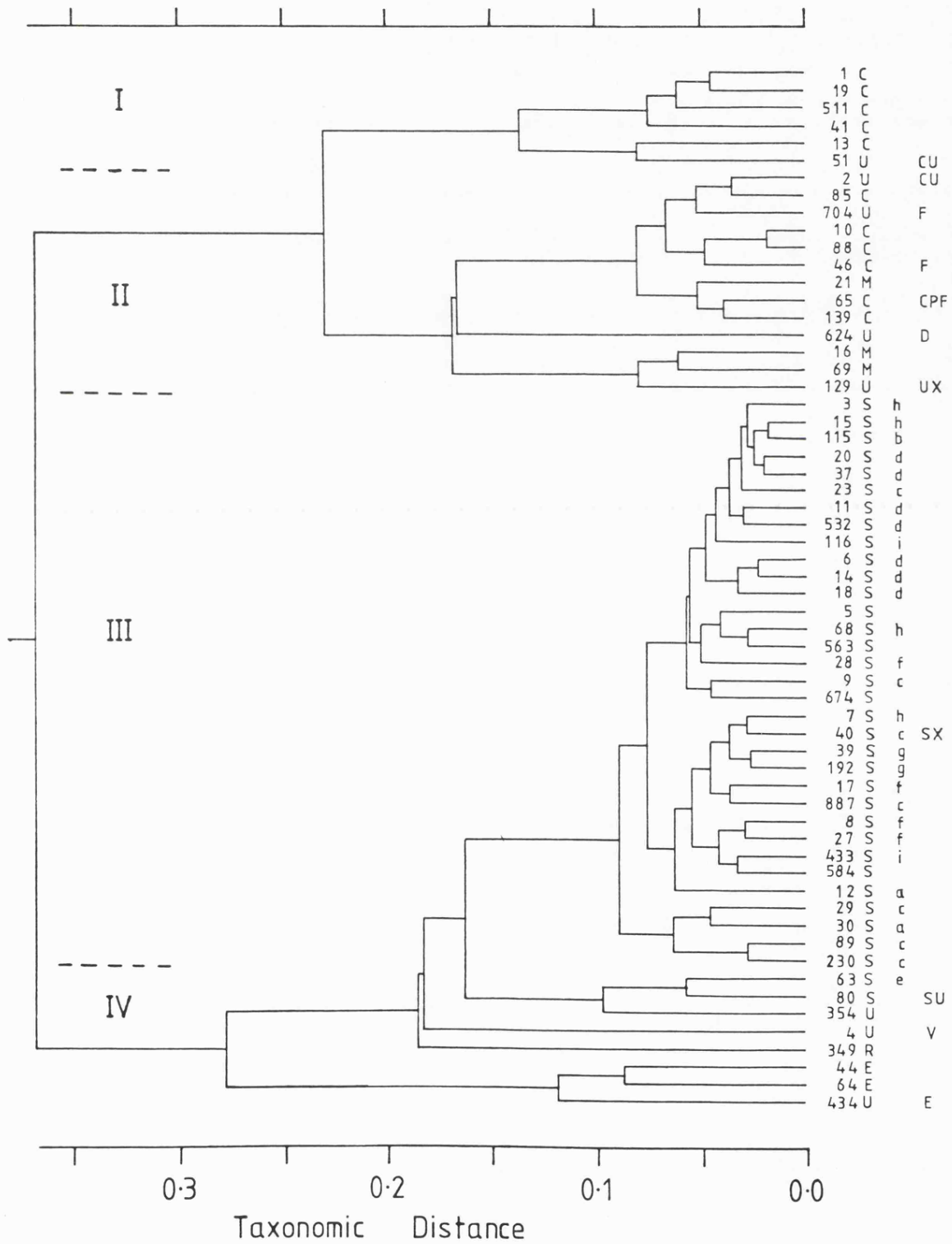
To provide a direct comparison with the dendrograms in Figures 2.4 and 2.5 a subset of the data, pertaining to the 60 asteroids, was used (ie. 60 asteroids with twelve wavelength points and 60 asteroids analysed by six parameters). An examination of the two dendrograms produced, for 60 and 82 asteroids from the twelve wavelength data revealed that, with the exception of the missing asteroids, the dendrograms are virtually identical, even to the lowest levels of taxonomic distances. This is also true of the corresponding dendrograms based on the spectral parameters U-B, B-V, R/B, BEND, DEPTH and the albedo. However, one object, the U-class 624 Hektor, does move from the C-like region (82 asteroids) to the S-like region (60 asteroids). In both pairs of dendrograms it is the C-like region which undergoes the most change, although these changes are still small. This is probably explained by the fact that most of the asteroids which only occur in one set of data make their appearance in the C-like regions of the dendrograms with 82 asteroids.

The effect of the introduction of  $P_{min}$  is, at first glance, quite dramatic (Figure 2.7). The dendrogram still splits into C-like and S-like regions, but this division occurs at a taxonomic distance of 0.37 compared to 0.23 (Figure 2.4) and 0.13 (Figure 2.5). This indicates that the two regions have become more dissimilar on the introduction of  $P_{min}$ . The connections between individual asteroids at lower levels also occur at slightly higher taxonomic distances, but this is partially explained by the introduction of another parameter into the analysis.

Four asteroids (4 Vesta - originally U-class, but now recognized as V-class, the only object of that class; 44 and 64 - both E-class; 434 - now classified as E-class, but previously U-class) have moved from the C-like region to the S-like region when Figure 2.7 is compared with Figure 2.4. The C-like region splits into two separate groups (I and II) at a relatively high taxonomic distance (0.23). Group I contains five C-classes and one object now identified as CU. The larger group II contains a few C-classes, but also embraces three M-class asteroids, two of which (16 and 69) together with 129 (UX) join at a high level within the region. The only D-class present (624 Hektor) joins at a similar taxonomic distance. The remaining asteroids (4 C-class, one M, two F's, one CU and one CPF) all cluster together at lower levels.

Considering the S-like region, it can be seen that three objects separate off at a high level; all three are now

Figure 2.7 Dendrogram of 60 asteroids analysed by the six parameters in Figure 2.5 plus  $P_{min}$ .



classified as E-class asteroids. Moving to lower taxonomic distances, two objects peel off individually - 349 Dembowska (R-class) and 4 Vesta. Next, another three asteroids separate into a small group 354 (U), 80 (SU), and 63 (S). It is interesting to note that Feierberg et al. (1982) found 63 to be the only representative of their subgroup e. All of these objects are in region IV. The remaining asteroids (all S-classes with the exception of 40 Harmonia which is SX) can be considered to fall into one group, region III. Returning to the subgroups of Feierberg et al. (1982) it is again apparent that there is a poor correlation, although the d-group cluster together at the top of region III. The two asteroids of the g-group also join together before connecting to other asteroids, though it is doubtful that this is significant since it does not happen in the other dendrograms.

#### ASTEROID COLOURS

Broadband photometric colours are one of the major means of classifying asteroids. Originally, visible colours (U-B, B-V) were used, but this has been extended to the infrared by Veeder et al. (1983). An assortment of UBVRIJHK colours have been obtained while observing the lightcurves presented in Chapters 3 and 4. Table 2.2 gives these colours, including asteroids for which only partial lightcurves were obtained.

The standard stars used for calibration were taken from Johnson et al. (1966); Neckel and Chini (1980); Vogt et al.

Table 2.2 Asteroid Colours

Asteroid	U-B	B-V	V-R	V-I	V-J	J-H	H-K
4					1.42	0.17	-0.07
5						0.35	0.03
19						0.34	0.12
20	0.51	0.86			1.47	0.36	0.04
29	0.44	0.80			1.47	0.45	-0.02
31	0.31	0.68	0.34	0.69			
31	0.34	0.71			1.21	0.45	0.17
39	0.52	0.90	0.48	0.93			
39	0.50	0.89			1.40	0.55	0.03
40	0.41	0.89	0.46	0.91			
44	0.23	0.70	0.38	0.71			
44	0.29	0.73			1.26	0.33	0.10
52						0.34	0.09
83						0.48	0.11
115						0.36	0.05
145						0.35	0.02
349						0.51	0.07
386						0.40	0.07
471						0.50	0.05

(1981); Elias et al. (1982) and Allen and Cragg (1983). Optical colours obtained using the simultaneous photometer (see Chapter 3) require correction factors to be added. This is necessary because the dichroic mirror used to separate the visible and infrared radiation has a transmission which is dependent on the wavelength of the radiation. In particular, it adds a short wavelength cutoff to the U filter. The corrections place the colours on the standard photometric system. The correction, in magnitudes, to a colour  $M_1 - M_2$  is calculated using the following equation:

$$\text{correction} = 2.5 \log (O_1 S_2 / S_1 O_2) \quad (2.2)$$

where  $S_1$  and  $S_2$  are the ratios in Table 3.1 for the spectral type of the standard and  $O_1$  and  $O_2$  are the ratios for the object. The subscripts refer to the filters used in the colour. Thus the correction to the U-B colour of a G0 star calibrated by a B0 standard is

$$\begin{aligned} \text{U-B correction} &= 2.5 \log (0.708 * 0.988 / 0.630 * 0.978) \\ &= 0.14 \text{ mag.} \end{aligned}$$

In the case of the asteroids, the corrections were 0.03 for U-B and 0.01 for B-V. The asteroids were assumed to have spectral types similar to G5 stars. The colours quoted are averaged over the lightcurve (or partial lightcurve) to remove the effect of any colour variations. Photometric errors are  $\pm 0.02$  for visible colours and  $\pm 0.04$  if a J, H or K filter is involved.

When the data in Table 2.2 are compared with previous observations (Veeder et al., 1983, Hansen, 1976 and references therein) on a two-colour diagram, it is found that the data plot within the regions usually associated with the appropriate classes. However, there appears to be a systematic error in the colours V-R, V-I and V-J, but not B-V, such that the colours are too red by  $\sim 0.2$  mag. The origin of this error is unknown, since the V-R and V-I data were obtained using different equipment on a different telescope and are compared with a different set of previous observations to the V-J data. Unfortunately, there are insufficient asteroids in Table 2.2 to be able to draw any conclusions from the two-colour diagrams concerning classification. As the number of asteroids which have infrared colours measured increases, it will prove possible to incorporate these colours into the data sets used for numerical taxonomy, in particular the data used to produce Figure 2.7. At present the number of asteroids which have measured infrared colours and also have known albedos,  $P_{\min}$ , etc., is too small for numerical taxonomy to be of any value.

## DISCUSSION

Figures 2.4 and 2.5 indicate that numerical taxonomy, when based on data obtained in the visible region of the electromagnetic spectrum, is very good at separating asteroids according to the general nature of their spectra. In particular, it is good for identifying S-class asteroids. The process is reasonably successful at identifying C-class

objects, but has difficulty distinguishing between some C-class and other classes such as E and M. This is similar to the situation with a plot of U-B vs. B-V, in which the C, M and E domains overlap to a large extent. Veeder et al. (1978) have shown that a plot of asteroid at  $1.6\mu\text{m}$  vs. the reflectance at  $2.2\mu\text{m}$  separates the M-class asteroids from the C-class asteroids, though these are coincident on the usual U-B vs. B-V colour plot. If these optical-infrared colours are included in the data set used by numerical taxonomy, it is probable that the M-class asteroids will be grouped together more strongly than in the dendrograms above. At present there are insufficient data available for this analysis to be performed.

The low level linking of asteroids in the dendrograms is of little, if any, significance, since the asteroids change position whenever the data are changed slightly. Observational errors will also affect the exact position of an asteroid. The linkages at large taxonomic distances are significant since this separates the asteroids into their basic classes. The level at which the linking becomes meaningful depends on the data used, since observational errors and incomplete data will affect the significance of the dendrogram. Large uncertainties in more than 10% of the input data are likely to generate large errors in the structure of the dendrogram (Sneath and Johnson, 1972). In general terms, the application of numerical taxonomy to asteroids produces result similar to those obtained with the more conventional techniques.

**CHAPTER 3**

**LIGHTCURVES**

**AND**

**COLOUR VARIATIONS**

## INTRODUCTION

Asteroid lightcurves have been observed for many years and were quickly attributed to the rotation of a non-spherical shape. Another possible origin of variations in the intensity of the light reflected by an asteroid is a change in the albedo, which may be related to mineralogy, across the surface of the asteroid. The lightcurves are also complicated by large-scale surface features, such as mountain ranges. These features would have to have sizes at least of the order of 1% of the parent body to be detectable by photometry. Lightcurves often show small-scale deviations superimposed on the smooth run of the overall shape of the lightcurve, which can be caused by such surface features. Repeated observations of the lightcurve should make it possible to construct a picture of the asteroid's surface morphology. The variation of the amplitude of the lightcurve with its position in the sky enables the overall shape and orientation of the rotation axis to be determined (see Chapter 4).

Asteroids exhibit a diversity of colours (e.g. in B-V) and albedos in the visible region which can, and have been, interpreted in terms of different surface mineralogies. By monitoring the colour of an asteroid, as it rotates, it should be possible to detect changes in the surface composition. A less probable cause of colour variations is a change in the size of the particles forming the regolith, but such variations would generally be smaller. Several asteroids have been searched for colour variations (Schober and Scholl,

1982) and a few such variations have been observed. These are usually small  $\leq 0^m.05$  (the exception being 944 Hidalgo with a variation of  $0^m.12$  in U-V) and are observed in optical colours (e.g. U-V, V-I). Recently, Veeder et al. (1978 and references therein) have extended the means of identifying surface compositions into the near-infrared with JHK colours. At these wavelengths, asteroids show a wider range of colour, particularly if the infrared magnitudes are combined with optical magnitudes to form such colours as V-K. Since the various classes of asteroids exhibit a larger range of optical-infrared colours than optical alone, it seems reasonable to assume that colour variations should be larger and thus easier to detect over this greater wavelength range.

This chapter presents BVJK lightcurves of ten asteroids (4 Vesta, 20 Massalia, 29 Amphitrite, 31 Euphrosyne, 39 Laetitia, 40 Harmonia, 43 Ariadne, 44 Nysa, 115 Thyra and 349 Dembowska). 40 Harmonia only has a V lightcurve, while the rest have B lightcurves together with simultaneous colour curves. Two of these asteroids, 29 and 39, were observed during two oppositions. Before presenting the results, the principal instrument used is described, followed by the method by which the data were acquired and subsequently reduced.

### INSTRUMENTATION

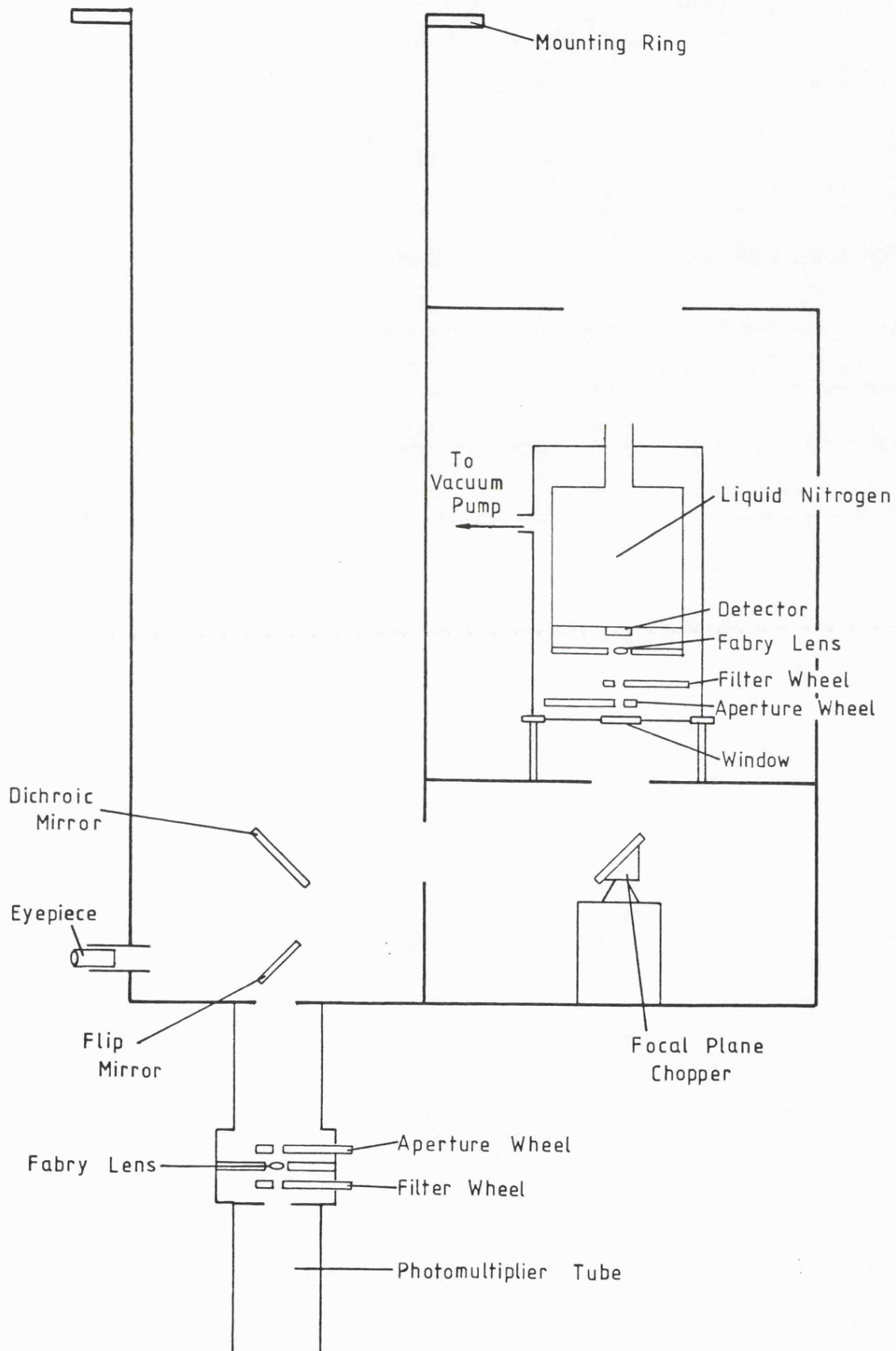
The majority of the data presented in this thesis were obtained with the Leicester simultaneous optical and infrared photometer attached to the 1.5m Infrared Flux Collector

(IRFC) at the Observatorio del Teide, Tenerife. The development of this instrument, in particular the infrared photometer, is described in detail by Sherrington (1980). Thus the following description of the instrument will be brief, although the transmission of the optical filters will be discussed in detail.

Figure 3.1 shows the layout of the simultaneous optical/ infrared photometer. The optical (UBV) radiation is separated from the infrared (JHK) by means of a 45° dichroic mirror which reflects the infrared radiation, but transmits the optical portion of the beam. The optical light then passes through the aperture, a quartz Fabry lens and either a U, B or V broadband filter before detection by an EMI 9502S photomultiplier tube. For all observations a 2mm aperture was used, corresponding to 21 arcseconds on the sky.

After reflection by the dichroic mirror, the infrared radiation is reflected to another 45° mirror which deflects the beam vertically into the cryostat housing the infrared detector. This second mirror is attached to a solenoid vibrator which moves the mirror vertically. This has the effect of alternately exposing the detector to two neighbouring regions of sky. The first region, or beam, contains the source plus an area of sky while the second only contains a region of sky. The difference between the beams, ie. the signal from the source, can be obtained by a phase sensitive detector. The distance (or chop) between the centres of the two beams was 40 arcseconds for all observations.

Figure 3.1 Diagram of optical/infrared photometer (not to scale).



The cryostat has a  $\text{CaF}_2$  window, a set of apertures, a selection of infrared filters (JHKL) and a Fabry lens (also  $\text{CaF}_2$ ), through which the radiation must pass in order to reach the indium antimonide detector. Again a 2mm aperture was used throughout. The detector is cooled by liquid nitrogen to 77K and can be 'pumped' to lower the temperature to  $\sim 63\text{K}$ . This improves the sensitivity of the detector and also serves to cool the aperture and filters, thus reducing their thermal radiation.

The spectral response of the optical filters is a convolution of the transmission of the dichroic and filter together with the response of the photomultiplier tube. The transmission curves for the UVB filters were obtained over the wavelength range 200 - 800nm using a monochromator of the chemistry department. This was also used to find the transparency of the dichroic mirror (which was placed such that the angle of incidence of the beam was  $45^\circ$ , to simulate its actual orientation in the photometer). The spectral response of the photomultiplier tube is supplied by the manufacturer. Figure 3.2 shows the percentage transmission of the three filters and the dichroic mirror; also presented is the efficiency of the photomultiplier tube as a function of wavelength.

Convolving the filter and dichroic transmission functions together with the tube response leads to the effective spectral response of the individual filters. These are shown in Figure 3.2 (solid lines); for comparison, the

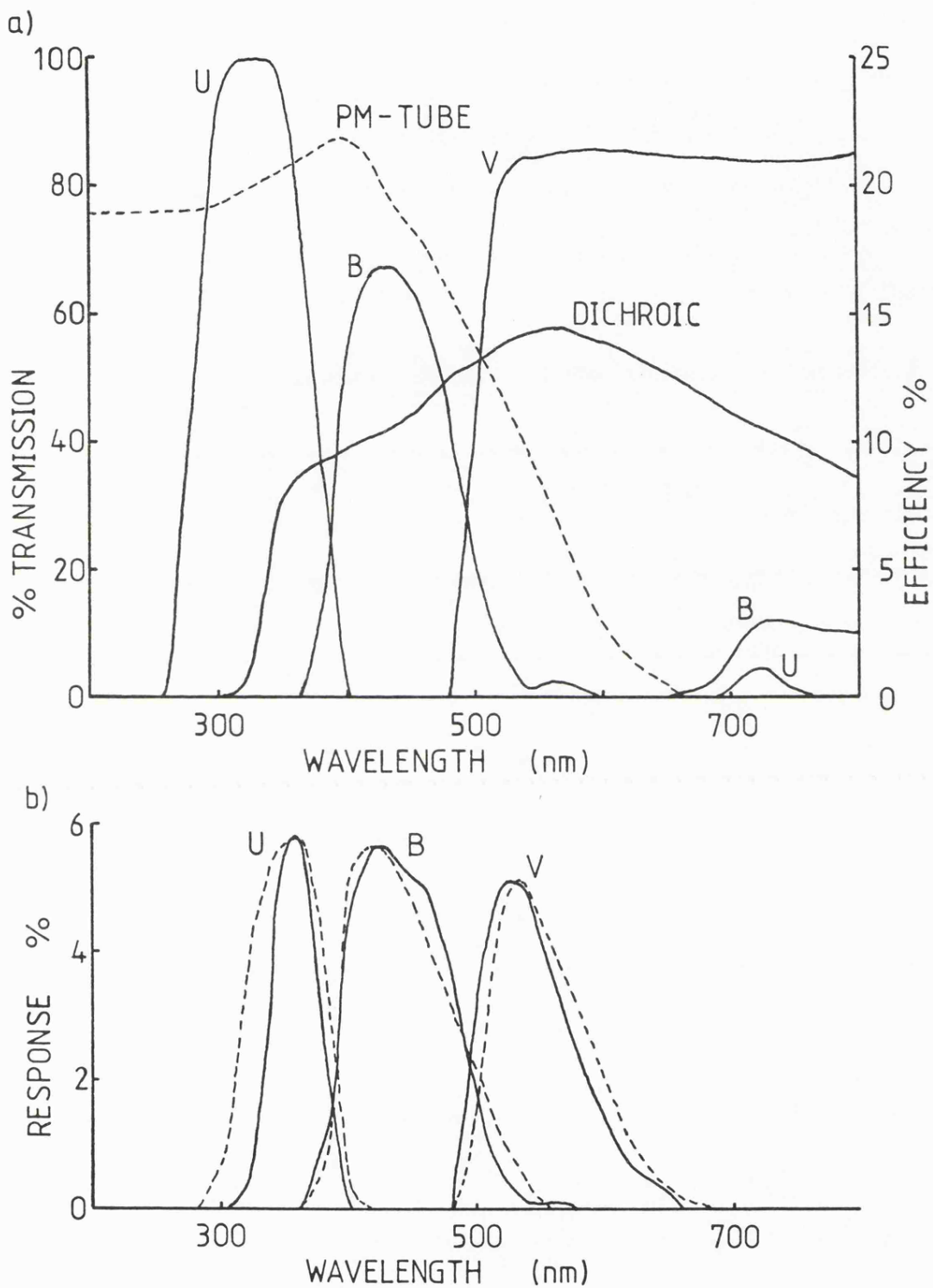


Figure 3.2 a) Transmission curves of the UVB filters and the dichroic mirror. Broken line is the efficiency of the photomultiplier tube. b) System response of the visible filters compared with standard filter profiles (broken lines).

response of the standard filters (Allen, 1973) are also shown (dashed lines). The mean wavelength ( $\lambda_m$ ) of the various filters can be calculated using Equation 3.1.

$$\lambda_m = \frac{\int T \lambda d\lambda}{\int T d\lambda} \quad (3.1)$$

where T is the transmission of the filter as a function of wavelength. The mean wavelengths of the Leicester filters and the standard filters are given in Table 3.1. Also given in Table 3.1 is the ratio of the number of photons detected by the system through the Leicester filters and through the standard filter set for various types of stellar spectra. These were obtained by converting the data given by Allen (1973) into photons, then multiplying by each of the filter sets and ratioing the resulting counts. This enables the colour corrections to be calculated. These corrections are required when the objects observed have different spectra from the standard stars used for calibration.

Table 3.1 Mean  $\lambda$  and correction factors for filters.

	Mean $\lambda$ (nm)		Correction factors for spectral type					
	Leic.	Standard	B0	A0	F0	G0	K0	M0
U	358	350	0.630	0.688	0.678	0.708	-----	-----
B	456	444	0.988	0.983	0.982	0.978	0.977	0.978
V	546	554	0.968	0.959	0.948	0.943	0.924	0.896

Other equipment used to obtain data was the 3-4 $\mu$ m circular variable filter (CVF) in UKT6 at the 3.8m UKIRT, Hawaii and the Peoples' Photometer on the 20" telescope at SAAO, South Africa. Both of these instruments are common user instruments and are described in the reference manuals for

their respective observatories.

### ACQUISITION AND REDUCTION

Lightcurve data were obtained at two observatories during five observing runs, (four at Observatorio del Teide, using the photometer described above, and one at SAAO, using the People's photometer). The observing technique was essentially the same at both sites. Observing runs at Tenerife yielded B, V, J and K lightcurves, with the exception of the first run in August 1982 when only B and V curves were obtained due to a failure of the infrared detector. The visit to SAAO only produced lightcurves in the V band.

Each asteroid was observed when it was within one degree ( $1.5^\circ$  for 349 Dembowska) of an SAO star, chosen to have solar-like colours. This comparison star was observed at intervals of 30-90 minutes to remove the effect of changing air mass on the asteroid's lightcurve. When infrared data were obtained, the measurements at J( $1.2\mu\text{m}$ ) were simultaneous with those at V( $0.55\mu\text{m}$ ), while K( $2.2\mu\text{m}$ ) was simultaneous with B( $0.44\mu\text{m}$ ), U( $0.36\mu\text{m}$ ) and H( $1.6\mu\text{m}$ ) were observed at the same time, but less frequently than the other wavelengths. Asteroids were observed alternately in BK and VJ wavebands at intervals of approximately five minutes. Each five-minute observation consisted of several asteroid-background subtractions and is plotted in the figures with its associated standard error of the mean. When only V data are presented the points plotted are the mean of two twenty-

Table 3.2 Aspect Data

ASTEROID	DATE	RA (1950)	DEC	$\lambda$	$\beta$	$r$	$\Delta$	PHASE
4 Vesta	27 Nov 83	05 36 45	18 13 18	84.5	-5.1	2.5740	1.6280	7.86
	28 Nov 83	05 35 48	18 14 19	84.2	-5.1	2.5739	1.6235	7.43 <sup>*</sup>
	29 Nov 83	05 34 51	18 15 20	84.0	-5.1	2.5736	1.6190	6.99
20 Massalia	28 Nov 83	01 03 07	06 31 23	17.0	-0.2	2.2172	1.4335	19.35
29 Amphitrite	01 Sep 82	23 20 59	-06 28 49	348.5	-2.1	2.4951	1.4959	4.21
	26 Nov 83	08 55 23	25 06 54	129.2	7.4	2.4257	1.8544	21.87
	27 Nov 83	08 55 49	25 07 13	129.3	7.5	2.4262	1.8435	21.70
31 Euphrosyne	25 Nov 83	01 19 40	13 05 29	23.3	4.3	2.6499	1.8092	13.57
	26 Nov 83	01 18 57	13 10 06	23.2	4.4	2.6479	1.8162	13.92
39 Laetitia	29 Aug 82	20 04 36	-13 47 29	300.4	6.4	2.5568	1.6663	13.26
	30 Aug 82	20 04 13	-13 54 12	300.3	6.4	2.5558	1.6728	13.60
	31 Aug 82	20 03 52	-14 00 51	300.2	6.3	2.5548	1.6794	13.94
	24 Nov 83	05 09 54	06 35 30	77.0	-16.3	2.6097	1.6706	8.37
40 Harmonia	07 Oct 83	19 35 01	-25 19 14	291.4	-3.6	2.1837	1.8037	26.94
	08 Oct 83	19 36 09	-25 16 31	291.7	-3.6	2.1833	1.8151	26.99
	09 Oct 83	19 37 17	-25 13 43	291.9	-3.6	2.1829	1.8265	27.03

43 Ariadne	29 Aug 82	01 17 15	14 13 43	23.2	5.6	2.0961	1.2822	21.02
	30 Aug 82	01 17 00	14 14 10	32.1	5.7	2.0979	1.2760	20.65
	31 Aug 82	01 16 44	14 14 23	23.1	5.7	2.0998	1.2698	20.26
	01 Aug 82	01 16 26	14 14 22	23.0	5.7	2.1017	1.2638	19.87
44 Nysa	05 Oct 83	02 31 15	08 35 59	38.2	-6.0	2.3448	1.4125	11.42
	06 Oct 83	02 30 39	08 31 00	38.1	-6.0	2.3430	1.4055	10.99
	09 Oct 83	02 28 44	08 15 32	37.5	-6.1	2.3376	1.3859	9.69
	30 Nov 83	01 46 57	04 41 40	26.5	-5.9	2.2465	1.4073	16.75
115 Thyra	13 Jan 83	09 18 43	16 37 16	136.9	0.9	2.2285	1.2969	10.64
	18 Jan 83	09 13 25	16 29 12	135.8	0.4	2.2389	1.2839	8.00
349 Dembowska	01 Jan 83	04 06 42	29 31 36	65.3	8.5	2.7674	1.9076	11.92
	09 Jan 83	04 03 17	29 19 29	64.6	8.4	2.7728	1.9821	14.32
	13 Jan 83	04 02 18	29 13 56	64.3	8.4	2.7757	2.0240	15.38
	18 Jan 83	04 01 45	29 07 52	64.2	8.3	2.7794	2.0801	16.55

second integrations on the object.

Table 3.2 contains the aspect data for each asteroid at 0<sup>h</sup> GMT for all the nights on which it was observed. The comparison stars are listed in Table 3.3 together with the associated asteroid and the range of dates for which it was used.

Table 3.3 Comparison Stars

Ast.	SAO star	R.A.	Dec.	Spectral Type	Year
4	094787	05 39 32	18 57 53	KO	1983
20	109654	01 02 14	06 46 47	F8	1983
29	146687	23 21 36	-06 01 06	G5	1982
	080525	08 53 50	25 12 00	G0	1983
31	092379	01 17 59	13 12 23	KO	1983
39	163259	20 03 08	-14 06 25	F2	1982
	112462	05 06 06	06 25 08	F8	1983
40	188347	19 34 00	-25 11 31	F8	1983
43	092397	01 19 34	14 04 46	G5	1982
44	110609	02 30 36	08 09 30	F8	1983
	110131	01 45 02	04 30 41	G0	1983
115	098504	09 17 15	16 08 59	G5	1983
349	076458	04 03 39	28 47 54	G5	1983

Since most of the asteroids were observed over several nights, it is necessary to correct for changing phase angle ( $\alpha$ ), Sun-asteroid distance ( $r$ ) and Earth-asteroid distance ( $\Delta$ ), all of which affect the apparent magnitude of the asteroid. However, the correction to the magnitude ( $\Delta m$ ) can be calculated from Equation 3.2

$$\Delta m = (|\alpha_j| - |\alpha_k|)\beta - 5\log(r_j\Delta_j/r_k\Delta_k) \quad (3.2)$$

where  $\beta$  = phase coefficient in magnitudes per degree.  $\Delta m$  is the correction which must be applied to observations obtained on night  $j$  in order to reproduce the observed

distances and phase angle encountered on night  $k$ . Strictly, Equation 3.2 can only be used when  $\alpha \geq 8^\circ$ , since most asteroids exhibit an opposition effect at phase angles of less than  $8^\circ$ . In practice, the observations were corrected to the phase angle encountered on the first night that the asteroid was observed, while  $r_k$  and  $\Delta_k$  were set to 1AU., in line with the definition of an asteroid's absolute magnitude.

The lightcurve data were folded with the period reported in TRIAD (Tedesco, 1979), or in Harris and Young (1983). Once the broadband lightcurves have been reduced it is a simple matter to calculate the colour lightcurves. For the simultaneous data, a straight subtraction is performed to acquire B-K and V-J curves. For the quasi-simultaneous, (B-V and J-K) lightcurves, it is necessary to interpolate between adjacent points (in time) for both colours.

Table 3.4 General Asteroid Data.

Ast.	B(1,0)	$\beta$	Period	Amplitudes	Class	Diameter
4	4 <sup>m</sup> 24	0.026	5 <sup>h</sup> 342 or 10.686	0 <sup>m</sup> 10 - 0 <sup>m</sup> 18	U	549km
20	7.59	0.031	8.098	0.17 - 0.27	S	137
29	7.02	0.031	5.390	0.06 - 0.13	S	194
31	7.73	-----	5.531	0.09	C	333
39	7.45	0.027	5.138	0.08 - 0.53	S	164
40	8.17	-----	9.136	0.22 - 0.28	S	121
43	9.02	0.047	5.753	0.13 - 0.66	S	77
44	7.95	0.019	6.421	0.22 - 0.50	E	72
115	8.56	-----	7.244	0.20	S	93
349	7.15	0.027	4.700	0.35 - 0.41	R	145

Absolute calibration of the objects is performed, where possible, by the observation of standard stars. These are then used to calibrate the comparison stars. Obtaining the absolute magnitudes, and hence colours, of the asteroids from

their comparison stars is relatively simple since they were observed at the same air mass and have similar colours. The lightcurves are shown with their maximum brightness set to zero magnitude while the colour curves are shown relative to the mean of all the points plotted. See Appendix A for the unfolded lightcurves.

Finally, Table 3.4 lists lightcurve and general information for each asteroid discussed below. The data were taken from TRIAD (Tedesco, 1979 and Bowell et al. 1979) and also from Degewij et al. (1979). The amplitudes of the lightcurves are listed in Table 3.5.

## RESULTS

### 4 Vesta

Observations of the lightcurve of 4 Vesta are reported in Stephenson (1951), Gehrels (1967), Blanco and Catalano (1979) and references therein. The observed amplitudes are in the range 0.10 - 0.18 mag. There is also some doubt as to whether the rotation period of Vesta is 5.342 hr., with one maximum, or 10.684 hr., with two maxima. Colour variations have been reported by Gehrels (1967) and Catalano and Blanco (1979) who found 4 Vesta to be redder just before maximum light. Degewij et al. (1979) report a change in the polarization of Vesta as it rotates. Colour and polarization changes both tend to favour the shorter period, since one contrasting spot is more likely than two symmetrically placed. In this case the principle cause of the variation in

Table 3.5 Amplitudes of Lightcurves

Asteroid	Maximum	Amplitude			
		B	V	J	K
4	$M_1 - m_1$	0.14±0.02	0.12±0.02	0.13±0.02	0.10±0.01
20	$M_1 - m_1$	0.21±0.02	0.21±0.01	0.24±0.01	0.21±0.01
	$M_2 - m_2$	0.18±0.01	0.16±0.01	0.20±0.02	0.19±0.01
29	$M_1 - m_1$	0.10±0.01	0.09±0.01	-----	-----
	$M_2 - m_2$	0.02±0.01	0.04±0.01	-----	-----
29	$M_1 - m_1$	0.07±0.01	0.07±0.01	0.07±0.02	0.07±0.02
	$M_2 - m_2$	0.03±0.01	0.03±0.01	0.05±0.03	0.03±0.03
31	$M_1 - m_1$	0.13±0.01	0.12±0.02	0.11±0.03	0.10±0.04
	$M_2 - m_2$	0.04±0.01	0.05±0.02	0.07±0.04	0.07±0.04
	$M_3 - m_3$	0.02±0.01	0.02±0.01	-----	-----
39	$M_1 - m_1$	0.15±0.02	0.16±0.02	-----	-----
	$M_2 - m_2$	0.01±0.02	0.03±0.02	-----	-----
39	$M_1 - m_1$	0.26±0.01	0.27±0.02	0.27±0.03	0.27±0.02
	$M_2 - m_2$	0.21±0.01	0.23±0.02	0.23±0.03	0.23±0.02
40	$M_1 - m_1$	-----	0.36±0.02	-----	-----
	$M_2 - m_2$	-----	0.27±0.02	-----	-----
	$M_3 - m_3$	-----	0.07±0.03	-----	-----
43	$M_1 - m_1$	0.37±0.04	0.36±0.04	-----	-----
	$M_2 - m_2$	0.25±0.04	0.24±0.04	-----	-----
44	$M_1 - m_1$	-----	0.43±0.01	-----	-----
	$M_2 - m_2$	-----	0.37±0.01	-----	-----
44	$M_1 - m_1$	0.52±0.01	0.51±0.01	0.56±0.01	0.52±0.01
	$M_2 - m_2$	0.40±0.01	0.39±0.01	0.38±0.01	0.40±0.01
115	$M_1 - m_1$	0.13±0.02	0.13±0.02	0.15±0.05	0.20±0.06
349	$M_1 - m_1$	0.39±0.04	0.39±0.05	0.33±0.05	0.34±0.06
	$M_2 - m_2$	0.24±0.03	0.21±0.04	0.28±0.05	0.29±0.05

the lightcurve must be a change in albedo across the surface of the asteroid.

4 Vesta was observed on three nights during November 1983. Figure 3.3 shows the composite lightcurve folded with the 5-hour period. Maximum light occurred at 03:52:24 GMT on 27 November 1983. The colour curves in Figure 3.3(b-e) show variations; B-V changes by  $0.05 \pm 0.03$ , B-K by  $0.07 \pm 0.03$ , J-K by  $0.06 \pm 0.03$ . The V-J colour does not show any variation greater than the scatter of the data, which is  $\pm 0.02$ . These variations all show Vesta to be bluer at maximum. The colour curves suggest that the surface of Vesta has a uniform V-J colour, but that the B-V, B-K and J-K colours vary across the surface.

A model has been proposed for 4 Vesta (Gaffey, 1983) which has eucrite as the main surface constituent, together with regions of relatively bright diogenite. This model is based on 10-hour (two maxima) period and thus has two regions of diogenite. Gaffey (1976) gives the reflectance spectra of these two minerals. From these spectra and the solar colours given by Johnson et al. (1975) and Allen (1973) it is possible to calculate the colours of the minerals. The resulting ranges of colours for eucrite are: B-V=0.70 - 0.84; B-K=2.16 - 2.50; V-J=1.40 - 1.56 and J-K=-0.27 - +0.10. For diogenite they are: B-V=0.78 - 1.10; B-K=2.04 - 2.40; V-J=1.38 - 1.52 and J-K=-0.40 - -0.13. Thus it is possible to compare the expected colour variations with those observed. The ranges of V-J colours exhibited by eucrite and diogenite samples are very similar. Hence it is not surprising that the

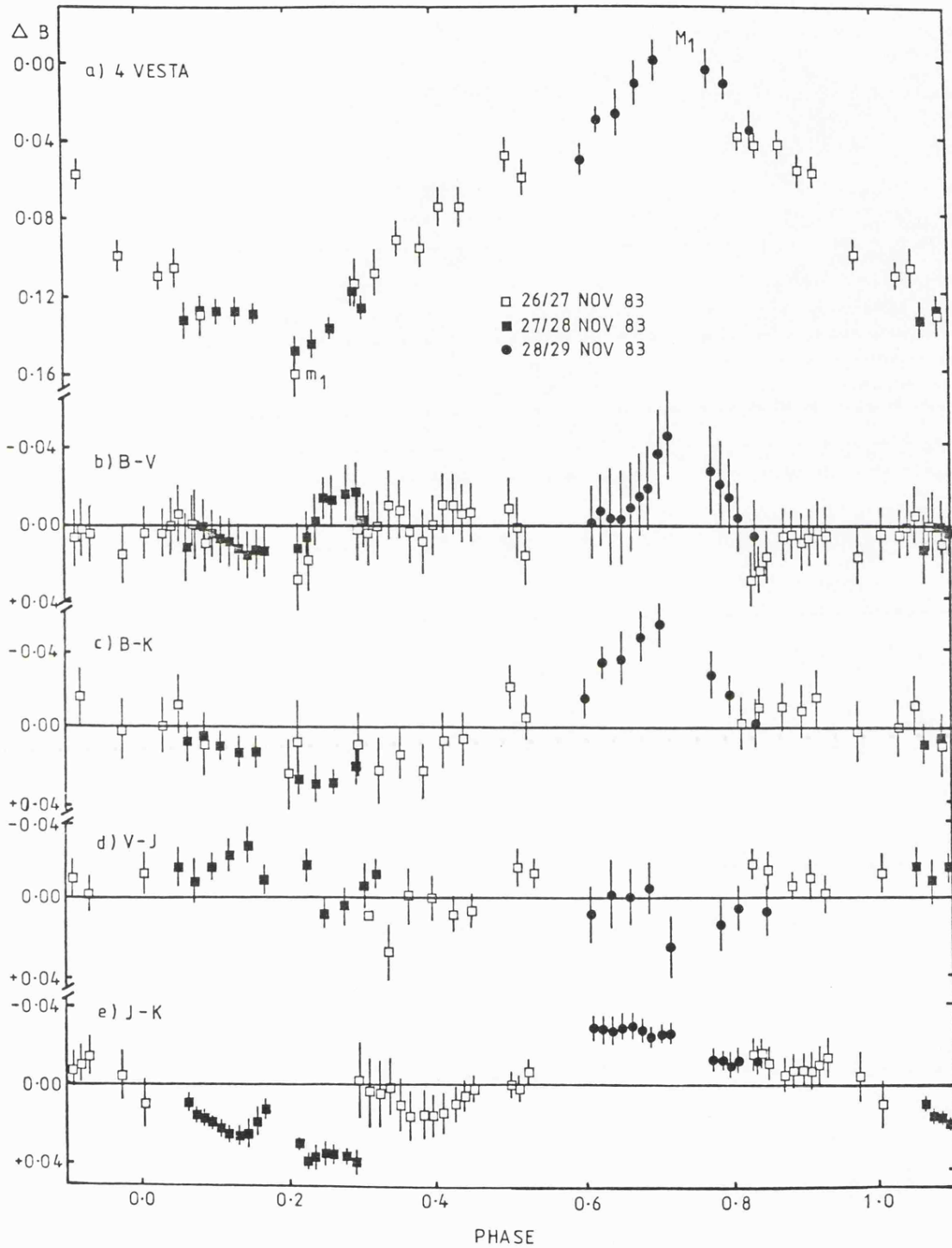


Figure 3.3 a) B lightcurve of the asteroid 4 Vesta. b) B-V colour curve. c) B-K colour curve. d) V-J colour curve. e) J-K colour curve.

V-J colour curve shows no variation; although, by selecting mineral samples from the extremes of the quoted ranges, it would be possible to produce some variation. Both the B-K and J-K ranges for diogenite are bluer than those of eucrite, but there is, nevertheless, a considerable overlap between the colours of the two minerals. From their B-V colours, it would be expected that Vesta should be redder at maximum light, since diogenite is generally redder than the darker eucrite. This tends to support the previous results of Gehrels (1967) and Blanco and Catalano (1979), rather than our observation of a bluer maximum. It should be added, however, that the overlap between the ranges of colours exhibited by eucrite and diogenite are such that a blue maximum is not entirely ruled out by the data. The observed mean colours of 4 Vesta would be expected to lie within the ranges shown by the minerals and this is, indeed, the case. It appears that the model of Vesta as a eucrite surface containing a region (or regions) of diogenite can be used to explain most of the observed properties of the asteroids lightcurve.

#### 20 Massalia

Complete lightcurves of this object have been obtained at four previous oppositions. Gehrels (1956) observed during 1955, when it had two maxima and minima (as do all lightcurves of the asteroid) with amplitudes from  $0^m.17$  to  $0^m.23$ . Observations in 1958 (Gehrels and Owings, 1962) showed 20 Massalia to have an amplitude of  $0^m.24$ . A third set of lightcurves was obtained in 1962 by Chang and Chang (1962). These also had an

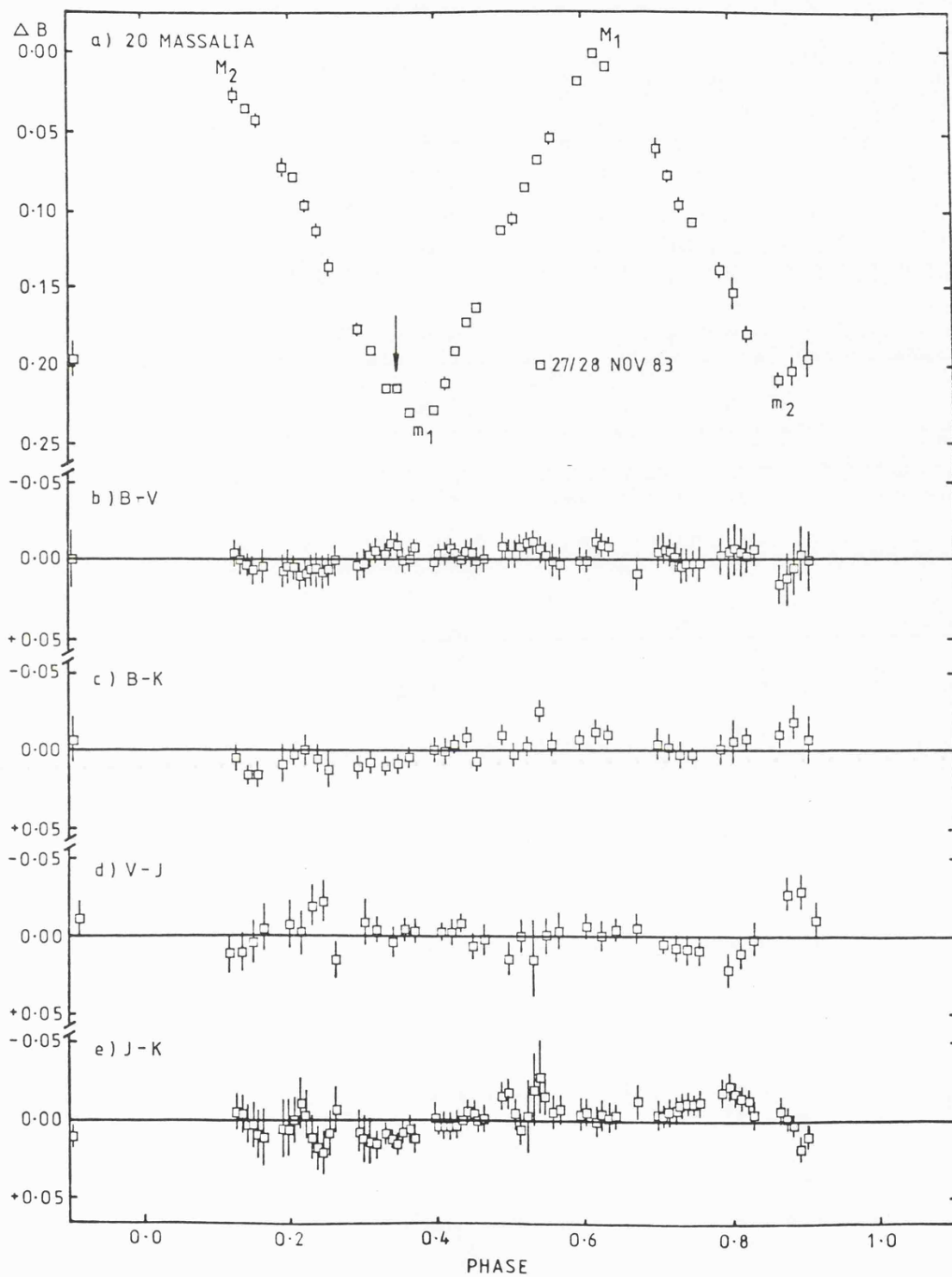


Figure 3.4 Same as Figure 3.3 but for 20 Massalia.

amplitude of  $0^m.24$ . A partial lightcurve is reported by Zhou et al. (1983) while Lupishko et al. (1982) present a complete lightcurve from the 1979 opposition. 20 Massalia has not previously been examined for colour variations.

Figure 3.4 presents data obtained in November 1983. Approximately 80% of the rotation period is covered and shows two minima and one maximum (the other, secondary, maximum occurred prior to the start of data acquisition). Maximum light was observed at 23:30:41 GMT on the 27 November 1983. Like previous lightcurves of 20 Massalia the B lightcurve in Figure 3.4 is generally smooth. However there is a point in the lightcurve (indicated by the arrow in Figure 3.4) which is slightly higher than the general trend of the lightcurve (it was also high in the V, J and K lightcurves). Detailed comparison of this latest lightcurve with earlier data shows that the 1955 and 1962 lightcurve also have a feature at a similar position. This would suggest that the deviation from the smooth curve is real and is probably caused by the surface morphology of the asteroid.

Figure 3.4(b-e) shows the B-V, B-K, V-J and J-K colour curves, none of which exhibit variations greater than the scatter of the data, which is  $\pm 0^m.01$ . This would indicate that the surface of 20 Massalia is of a uniform composition.

### 29 Amphitrite

The lightcurves of 29 Amphitrite can change considerably from one opposition to the next and are complex,

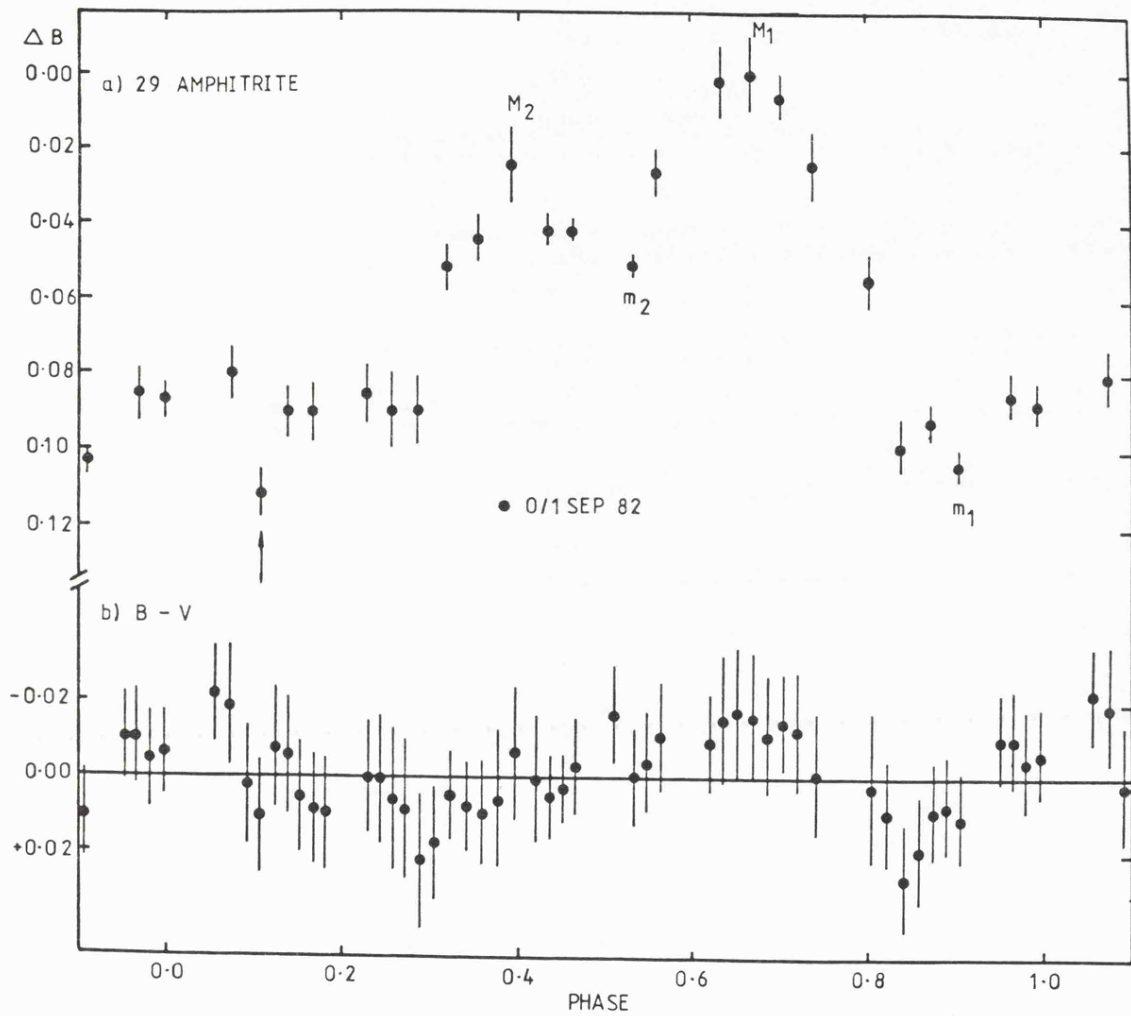


Figure 3.5 a) B lightcurve for 29 Amphitrite (1982 opposition). b) B-V colour curve.

with the number of maxima varying from one (1972) to five (1970) and exhibiting amplitudes in the range 0.06 - 0.13 mag. These lightcurves are reported in Tedesco and Sather (1981 and references therein). 29 Amphrite has previously been searched for a colour variation in V-I (Degiwij et al., 1979); no variation  $>0.01$  mag. was detected.

29 Amphrite was observed at two oppositions: August 1982 and November 1983. The first of these B lightcurves is shown in Figure 3.5 together with a B-V colour curve. Figure 3.6 shows the B lightcurve from the latter opposition accompanied by optical and near-infrared colour curves. The first lightcurve shows two peaks separated by approximately 0.3 in phase. The maximum  $M_1$  occurred at 03:19:32 GMT on the 1 Sep 1982, (uncorrected for light travel time). The B-V curve does not show any significant deviation from the mean. The second lightcurve also shows two maxima, but they have shifted with respect to each other and are now separated by nearly half a period. It should be noted that the labelling of the extrema,  $M_1$ ,  $m_2$  etc. is applied so that  $M_1 - m_1$  is the maximum amplitude of the lightcurve; thus the minimum identified as  $m_1$  in Figure 3.5 is not the same physical minimum identified as  $m_1$  in Figure 3.6. None of the four colour curves exhibit any variation greater than the scatter of the data ( $\pm 0.02$  for V-J and  $\pm 0.01$  for the others). The lack of any colour variations at both oppositions indicates that the composition of 29 Amphrite is uniform to within the limits of the measurements.

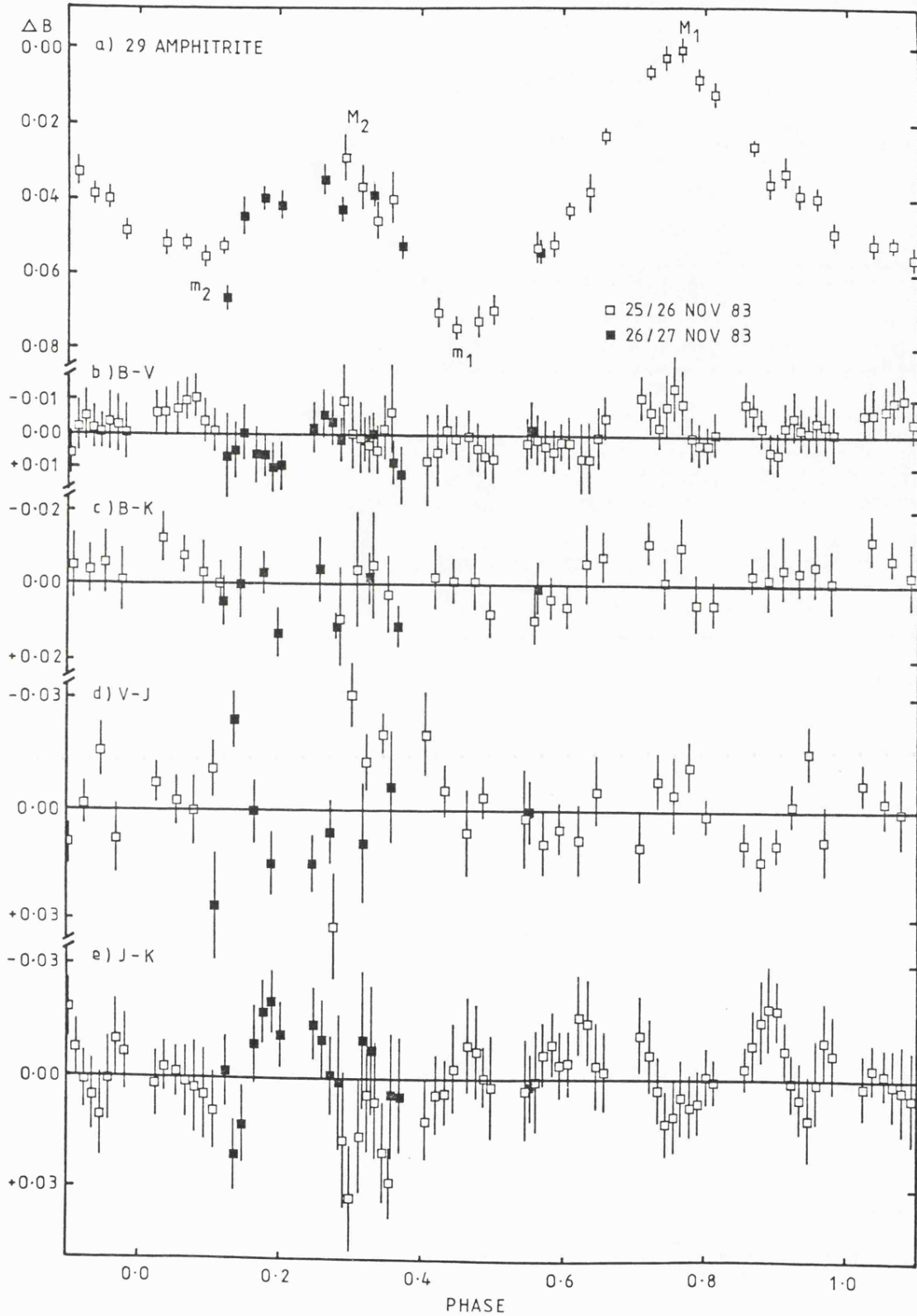


Figure 3.6 Same as Figure 3.3 but for 29 Amphitrite (1983 opposition)

### 31 Euphrosyne

Schober et al. (1980) is the only published paper dealing with the lightcurves of this asteroid. The reported lightcurves were obtained at two oppositions, in 1977 and 1978, and all had an amplitude of 0.08 mag. with two maxima and minima. 31 Euphrosyne has not previously been searched for the presence of colour variations.

The B lightcurve and the four colour curves are shown in Figure 3.7. These data were obtained in November 1983, observing from Tenerife. The lightcurve exhibits three maxima, although the tertiary amplitude is small. The infrared lightcurves did not show this third peak, but such a small maximum could have been hidden by the larger scatter in the data at these wavelengths. Details of the amplitudes are listed in Table 3.5. Maximum light was observed at 19:43:55 GMT on 24 November 1982. In correcting for the different phase angles encountered on the two nights when this object was observed, a phase coefficient of 0.025 mag/deg. was assumed since no value has been reported in the literature. The J-K colour curve does not show any variation beyond the scatter of the data,  $\pm 0.02$  mag. The other three colour curves all show 31 Euphrosyne to be slightly redder at phases 0.7 - 0.2, corresponding to the region of minimum light. The variation is  $0.04 \pm 0.03$  in B-V,  $0.05 \pm 0.03$  in B-K and  $0.05 \pm 0.03$  in V-J.

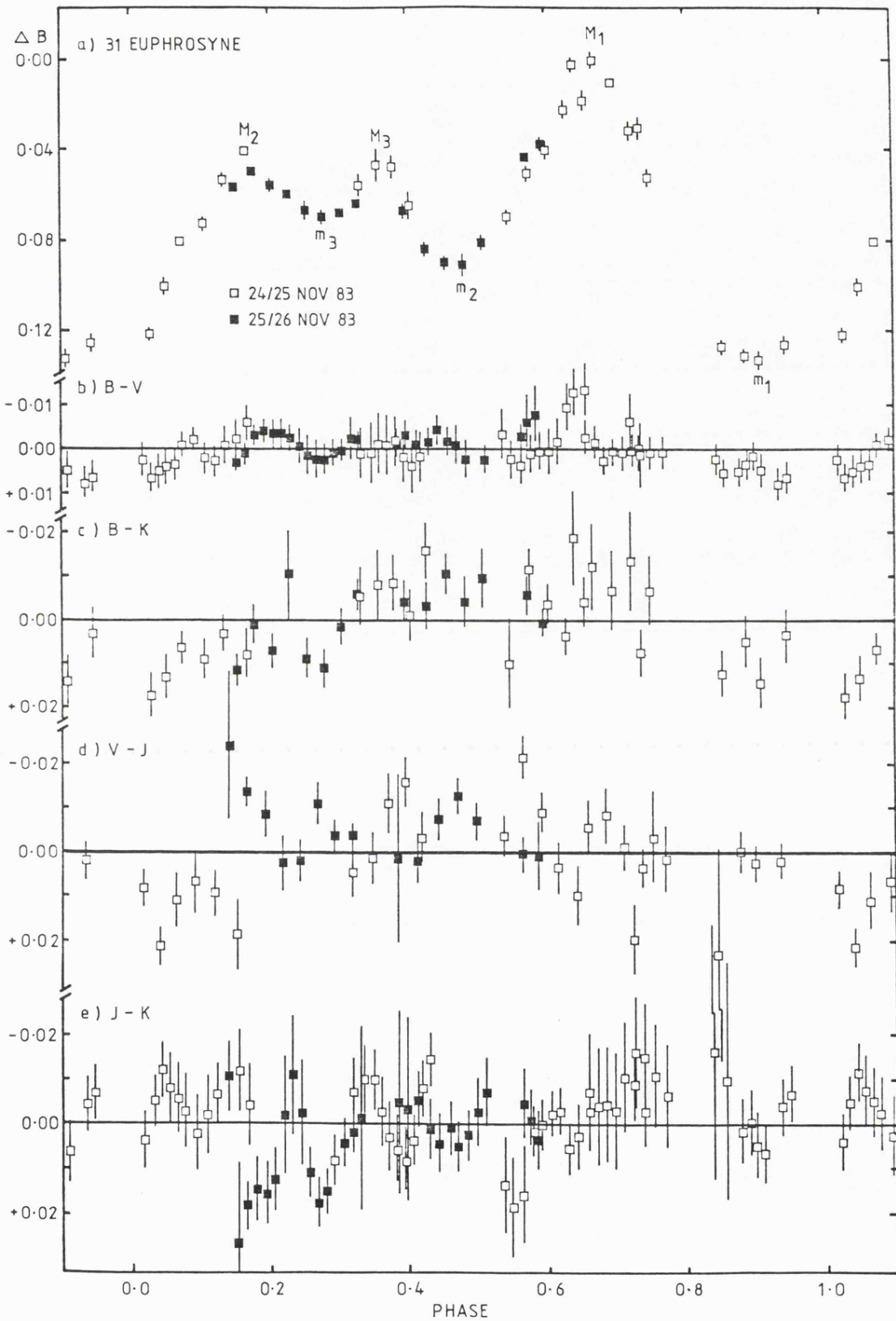


Figure 3.7 Same as Figure 3.3 but for 31 Euphrosyne.

### 39 Laetitia

39 Laetitia has one of the most extensively observed lightcurves. Observations have been published by Groeneveld and Kuiper (1954a,b), van Houten-Groeneveld and van Houten (1958), Gehrels and Owings (1962), Yang et al. (1965), Wamsteker and Sather (1974) and Sather (1976). The lightcurves are generally smooth, double peaked and have amplitudes in the range 0.15 to 0.54 mag. This asteroid has been searched for colour variations on several occasions (Degiwiij et al., 1979), but only Wamsteker and Sather (1974) report any variation, with V-U being slightly bluer at both maxima.

Two lightcurves were obtained, the first in August 1982 and the second in November 1983. Figure 3.8 shows the earlier of these curves. This lightcurve was obtained at similar aspect and phase angles as that of 1-2 August 1968 (Wamsteker and Sather, 1974). Both of these lightcurves show a small feature (indicated by an arrow in Figure 3.8) suggesting that it is real. Maximum light was observed at 23:45:30 GMT on 30 August 1982. The B-V plot in Figure 3.8 appears to be bluer at the secondary maximum by  $0.04 \pm 0.03$  mag. as compared with the region preceding primary maximum. The second lightcurve (Figure 3.9) has a larger amplitude with a more pronounced secondary peak.  $M_1$  occurred at 23:18:37 GMT on 23 November 1983. None of the accompanying colour curves show any variation greater than the scatter of data ( $\pm 0.01$  for B-V,  $\pm 0.02$  for B-K and  $\pm 0.03$  for V-J and J-K).

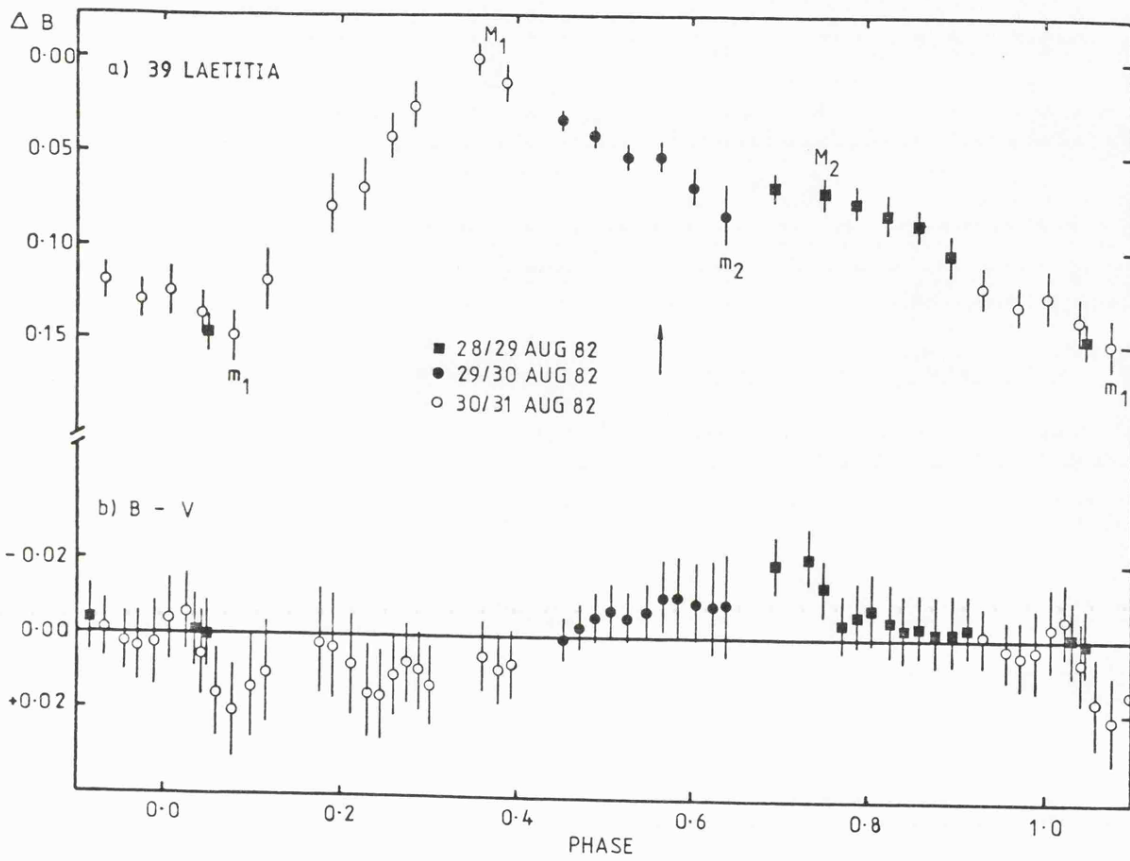


Figure 3.8 Same as Figure 3.5 but for 39 Laetitia (1982 opposition).

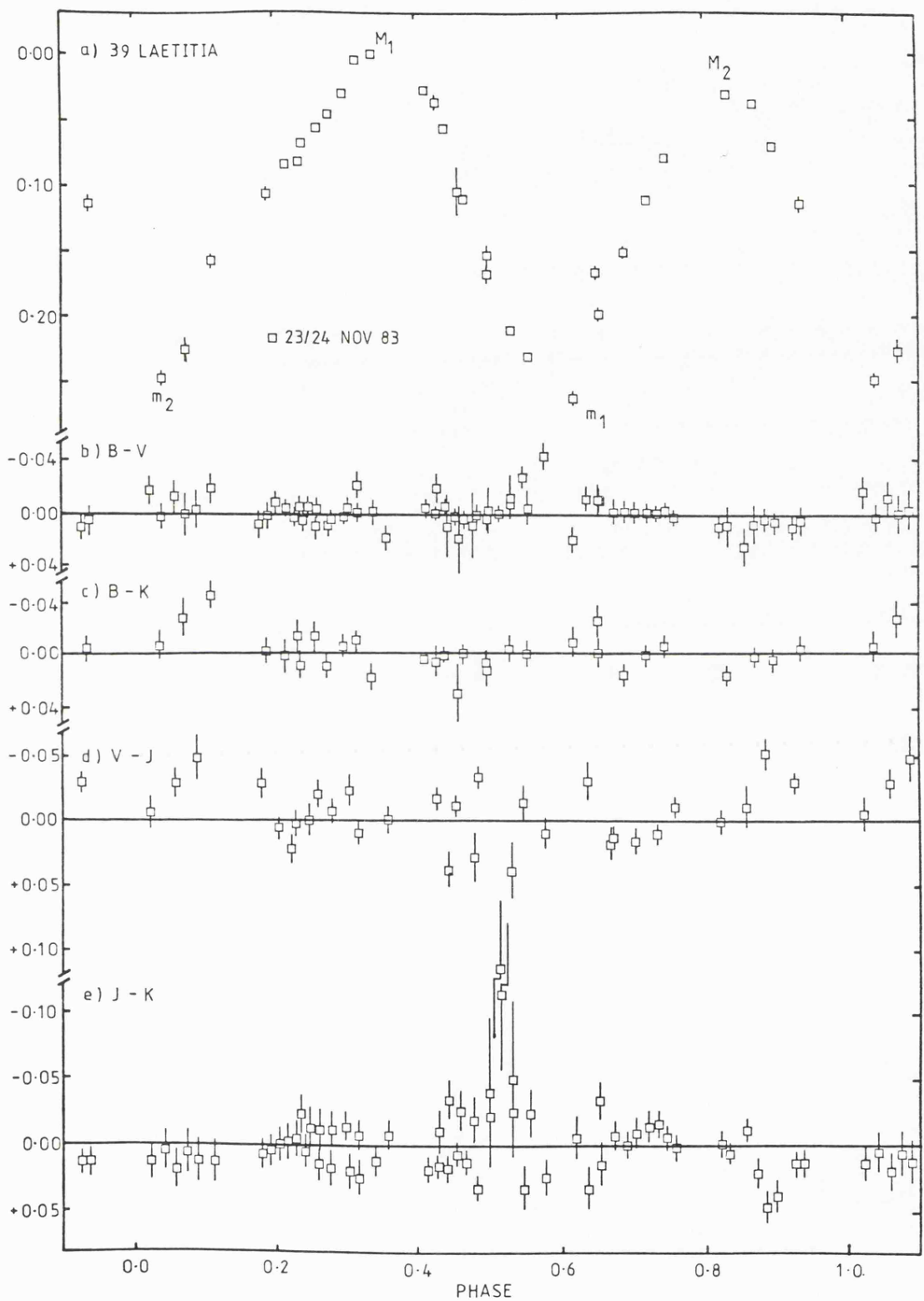


Figure 3.9 Same as Figure 3.3 but for 39 Laetitia (1983 opposition).

It is interesting to note that both of the detections of colour variations have occurred when 39 Laetitia has been at ecliptic longitudes around  $290^\circ$  and when the amplitudes of the lightcurves have been at the lower end of the range exhibited by the asteroid. The small amplitudes indicate that the asteroid is being viewed close to pole-on and the similar longitudes mean that it is the same pole which is observed. If the region responsible for the colour change was situated close to this pole, then the variation would be smaller (and thus possibly below the detection threshold) when the aspect angle is around  $90^\circ$  (maximum lightcurve amplitude). It would not be visible when viewing the other pole (ie. when the asteroid is at ecliptic longitudes of approximately  $100^\circ$ ). This could explain the lack of detectable colour variations other than at longitudes around  $290^\circ$ . Thus it appears that the surface of 39 Laetitia is not homogeneous, but has a region with different optical colours situated close to one pole of the rotation axis.

#### 40 Harmonia

The first lightcurve of this asteroid was published by Gehrels and Owings (1962) who observed an amplitude of 0.22 mag. and displayed two peaks. The secondary maximum had a couple of features on its rising side. Lagerkvist (1978) obtained a partial photographic lightcurve with an amplitude of 0.28 mag., but it is not possible to tell whether this was the primary or secondary amplitude.

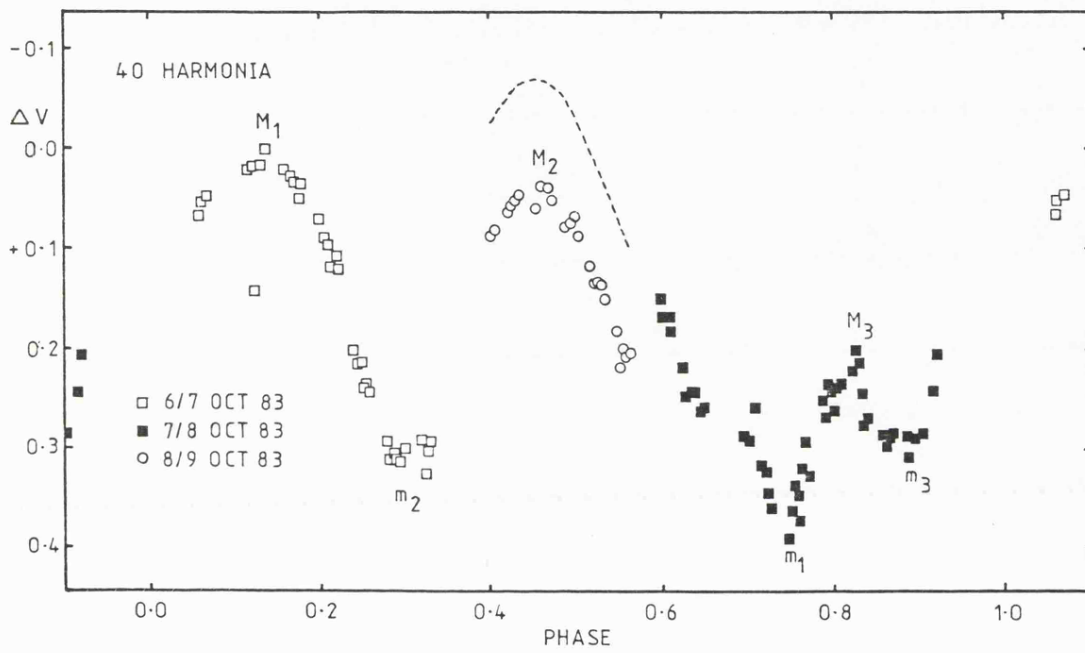


Figure 3.10 V lightcurve of 40 Harmonia.

40 Harmonia was observed on three nights in October 1983 using the 20-inch telescope at SAAO. Only a V lightcurve was obtained, Figure 3.10. The data show two main peaks with a large feature, which could be considered a third peak, just after the minimum  $m_1$ . None of the data obtained on different nights overlap, so it is not possible to check on the phase and distance corrections applied. There appears to be a discontinuity between the data at a phase of 0.55. The fault, if any, probably lies with the data of 8/9 October 1983, since data on another asteroid (44 Nysa) obtained on the same night did not match up correctly either. If the slopes on either side of the discontinuity are used to shift this portion to brighter magnitudes then the peak labelled as  $M_2$  in Figure 3.10 is, in fact, the primary maximum. The adjusted position of the data is indicated by the dashed curve in Figure 3.10. In this case the primary amplitude would be 0.49 mag. and the secondary 0.29 mag. The maximum labelled as  $M_1$  was observed at 19:29:18 on 6 October 1983, while  $M_2$  occurred at 20:07:07 GMT on 8 October 1983.

#### 43 Ariadne

Lightcurves of this asteroid have previously been obtained during two oppositions, in 1965 (van Houten-Groeneveld et al., 1979) and in 1972 (Burchi and Milano, 1974). At both oppositions the lightcurves exhibited two maxima and minima but with completely different amplitudes: 0.13 mag. at the earlier opposition and around 0.64 mag. in 1972. The lightcurve presented here was obtained in August 1982. A lightcurve obtained by Zappalà (Di Martino and

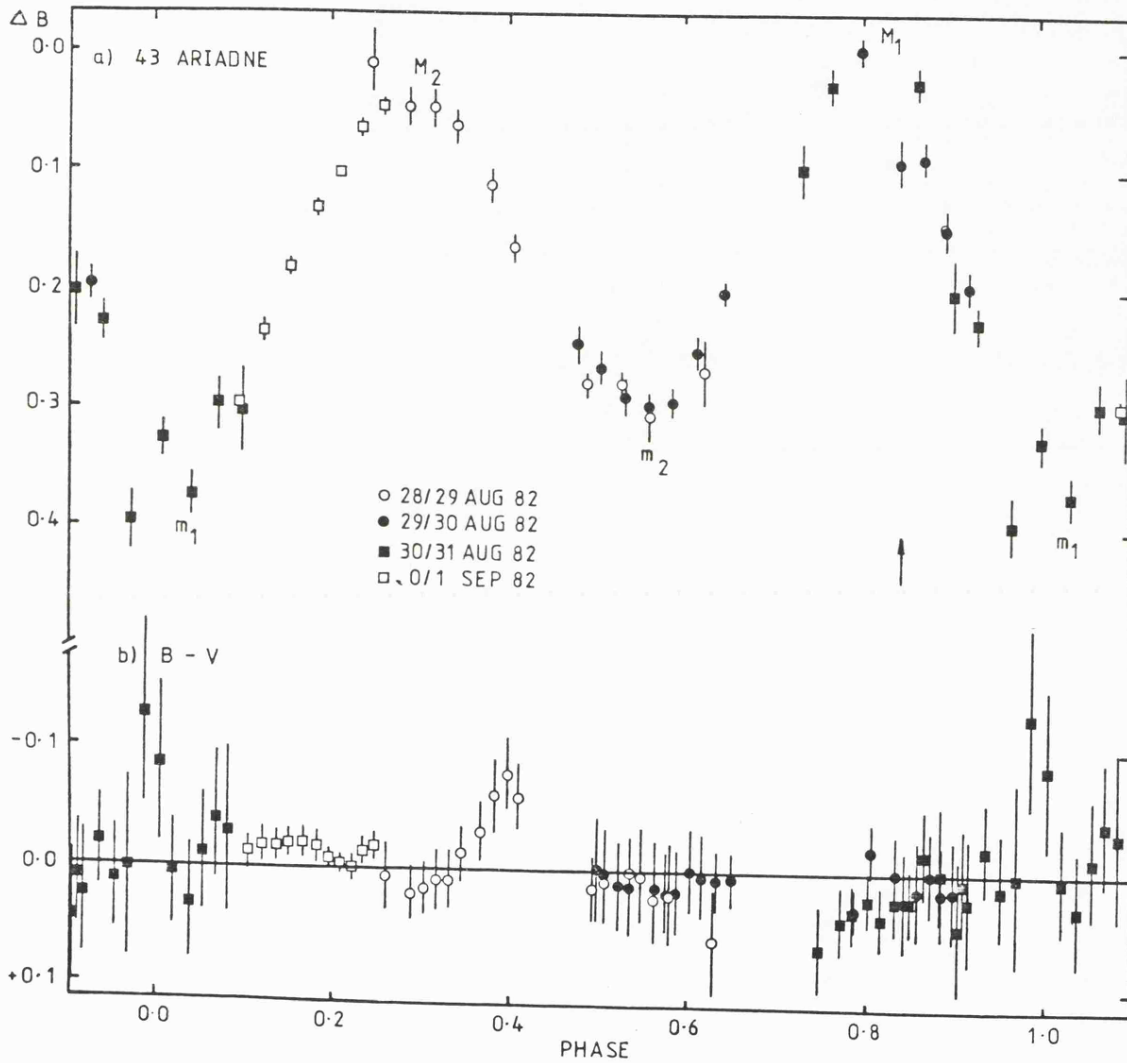


Figure 3.11 Same as Figure 3.5 but for 43 Ariadne.

Cacciatori, 1984) in October 1982 has a amplitude of 0.31 mag. and also has two maxima and minima.

Since the data were obtained in small sections on five consecutive nights, it was not possible to calculate the period directly. However, folding the data with a period of 5.7506 hours produced a reasonably complete lightcurve (after corrections for changing distances and phase angles, with  $\beta=0.047$  mag/deg, using Equation 3.2). The resulting B lightcurve is depicted in Figure 3.11a. The arrow indicates a possible feature which appeared in both the B and V data. Burchi and Milano (1974) also observed a small feature which repeated in several lightcurves, but was at a different phase and aspect to that reported here. Generally, 43 Ariadne's lightcurves are smooth. Figure 3.11b shows the B-V lightcurve. There are no significant deviations from the mean value of B-V, indicating that, to within the limits of the measurements, 43 Ariadne has uniform surface properties. 43 Ariadne had not previously been searched for possible colour variations.

#### 44 NYSA

The lightcurve of 44 Nysa has been extensively observed and is reported in Shatzel (1954), Groeneveld and Kuiper (1954b), Chang and Chang (1962), Gehrels and Owings (1962), Yang et al. (1965), Zappalà and van Houten-Groeneveld (1979), Birch et al. (1983) and Taylor and Tedesco (1983). All the lightcurves have two maxima and minima. Although the asteroid has not been examined for colour variation, Degewij et al.

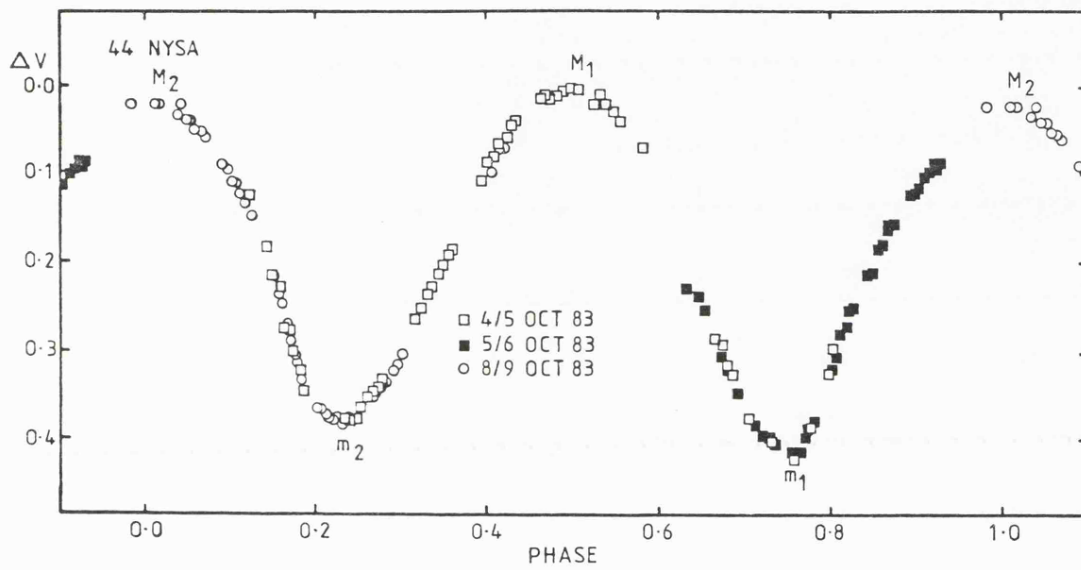


Figure 3.12 V lightcurve of 44 Nysa.

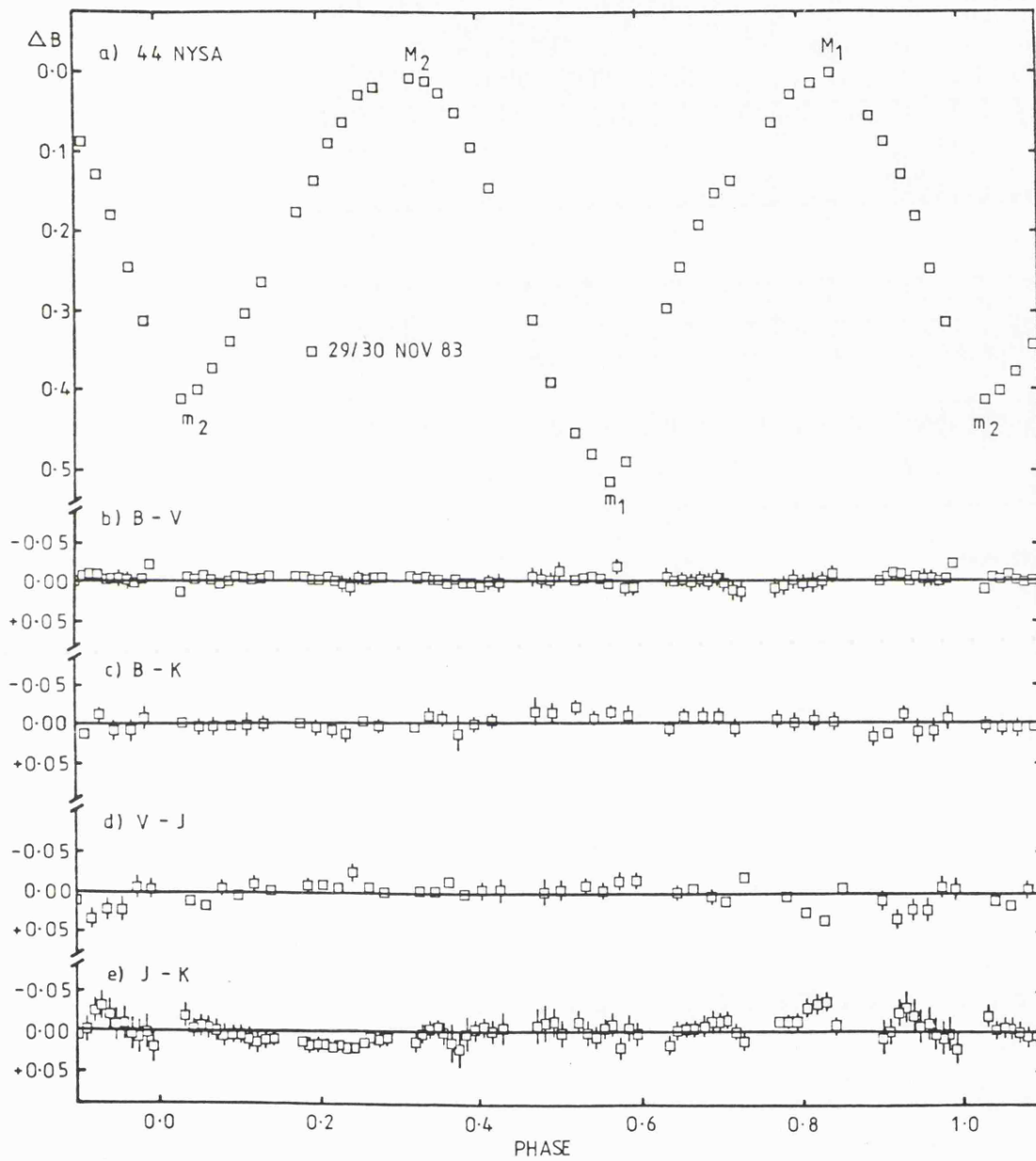


Figure 3.13 Same as Figure 3.3 but for 44 Nysa.

(1979) report that no change in the polarization was detected which was greater than the scatter of the data.

Lightcurves were obtained on two occasions during 1983. A V lightcurve was obtained in October (Figure 3.12) and BVJK lightcurves in November (Figure 3.13). Both lightcurves are typical for the asteroid. It was found that the data from the night of 8/9 October in Figure 3.12 did not align correctly with the other data, but were too bright by 0.04 mag. The data are shown reduced by this amount in Figure 3.12. Accompanying the B lightcurve in Figure 3.13 are the four colour curves, none of which show significant variations greater than the scatter of the data (which is  $\pm 0.01$  in all cases).

#### 115 Thyra

This asteroid's lightcurve has only previously been observed in 1978 by Scaltriti and Zappalà (1981) and Chang et al. (1981); the latter reference only presents a partial lightcurve. The complete lightcurve had an amplitude of 0.20 mag. and displayed the typical shape of two maxima and minima. No previous searches for colour variation have been conducted.

The composite B lightcurve is presented in Figure 3.14 and was obtained from Tenerife on two nights in January 1983. The lightcurve is only 80% complete. The data on either side of the missing portion indicate that one of the maxima is absent, although it is not possible to determine whether it

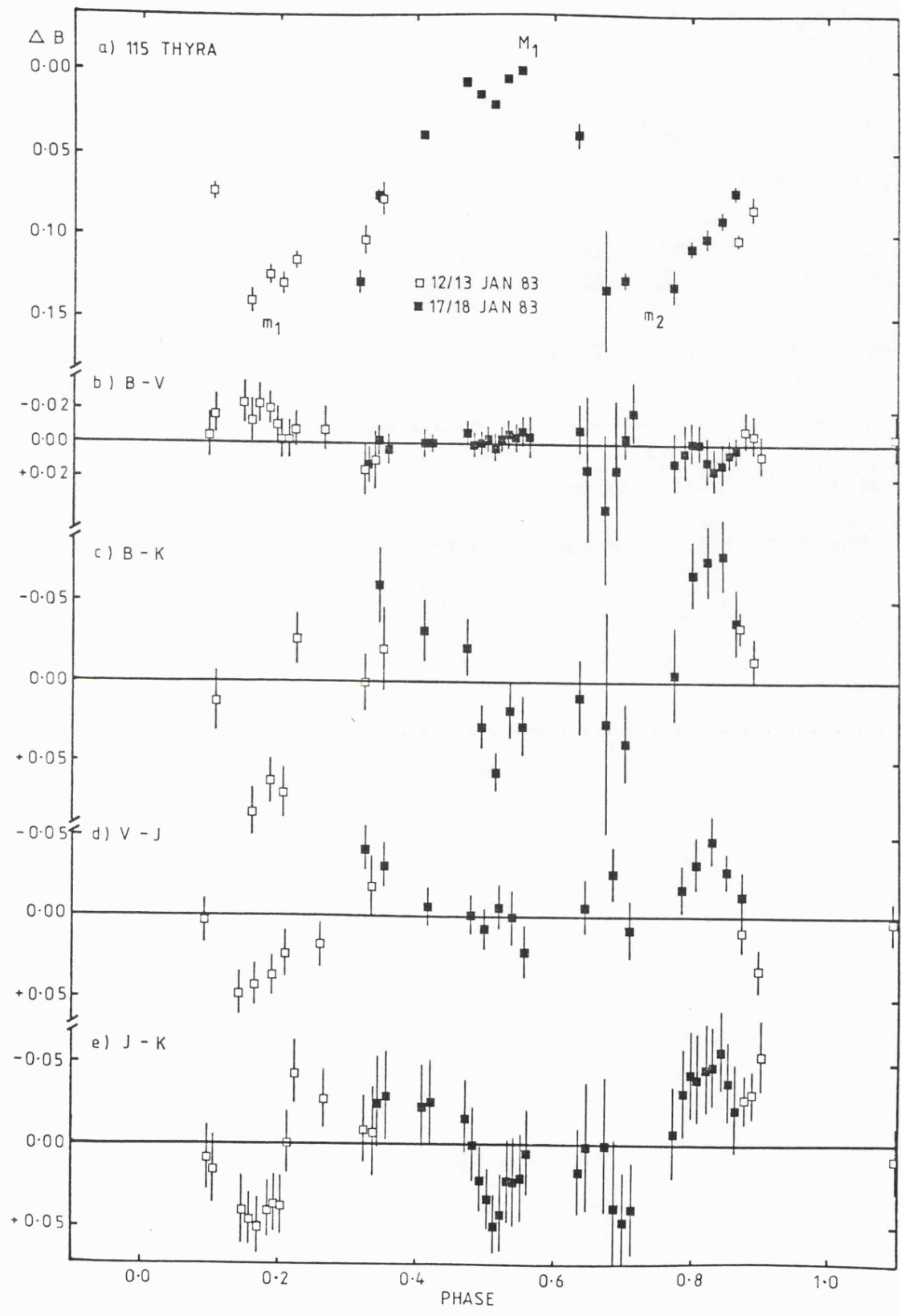


Figure 3.14 Same as Figure 3.3 but for 115 Thyra.

is the primary or secondary. Maximum light was observed at 4:15:11 GMT on 18 January 1983. The phase coefficient could only be estimated from the small overlap between the two nights (there are no published values for  $\beta$ ). It was found that a phase coefficient of 0.03 mag/deg. was suitable in all four wavebands.

The colour curves are also shown in Figure 3.14. B-K, V-J and J-K all show a change in colour with amplitudes of  $0.12 \pm 0.04$ ,  $0.06 \pm 0.03$  and  $0.07 \pm 0.03$  mag. respectively. These colour curves are all redder at  $m_1$  and bluer after  $m_2$ . The B-V curve appears to show a much smaller variation, which is anti-correlated with that of the other curves (ie. bluer at  $m_1$  and redder after  $m_2$ ). The amplitude of this variation is  $0.03 \pm 0.02$  mag. The amplitude of the colour variation increases with increasing wavelength base. This can be explained by a change in the slope of the spectrum across the surface of the asteroid. The change in slope in the B-V region would have to be in the opposite direction to that at longer wavelengths in order to account for the observed behaviour of the colour variations. Thus, it appears, that 115 Thyra has an inhomogeneous surface composition.

#### 349 Dembowska

Remarkably, this unusual asteroid has only had its lightcurve observed during three oppositions: in 1962 by Chang and Chang (1963); in 1965 by Zappalà et al. (1979) and in 1977 by Haupt (1980). The 1965 observations enabled an amplitude-phase coefficient (see Chapter 4) of 0.005 mag/deg.

to be determined;  $\beta_V$  was determined as 0.023 mag/deg. All the lightcurves are typical in that they have two peaks. The overall amplitudes lie in the range 0.31 - 0.41 mag. Degewij et al. (1979) report observations which found 349 Dembowska to be redder at primary maximum by 0.04 mag. in U-I, smaller variations were found when a shorter wavelength base was used.

The lightcurves of 349 Dembowska in Figure 3.15 were obtained in January 1983 at the Observatorio del Teide, Tenerife. The resulting folded lightcurve has the same general appearance as the earlier data. However in order for the data from different nights to overlap and join up correctly, the phase coefficient quoted above was found insufficient to account for the change in magnitude observed from night to night. The following values were required to align the lightcurve correctly:

$$\beta_B = 0.048 \pm 0.05 \text{ mag/deg.} \quad \beta_J = 0.032$$

$$\beta_V = 0.056 \quad \beta_K = 0.031$$

These values of  $\beta_B$  and  $\beta_V$  are very large. It should be emphasized that they are based on a small number of points over a small range of phase angles (12 - 17°) and could thus be unreliable when extended to different phase angles.  $\beta_J$  and  $\beta_K$  are close to the optical coefficients already published. Maximum light was observed at 00:08:07 GMT on 13 January 1983.

The colour curves in Figure 3.15 do not show any significant variations greater than the scatter of the data:  $\pm 0.02$  for B-V,  $\pm 0.04$  for B-K and  $\pm 0.03$  for V-J and J-K. The

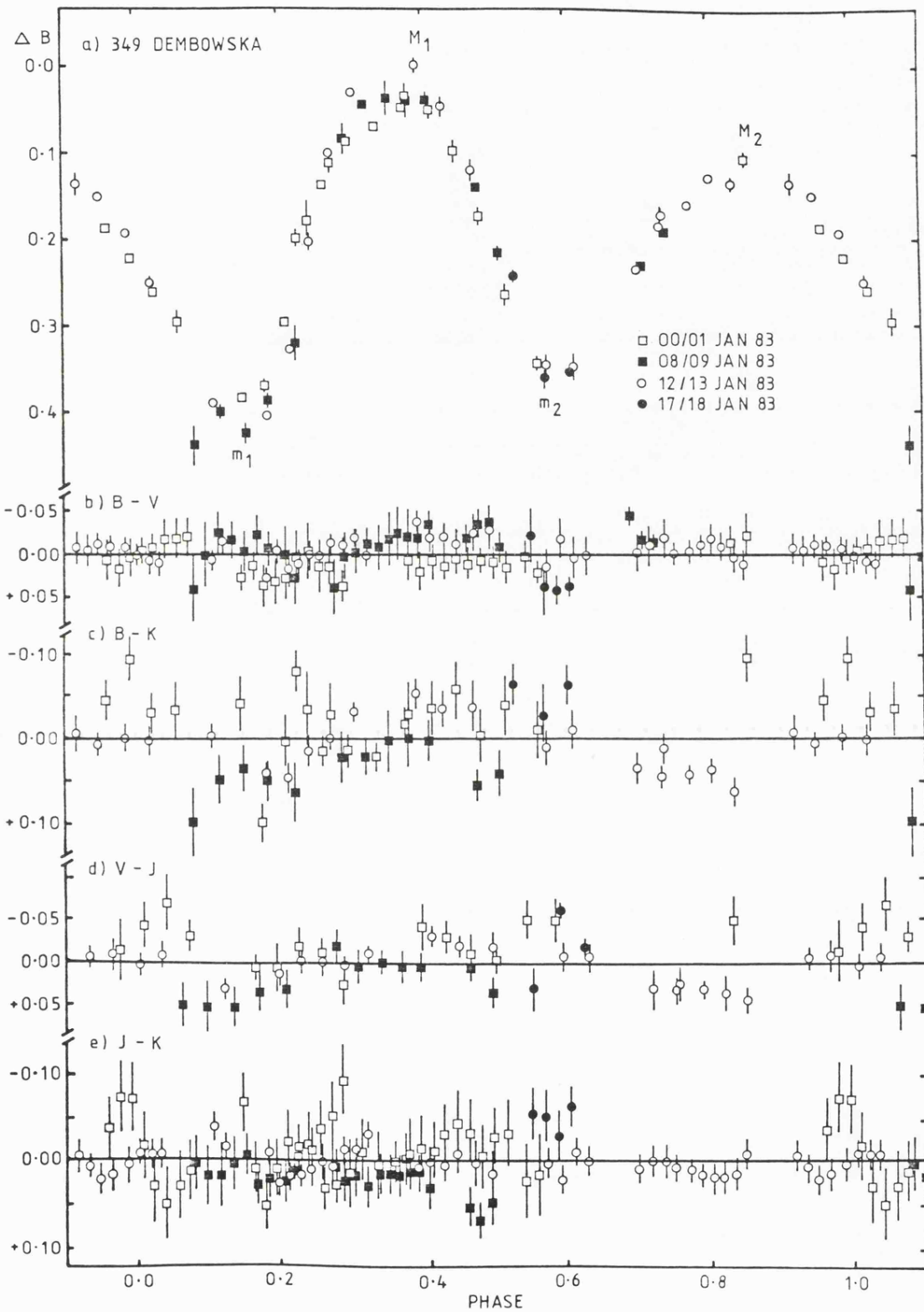


Figure 3.15 Same as Figure 3.3 but for 349 Dembowska.

dependence of the phase coefficient on wavelength was taken into account when correcting the colour curves for changing phase angles. This had the effect of reducing the scatter of the data.

## DISCUSSION

Lightcurves were obtained for a total of ten asteroids, of which two were observed at two oppositions. With one exception, 40 Harmonia, simultaneous colour curves were also obtained. Colour variations were detected for four of these asteroids (4, 31, 39 and 115). The amplitudes of the variations generally tend to increase as the wavelength base of the colour increases.

39 Laetitia was seen to vary in B-V at one opposition, but not at the other. This behaviour can be explained by the different aspects encountered at the two oppositions (see Chapter 4). This effect could also explain the discrepancy between the non-detection of variation in 349 Dembowska, while Degewij et al. (1979) report observing variations in the colour curves; but at present there is insufficient data to estimate the orientation of the axis of rotation and thus calculate the aspect angle.

The colour curves presented here, when combined with those listed in Schober and Scholl (1982), bring the total number of asteroids examined for colour variations to 53, of which, 12 have had variations detected. The majority of these asteroids have only been examined at one opposition, so it

is possible that this proportion may increase if they are observed at another opposition (see 39 Laetitia above). Based on this small sample, it appears that approximately 1 in 4 asteroids exhibit colour variations. However, it is not possible to analyse the data for correlations with diameter or class because of the small sample size. There does not appear to be any tendency for the colour curves to be systematically redder (or bluer) at maximum light. This indicates the existence of different combinations of surface mineralogies: a deduction supported by the infrared data, since the infrared colour variations also differ from one asteroid to the next.

Although broadband photometry does not permit a detailed analysis of the surface composition, it can serve a useful purpose by indicating which asteroids exhibit colour variations. These become targets for spectroscopic lightcurves which can provide the necessary information for a detailed analysis. Photometry can also be used to check a model, which has been developed on the basis of optical spectra, at other wavelengths.

**CHAPTER 4**

**SHAPES AND**

**POLE ORIENTATIONS**

## INTRODUCTION

Various methods to determine the orientation of the pole, sidereal period and sense of rotation of an asteroid have been devised. A summary of several of these methods is given by Vesely (1971). There are two basic techniques; photometric astrometry and magnitude-amplitude-longitude relations, the method used in this Chapter falls into this second category.

The basis of photometric astrometry is that the observed synodic period of an asteroid is longer than the sidereal period when the longitude of the asteroid, as seen from the Earth, is increasing and the asteroid's rotation is prograde. The ideal input data in several lightcurve from one opposition, to enable the synodic period to be determined, and at least one good lightcurve from each of several other oppositions. This method is described in detail by Taylor (1979) with refinements to the technique by Taylor and Tedesco (1983). The results of applying photometric astrometry to an asteroids lightcurves are the sidereal period, pole orientation and sense of rotation. Like magnitude-amplitude-longitude relations photometric astrometry also produces two ambiguous solutions to the pole orientation. These solutions have similar ecliptic latitudes but their longitudes differ by approximately  $180^\circ$ .

Sather (1976) used unit distance magnitudes,  $V(1, \alpha)$  and phase angles to determine the pole position and shape of

39 Laetitia. Various pole positions and axial ratios were assumed for the asteroid and the  $V(1,\alpha)$  magnitudes corrected to an aspect of  $90^\circ$ . The adopted solutions were those that resulted in the least scatter of the magnitude vs. phase angle from a straight line. An infrared technique described by Matson (1971) and Morrison (1977) uses the temperature difference between the "morning" and "afternoon" sides of an asteroid to determine the sense of rotation. This technique has not been applied to many asteroids since the results are less than definitive. The overall shape of the asteroid as well as the pole orientation can be found from the amplitude-longitude relations detailed by Zappalà (1981). This is the method used in this Chapter and is described in detail below.

The distribution of asteroid poles conveys information concerning the evolution of these solar system objects. If, as is believed, the asteroids are collisionally evolved (i.e. have undergone many collisions), then the poles would be expected to have random orientations and be evenly distributed across the sky. If this is not the case, then a significant number should retain their original pole positions, which may either be randomly distributed, or may all point to one region of the sky. This last case would offer the possibility of identifying "unevolved" asteroids.

The next section describes the amplitude-longitude method used to determine the shape and pole position of 20 Massalia, 29 Amphitrite, 31 Euphrosyne, 39 Laetitia, 43 Ariadne and 44 Nysa. The assumptions of the technique are discussed. The lightcurves presented in Chapter 3 have

enabled the pole orientation to be determined for 31 and 43 for the first time. Thus, although lightcurves of these objects have been observed on previous occasions the additional lightcurve has made possible the calculation of the spin axis orientation and the axial ratios. Only 29, 39 and 44 have previously had their overall shape determined. The results section also contains a discussion of the behaviour of the lightcurve of 4 Vesta in terms of albedo changes across its surface. An examination of the errors of the results and comments on the distribution of the pole positions conclude the Chapter.

#### AMPLITUDE-LONGITUDE RELATION

The method employed here to determine the orientation of the rotation axis and shape of an asteroid is the amplitude-longitude relation detailed by Zappalà (1981). The advantages of this method over photometric astrometry are twofold: firstly, it generally requires fewer lightcurves in order to obtain a result and, secondly, it also yields estimates of the shape of the asteroid. Naturally, the method also has disadvantages, in that the amplitude of a lightcurve, in many cases, can depend on the phase angle and that assumptions concerning the surface properties of the asteroid are required.

The assumptions used to derive Equation 4.1 are that:

1. The asteroid is a triaxial ellipsoid, with semi-axes  $a > b > c$ .

2. It is rotating about the shortest axis, which is set equal to unity.
3. The asteroid is at opposition.
4. The amount of reflected light is proportional to the cross-sectional area.
5. The asteroid is neither precessing nor rotating about three or more axes (tumbling).

The amplitude (A) of the lightcurve, in magnitudes, is then given by (Zappala, 1981)

$$A = 2.5 \log(ad/bd') \quad (4.1)$$

with

$$d = [b^2 \cos^2(\xi) + \sin^2(\xi)]^{0.5}$$

$$d' = [a^2 \cos^2(\xi) + \sin^2(\xi)]^{0.5}$$

and where

$$\cos(\xi) = -[\cos\beta\cos\beta_0 + \sin\beta\sin\beta_0\cos(\lambda-\lambda_0)]$$

where  $\lambda_0, \beta_0$  are the ecliptic coordinates of the pointing of the rotation axis;  $\lambda, \beta$  are the ecliptic coordinates of the asteroid and  $\xi$  is then the aspect angle (angle between the line of sight and the direction to the pole). The maximum amplitude occurs when  $\xi=90^\circ$ , in this case

$$A = 2.5 \log(a/b) \quad (4.2)$$

A solution to the pole position and shape is found by varying the values of the parameters  $\lambda_0, \beta_0, a$  and  $b$  to minimise the sum of the squares of the difference between the observed amplitude and the calculated amplitude. This method

cannot distinguish between prograde and retrograde rotation, and also it cannot distinguish between poles which have the same latitude but whose longitudes differ by  $180^\circ$ . Thus a total of four solutions to the pole position are found. Generally, only the northern ecliptic solutions will be quoted.

A lightcurve produced by a rotating ellipsoid will exhibit two maxima of equal magnitudes separated by half a rotation period. Most asteroids for which lightcurves have been obtained have two maxima, although they are usually of differing sizes and not exactly half a period apart. Some asteroids have lightcurves which show either only one, or more than two, peaks, while a few (eg. 29 Amphitrite) have a variable number of maxima. Clearly, these asteroids are not simple triaxial ellipsoids. The method should give a first estimate of the overall shape of the body, although the errors in the various parameters for these asteroids will undoubtedly be larger.

The minimum energy state for a body which has a fixed angular momentum is when the angular momentum vector is aligned with the axis of maximum moment of inertia (ie. the shortest axis). However, collisions with other asteroids will change this alignment. A damping mechanism is then required to realign the rotation axis with the shortest axis. This mechanism is believed to be internal friction, since any material which is subject to a stress-strain cycle will lose energy. The characteristic time for alignment is  $10^5$  years for objects with diameters of  $\sim 100$ km, increasing to  $10^7$  years

for a rapidly spinning irregular 1km asteroid (Burns and Tedesco, 1979). These must be compared with the timescale for collisions. A rough estimate of the collision timescale can be made as follows: assume that 20000 asteroids occupy a torus with an inner radius of 2.2 A.U. and an outer radius of 3.2 A.U. and that the relative velocity of the asteroid is  $5 \text{ Kms}^{-1}$ . The volume of the torus is  $\sim 10^{34} \text{ m}^3$ . The probability of collision is then

$$P = 10^{-18} R^2 \text{ m}^{-2} \text{ year}^{-1} \quad (4.3)$$

where  $R$  is the radius of the asteroid. For a 50Km radius asteroid the timescale for collisions is  $3 \times 10^9$  years, considerably greater than the time required for alignment of the angular momentum vector with the shortest axis. Thus the majority of asteroids will be rotating about the shortest axis.

Asteroids are rarely observed exactly at opposition: generally, observations are made with phase angles in the range  $0^\circ$  to  $25^\circ$ . Assumption 3 above will only introduce errors if the amplitude of the lightcurve varies as a function of phase angle. Such relationships have been observed in some asteroids (eg. Scaltriti and Zappalà, 1976) and in lightcurves of model asteroids (Barucci and Fulchigoni, 1983). In both cases, the relationship was found to be linear, with the amplitude increasing with increasing phase angle. The determination of the amplitude-phase coefficient ( $\gamma$ ) requires several observations of the lightcurve over a range of phase angles, but with the asteroid restricted to a small range of ecliptic longitudes. Once  $\gamma$  has been found, Equation 4.1 can be modified so that

assumption 3 is no longer required. The modified equation is

$$A = 2.5 \text{ Log}(ad/bd') + \alpha\gamma \quad (4.4)$$

where  $\alpha$  is the phase angle.

The assumption that the amount of reflected light is proportional to the cross-sectional area is only valid if the surface material of the asteroid scatters light according to the Lommel-Seelieger relation

$$I_r = \frac{I_i A \cos(i) \cos(r) dS}{[\cos(i)+\cos(r)]} \quad (4.5)$$

where  $I_i$  is the amount of sunlight incident on area  $dS$  which has an albedo  $A$ .  $I_r$  is the amount of light reflected;  $i$  and  $r$  are the angles of incidence and reflection, respectively. A study of asteroid models by Barucci and Fulchigoni (1983) has shown that the scattering properties of the materials used in the models affects the amplitude of the lightcurve, leading to the over-estimation of the parameters  $a$  and  $b$  by a factor of 1.25 or more, depending on the material used.

From their lightcurves, it is apparent that the vast majority of asteroids are not spherical and will therefore be subject to a torque from the gravitational attraction of the Sun. The result is a precession of the rotation axis. The time scale for the precession is of the order of  $10^3 - 10^4$  years for an elongated body such as 433 Eros (Burns and Tedesco, 1979). Since this precession period is much longer than the time span of available observations, which cover

approximately 35 years, the effects of precession can be ignored.

The amplitude-longitude diagrams show the data used together with smooth curves which represent the expected lightcurve amplitude when the asteroid is at opposition. The effect of the asteroid's orbital inclination and eccentricity are taken into account, when drawing these curves, by introducing these elements into the calculation of the aspect angle through the geocentric ecliptic coordinates of the asteroid. All the data utilised in the calculation of the asteroids' pole positions and shapes are listed in Table 4.1. The various parameters were constrained to the following limits  $0^\circ \leq \lambda_0 \leq 360^\circ$ ;  $-90^\circ \leq \beta_0 \leq 90^\circ$ ;  $1 \leq a \leq 15$  and  $1 \leq b \leq 15$ .

#### 4 Vesta

A large number of lightcurves are available for this asteroid (Blanco and Catalano, 1979 and references therein) including thirteen obtained during one opposition. The pole position has been calculated by photometric astrometry (Taylor, 1979) as  $139^\circ, 47^\circ$  or  $333^\circ, 39^\circ$ , if it has a 10 hour period, but  $151^\circ 49'$  or  $350^\circ, 47'$  if the period is 5 hours. Gehrels (1967) calculated the ecliptic longitude and latitude of the pole as  $126^\circ, 65^\circ$ .

If Vesta's lightcurve is produced by albedo contrasts on the surface, then it would not exhibit an amplitude-longitude relation of the form of Equation 4.1, since the lightcurve amplitude would also depend on the size of the

Table 4.1 Asteroid lightcurves.

Ast.	Date	$\lambda$	$\beta$	$\alpha$	Amp.	Reference.	
4	22 Dec 50	36	-8	18	0.12	Blanco & Catalano (1979)	
	7 Mar 52	155	10	4	0.12	Blanco & Catalano (1979)	
	21 Dec 54	83	-4	3	0.13	Blanco & Catalano (1979)	
	2 Nov 58	128	0	23	0.12	Blanco & Catalano (1979)	
	5 Nov 58	129	0	23	0.12	Blanco & Catalano (1979)	
	11 Dec 58	133	2	19	0.14	Blanco & Catalano (1979)	
	19 Jan 59	127	4	4	0.11	Blanco & Catalano (1979)	
	24 Jan 59	126	4	2	0.10	Blanco & Catalano (1979)	
	26 Jan 59	125	4	2	0.10	Blanco & Catalano (1979)	
	28 Jan 59	125	4	2	0.10	Blanco & Catalano (1979)	
	31 Jan 59	124	5	3	0.10	Blanco & Catalano (1979)	
	5 Feb 59	123	5	6	0.11	Blanco & Catalano (1979)	
	20 Feb 59	119	5	12	0.12	Blanco & Catalano (1979)	
	25 Feb 59	119	5	14	0.13	Blanco & Catalano (1979)	
	6 May 59	126	5	25	0.14	Blanco & Catalano (1979)	
	10 May 59	127	5	25	0.13	Blanco & Catalano (1979)	
	7 Dec 61	54	-8	9	0.12	Blanco & Catalano (1979)	
	10 Apr 67	240	10	18	0.13	Blanco & Catalano (1979)	
	26 Oct 68	26	-11	5	0.10	Blanco & Catalano (1979)	
	4 Dec 68	20	-9	18	0.12	Blanco & Catalano (1979)	
	23 May 71	305	1	25	0.12	Blanco & Catalano (1979)	
	16 Jun 71	306	-1	18	0.13	Blanco & Catalano (1979)	
	19 Jul 71	300	-3	3	0.09	Blanco & Catalano (1979)	
	29 Jul 71	298	-4	4	0.18	Blanco & Catalano (1979)	
	21 Jan 73	61	-4	19	0.14	Blanco & Catalano (1979)	
	24 Jan 73	61	-4	20	0.15	Blanco & Catalano (1979)	
	25 Jan 78	249	5	11	0.11	Blanco & Catalano (1979)	
	28 Nov 83	84	-5	7	0.12	This thesis	
	20	1 Apr 55	185	0	1	0.17	Gehrels (1956)
		15 Apr 55	178	0	20	0.23	Gehrels (1956)
		25 Jan 58	48	0	27	0.24	Gehrels & Owings (1962)
9 Jan 62		98	-1	2	0.24	Chang & Chang (1962)	
8 Sep 79		350	1	2	0.19	Lupishko et al. (1982)	
28 Nov 83	17	0	19	0.21	This thesis		
29	25 Oct 62	44	7	6	0.13	Tedesco & Sather (1981)	
	4 Jul 65	271	-10	4	0.13	Tedesco & Sather (1981)	
	18 Oct 70	17	4	3	0.11	Tedesco & Sather (1981)	
	11 Mar 72	149	3	8	0.06	Tedesco & Sather (1981)	
	30 May 77	247	-9	3	0.12	Tedesco & Sather (1981)	
	1 Sep 82	348	-2	4	0.09	This thesis	
27 Nov 83	129	7	22	0.07	This thesis		
31	24 Sep 77	354	-23	7	0.07	Schober et al. (1980)	
	14 Nov 78	111	31	22	0.07	Schober et al. (1980)	
	1 Jan 79	107	40	15	0.07	Schober et al. (1980)	
	26 Nov 83	23	4	14	0.12	This thesis	

Ast.	Date	$\lambda$	$\beta$	$\alpha$	Amp.	Reference.	
39	9 May 49	232	15	6	0.43	Groeneveld & Kuiper(1954b)	
	29 Jan 52	97	-12	11	0.18	Groeneveld & Kuiper(1954a)	
	10 Apr 53	180	7	7	0.22	Groeneveld & Kuiper(1954a)	
	18 Dec 55	25	-13	20	0.50	van Houten-G & vH (1958)	
	28 Dec 55	26	-12	22	0.53	van Houten-G & vH (1958)	
	5 Mar 58	221	10	16	0.44	Gehrels & Owings (1962)	
	20 Nov 64	355	-9	21	0.26	Yang et al. (1965)	
	1 Aug 68	281	12	11	0.23	Wamsteker & Sather (1974)	
	22 Aug 68	279	10	17	0.18	Sather (1976)	
	1 Feb 70	51	-12	22	0.54	Sather (1976)	
	3 Apr 71	144	0	15	0.15	Sather (1976)	
	22 Apr 72	231	14	8	0.48	Sather (1976)	
	22 Dec 74	100	-14	6	0.23	Sather (1976)	
	3 Nov 78	23	-13	8	0.35	Chang et al. (1981)	
	30 Aug 82	300	6	14	0.16	This thesis	
	24 Nov 84	77	-16	8	0.27	This thesis	
	43	4 May 65	221	-5	3	0.13	van Houten-G et al. (1979)
		8 Aug 72	345	6	15	0.64	Burchi & Milano (1974)
		13 Aug 72	344	6	12	0.63	Burchi & Milano (1974)
		8 Oct 72	334	6	19	0.66	Burchi & Milano (1974)
31 Aug 82		23	6	21	0.36	This thesis	
44	15 Oct 82	13	6	5	0.31	Di Martino & Caccia (1984)	
	6 Nov 49	18	-6	11	0.46	Shatzel (1954)	
	7 Nov 49	18	-6	11	0.47	Shatzel (1954)	
	6 Jan 54	52	-5	22	0.32	Groeneveld & Kuiper(1954b)	
	11 Jan 54	52	-5	23	0.32	Groeneveld & Kuiper(1954b)	
	13 Jan 58	99	-3	7	0.22	Gehrels & Owings (1962)	
	2 Mar 62	144	2	7	0.24	Chang & Chang (1962)	
	10 Jun 70	211	5	17	0.45	Taylor & Tedesco (1983)	
	17 May 74	247	6	5	0.23	Zappalà & van Hou-G (1979)	
	31 Jul 79	10	-3	21	0.51	Taylor & Tedesco (1983)	
	1 Aug 79	10	-3	20	0.57	Taylor & Tedesco (1983)	
	22 Aug 79	10	-4	15	0.46	Taylor & Tedesco (1983)	
	24 Aug 79	10	-4	15	0.52	Taylor & Tedesco (1983)	
	10 Sep 79	7	-5	8	0.39	Taylor & Tedesco (1983)	
	25 Sep 79	4	-5	2	0.41	Taylor & Tedesco (1983)	
26 Sep 79	4	-5	2	0.43	Taylor & Tedesco (1983)		
17 Oct 79	359	-5	10	0.45	Taylor & Tedesco (1983)		
22 Oct 79	358	-5	12	0.49	Taylor & Tedesco (1983)		
6 Oct 83	30	-6	11	0.41	This thesis		
12 Oct 83	37	-6	8	0.39	Di Martino (Private commu)		
30 Nov 83	27	-6	16	0.52	This thesis		

spot and its position on the asteroid. A plot of amplitude vs. longitude shows that there is very little variation of amplitude with ecliptic longitude. (This could be explained by the pole being perpendicular to the ecliptic plane.)

However, the effect of solar phase angle on the lightcurve amplitude has been noted by Gehrels (1967) and Blanco and Catalano (1979). From the lightcurves of the 1958/59 opposition, Gehrels (1967),  $\gamma$  can be determined as  $0.0013 \pm 0.0002$  mag/deg. It is also possible to calculate  $\gamma$  for the 1968 opposition (0.0015 mag/deg.) and for 1971 (0.0018 mag/deg.). (Note: the 29 July 1971 lightcurve has been ignored because the amplitude is anomalously large for its phase angle; it has also been omitted from the amplitude vs. phase angle plot of Blanco and Catalano, 1979). The errors of these last two values of  $\gamma$  are large and incorporate the earlier result, Thus the 1958/59 value will be adopted for all longitudes. Figure 4.1 shows the amplitude of one lightcurve (that with the smallest solar phase angle) from each opposition, corrected to zero phase angle with  $\gamma=0.0013$  mag/deg. vs. ecliptic longitude. Correcting the data to zero phase reduces the spread of amplitudes, but only by 0.01 magnitudes.

If Vesta's lightcurve is caused by albedo differences, then in order to produce a lightcurve of amplitude 0.1 magnitudes, the albedo must change by approximately 10% (eg. an albedo of 0.2 on one side and 0.22 on the other). Bowell and Lumme (1979) have tabulated mean phase coefficient and mean albedo for various asteroid classes. The slope of  $\beta_V$  vs.

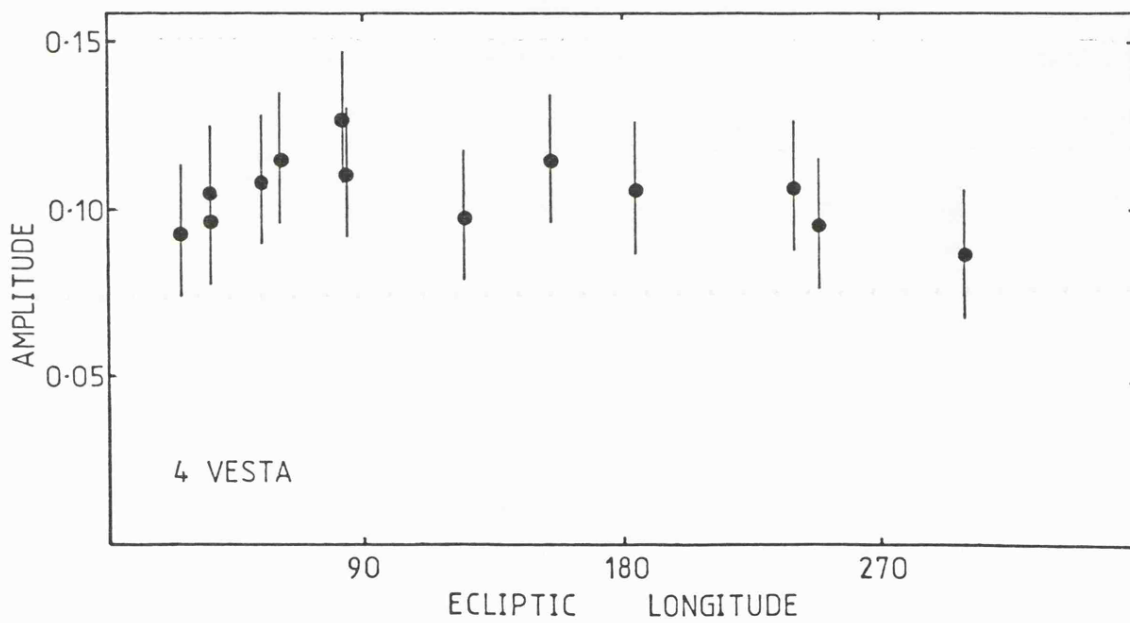


Figure 4.1 Lightcurve amplitude vs. ecliptic longitude for 4 Vesta. Only the lightcurve with the smallest solar phase angle is plotted reduced to zero phase angle using  $\gamma=0.0013$  mag/deg.

$P_V$  at an albedo of  $\sim 0.25$  (Vesta's albedo - Morrison and Zellner, 1979) is  $-0.042$  mag/deg. This means that dark material gets fainter more quickly than bright material as the phase angle increases. The difference in the values of  $\gamma$  for the bright and dark sides gives the expected value of the amplitude-longitude coefficient. This expected value is  $0.001$  mag/deg., compared with the observed value of  $0.0013$  mag/deg. Thus it is possible to explain the behaviour of the amplitude of Vesta's lightcurve in terms of albedo changes across the surface.

#### 20 Massalia

Based on data obtained in 1955 (Gehrels, 1956) and 1958 (Gehrels and Owings, 1962), it was suggested in the latter paper that the rotational axis was either perpendicular to the ecliptic plane, or that the longitude of the pole was near  $120^\circ$  ( $300^\circ$ ) or  $30^\circ$  ( $210^\circ$ ). The pole position has also been calculated by Chang and Chang (1962) as being at  $289^\circ.9, 65^\circ.8$ .

From the observations of Gehrels (1956),  $\gamma$  can be determined as  $0.003$  mag/deg. After correcting the amplitudes in Table 4.1 to zero phase angle, the pole position was calculated as  $30^\circ, 54^\circ$  or  $205^\circ, 79^\circ$  with corresponding axial ratios of  $1.25:1.00:1.00$  and  $4.88:3.85:1.00$ . Both solutions for the pole lie close to the second possibility suggested by Gehrels and Owings (1962), but not to that calculated by Chang and Chang (1962). Clearly, the first shape is the preferred solution, since the second shape is physically unlikely. If the lightcurve of 15 April 1955 is ignored (thus

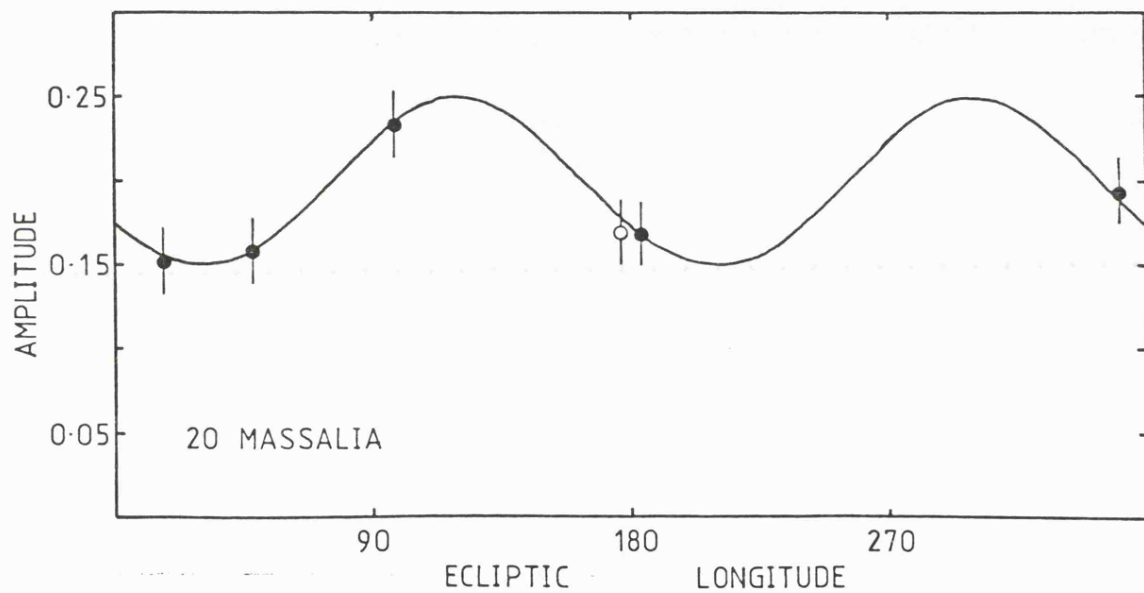


Figure 4.2 Amplitude vs. longitude for 20 Massalia. The curve is the best fit to the solid symbols and has the pole at  $32^{\circ}, 54^{\circ}$  and axial ratios 1.26:1.00:1.00.

giving equal weight to each opposition) and the parameters redetermined, then the solutions are found to be  $31^{\circ}, 54^{\circ}$  and  $206^{\circ}, 77^{\circ}$  with shapes of 1.26:1.00:1.00 and 4.12:3.25:1.00. The first of these new solutions is, again, the more likely solution.

In all cases, the predicted range of amplitudes for 20 Massalia was approximately 0.15 - 0.25 mag. Figure 4.2 shows the expected amplitude of the lightcurve with the pole at  $31^{\circ}, 54^{\circ}$  and a shape of 1.26:1.00:1.00. The solid symbols are the data used to obtain this solution, the open circle is the 15 April 1955 lightcurve. The data are plotted reduced to zero phase angle. All four solutions gave very similar curves.

### 29 Amphitrite

The complex nature of 29 Amphitrite's lightcurves led van Houten-Groeneveld et al. (1979) to suggest a "pyramidal" shape for the asteroid. Tedesco and Sather (1981) fitted the observed amplitude-longitude data with a biaxial ellipsoid having axial ratios of 1.14:1.00:1.00 and a pole positioned at  $\lambda_0 = 165^{\circ}$ ,  $\beta_0 = 45^{\circ}$ . Zappalà and Knežvić (1984) calculated the pole to be at  $142^{\circ}, 50^{\circ}$  or  $308^{\circ}, 40^{\circ}$  with axial ratios of 1.13:1.00:1.00 using a more elaborate version of the method employed here. 29 Amphitrite has also been observed by speckle interferometry (Baier and Weigelt, 1983). The shape of the asteroid was derived as elliptical with the ratio of the long axis to the short axis being  $1.6 \pm 0.5$ .

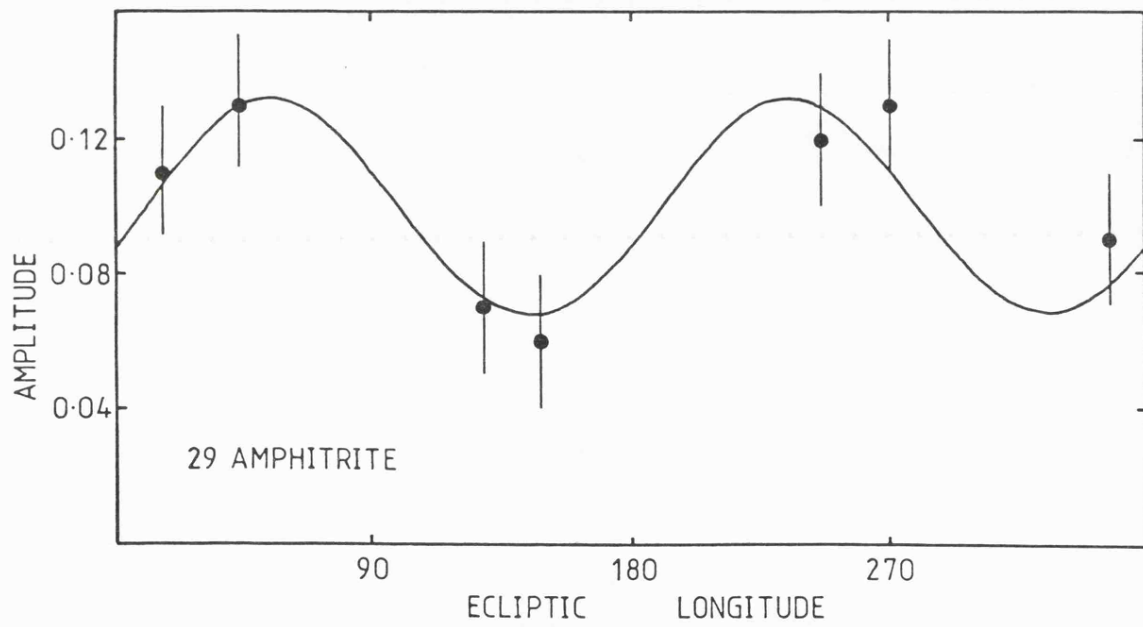


Figure 4.3 Amplitude vs. longitude for 29 Amphitrite with the pole at  $157^{\circ}, 52^{\circ}$  and axial ratios 1.13:1.00:1.00.

Combining all published lightcurves of this asteroid with those presented in Chapter 3, it is possible to calculate the pole orientation and shape of the body. The ecliptic coordinates of the pole were found to be  $157^\circ, 52^\circ$  or  $318^\circ, 43^\circ$ , both with axial ratios of 1.13:1.00:1.00, making the asteroid biaxial. The first pole position lies within the error boxes of both the earlier solutions and agrees with their shapes. It should be noted that calculation of the shape and pole position assumes that the asteroid is a smooth triaxial ellipsoid; but the complexity of 29 Amphitrite's lightcurves show that this is not the case. However, the solutions should give a first estimate of the parameters.

It is not possible to calculate the amplitude-phase coefficient for 29 Amphitrite because each lightcurve has been obtained at widely different longitudes. However, all but the latest lightcurves were obtained at small phase angles ( $3 - 8^\circ$ ). If this subset of data is used to calculate the parameters, thus minimising any errors which would be introduced by an amplitude-phase relation, then it is found that the pole positions are the same as before to within  $3^\circ$ , and the shapes are identical. This could indicate that the value of  $\gamma$  for this asteroid is small or zero. Figure 4.3 represents the expected amplitude-longitude plot for the solution  $\lambda_0 = 157^\circ$ ,  $\beta_0 = 52^\circ$ , assuming that the asteroid is observed at opposition. The alternative solution gives virtually the same curve. This shows that the expected range of amplitudes is 0.07 - 0.13 mag.

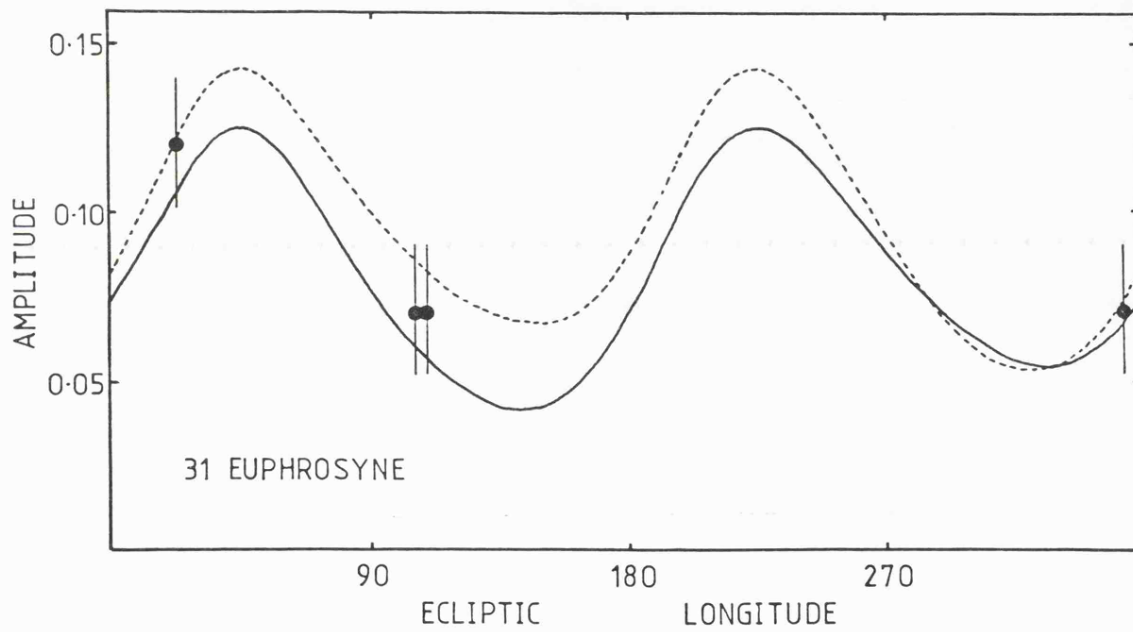


Figure 4.4 Amplitude vs. longitude for 31 Euphrosyne. The solid curve has the pole at  $178^\circ, 72^\circ$  with a shape of 1.12:1.00:1.00; the broken line has the pole at  $315^\circ, 5^\circ$  with axial ratios 1.14:1.00:1.00.

### 31 Euphrosyne

An estimate of the pole position or shape has not previously been published for 31 Euphrosyne. All available data are listed in Table 4.1. Because of the small amount of data, the pole position and shape obtained can only be considered as first approximations. The solutions are  $178^{\circ}, 72^{\circ}$  and  $315^{\circ}, 5^{\circ}$  with axial ratios of 1.12:1.00:1.00 and 1.14:1.00:1.00, making 31 Euphrosyne biaxial and not far from spherical. Figure 4.4 shows the data and the expected amplitudes for the two solutions (solid line =  $178^{\circ}, 72^{\circ}$ ; broken line =  $315^{\circ}, 5^{\circ}$ ). The asymmetry in these curves is caused by the large eccentricity and inclination of the asteroid's orbit.

### 39 Laetitia

The orientation of the axis of rotation of 39 Laetitia has been calculated on five occasions: firstly by van Houten-Groeneveld and van Houten (1958) -  $117^{\circ}, 24^{\circ}$  or  $112^{\circ}, 31^{\circ}$ ; Gehrels and Owings (1962) -  $130^{\circ}, 10^{\circ}$ ; Sather (1976) -  $121^{\circ}, 37^{\circ}$ , who also calculated the shape as 3.0:1.8:1.0; Zappalà and Scaltriti (1982) -  $116^{\circ}, 53^{\circ}$  or  $340^{\circ}, 62^{\circ}$  and Zappalà and Knezvic (1984) -  $116^{\circ}, 49^{\circ}$  or  $338^{\circ}, 57^{\circ}$  with axial ratios of 3.29:2.08:1.00.

A total of sixteen lightcurves at fourteen oppositions (Table 4.1) are available for calculation of the pole position and shape parameters. Utilizing all the data, two solutions were obtained; the first has the pole at  $114^{\circ}, 47^{\circ}$

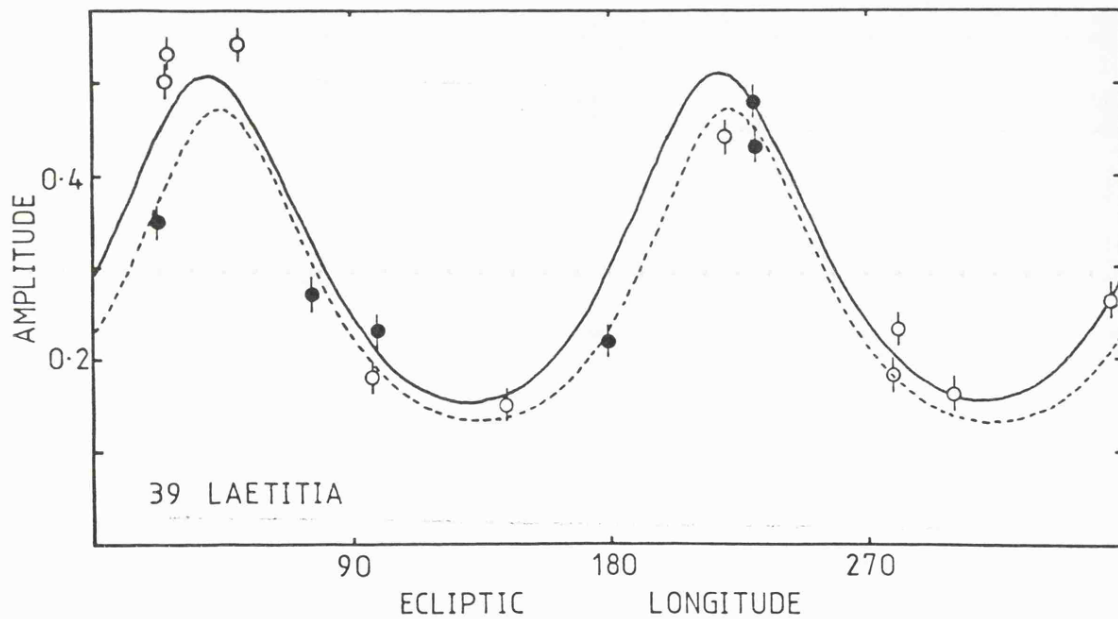


Figure 4.5 Amplitude vs. longitude for 39 Laetitia. The solid curve is a fit to all the data and has the pole at  $114^{\circ}, 47^{\circ}$  with  $2.86:1.79:1.00$  as the shape. The broken line has  $111^{\circ}, 56^{\circ}$  as the pole and  $4.23:2.74:1.00$  as the axial ratios and is a fit to the solid symbols only.

with axial ratios of 2.86:1.79:1.00, while the second has the pole at  $340^{\circ}, 62^{\circ}$  with a shape of 3.67:2.31:1.00. It should be noted that the data cover a wide range of phase angles and have not been corrected for any possible amplitude-phase relation. Using the two lightcurves from the 1955 opposition together with the lightcurve from Chang et al. (1981), which has a similar ecliptic longitude, an average value of the slope of  $\gamma$  was obtained as 0.015 mag/deg. However, using data from the 1968 opposition, it is found that  $\gamma = -0.008$  mag/deg. Applying the first value of  $\gamma$  to the data results in several lightcurves having negative amplitudes, which are physically meaningless, while the second value is of the opposite sign to any reported in the literature. Obviously, more data are required for 39 Laetitia in order to determine the value of  $\gamma$  accurately.

The effect of any amplitude-phase relation can be minimised by eliminating those data which were obtained at large phase angles ( $\geq 8^{\circ}$ ). This leaves six lightcurves each from a different opposition. The two solutions calculated using this subset of data are:  $111^{\circ}, 56^{\circ}$  with 4.23:2.74:1.00 and  $5^{\circ}, 70^{\circ}$  with 5.32:3.51:1.00. Figure 4.5 shows the first solution above as the solid line while the broken line represents the solutions obtained with the subset of data. This subset is indicated by the solid symbols. Most of the solutions have the latitude of the pole higher than any of the previously published values; there is a better agreement in the longitude of the pole. Of the shapes, the first solution is similar to that of Sather (1976), and the shapes obtained using all the data lie on either side of the Zappalà

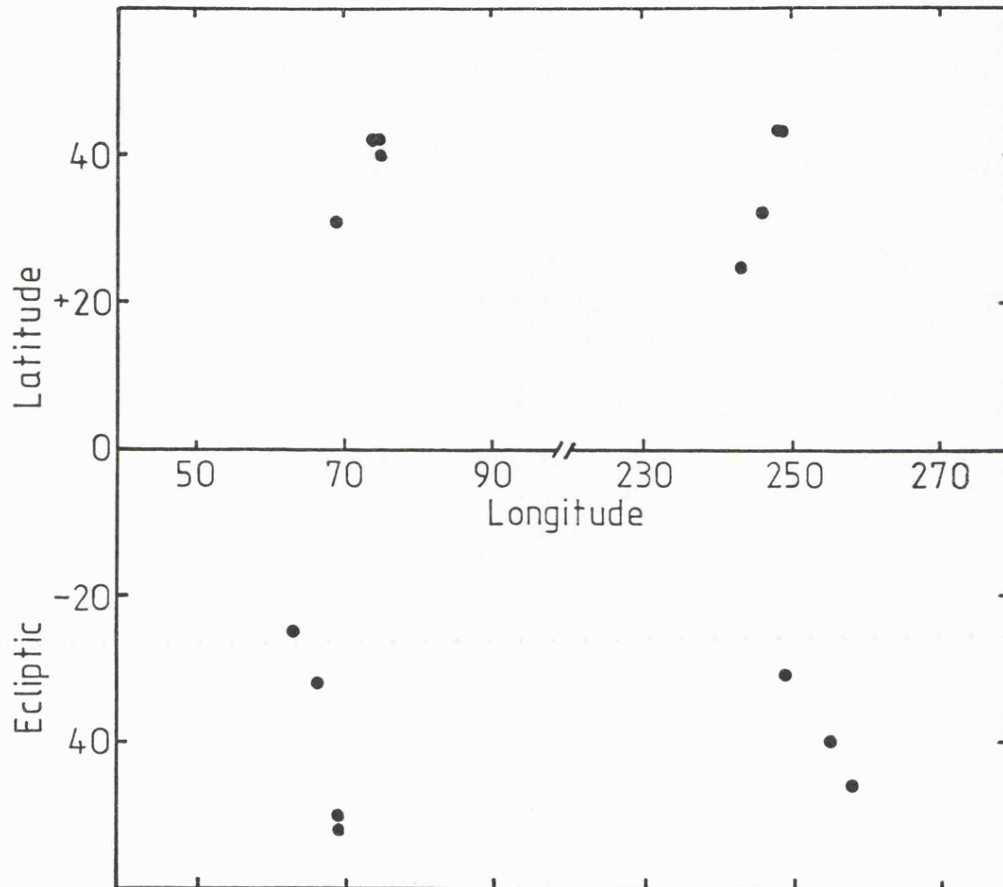


Figure 4.6 Shows the ecliptic coordinates for all the solutions to the pole orientation for 43 Ariadne.

and Knezvic (1984) result.

### 43 Ariadne

Neither a pole position nor a shape have been published previously for 43 Ariadne; although van Houten-Groeneveld et al. (1979) suggested that the rotation axis was highly inclined and that the asteroid was quite elongated. All the available lightcurves are listed in Table 4.1.

Using all of these data, the pole positions are calculated as  $68^{\circ}, 31^{\circ}$  and  $243^{\circ}, 25^{\circ}$ , both with shapes of 1.84:1.00:1.00. However, three of the lightcurves were obtained at the 1972 opposition. From these,  $\gamma$  is estimated to be  $0.004 \pm 0.001$  mag/deg. After correcting the data to zero phase angle, the pole position and shape were recalculated as  $75^{\circ}, 38^{\circ}$  and  $246^{\circ}, 31^{\circ}$  with 2.52:1.45:1.00 and 2.34:1.35:1.00 as their respective shapes. Solutions can also be obtained by utilizing only one lightcurve from each opposition (chosen to have the smallest phase angle), thus giving equal weight to each opposition. The solutions obtained were;  $74^{\circ}, 42^{\circ}$  and  $248^{\circ}, 43^{\circ}$  with axial ratios 2.95:1.62:1.00 and 3.69:2.06:1.00 with the data uncorrected for amplitude-phase effects and  $75^{\circ}, 42^{\circ}$  and  $249^{\circ}, 43^{\circ}$  with 2.96:1.70:1.00 and 3.66:2.13:1.00 after correction. Unlike the results obtained with the complete data sets, the solutions which have the pole in the southern ecliptic sky were not directly opposite the northern pole positions and the shapes differed by a considerable amount. The reason for this is that the solutions are obtained from only three lightcurves. Figure 4.6 shows all

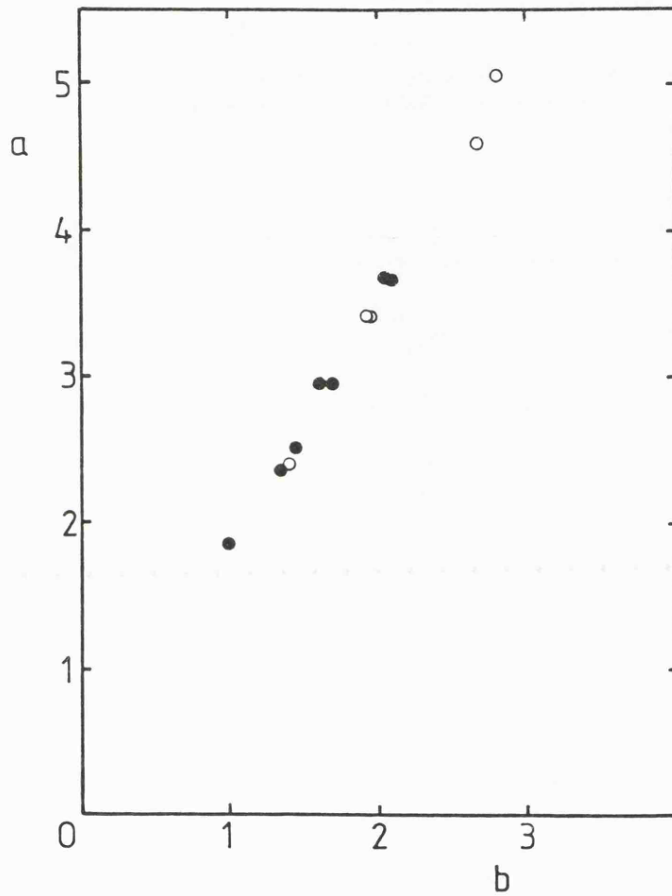


Figure 4.7 Shows all the derived values of the parameters a and b for 43 Ariadne. Open circles are those corresponding to pole positions in the southern ecliptic sky. The slope of the line through the points is  $1.75 \pm 0.01$ .

the solutions of the pole position and Figure 4.7 shows all the shapes (those corresponding to the southern poles are represented by open symbols). The shapes plotted in Figure 4.7 lie on a straight line the slope of which gives the ratio of a:b as  $1.75 \pm 0.01$ . Of the four groups of pole positions in Figure 4.6, those around  $\lambda_0 = 75^\circ$ ,  $\beta_0 = 35^\circ$  are clustered closest. This could indicate that the actual pole lies in this region. Figure 4.8 depicts the expected variation of amplitude with longitude for the solution  $75^\circ, 38^\circ$  2.52:1.45:1.00. The data are plotted after removal of the amplitude-phase effect.

#### 44 Nysa

This asteroid has probably the most frequently determined pole position of any asteroid. Chang and Chang (1962) give Nysa's pole as  $285^\circ.6, 65^\circ.5$ ; Tedesco (1979) lists the pole as  $105^\circ, 30^\circ$ ; while Zappalà and van Houten-Groeneveld (1979) calculate  $100^\circ, 50^\circ$ ; Zappalà and Scaltriti (1982) give the pole as  $101^\circ, 42^\circ$  or  $288^\circ, 53^\circ$ ; Magnusson (1983) gives  $94^\circ, 59^\circ$  or  $288^\circ, 63^\circ$ ; finally Zappalà and Knezvic (1984) have calculated the pole coordinates as  $99^\circ, 49^\circ$  or  $295^\circ, 54^\circ$  and also gives the axial ratios as 1.78:1.18:1.00.

There are a large number of lightcurves available for this asteroid, in particular during the 1979 opposition. These are listed in Table 4.1. Utilizing all of these data to calculate  $\lambda_0$ ,  $\beta_0$ , a and b places the pole at  $96^\circ, 58^\circ$  or  $294^\circ, 61^\circ$  with shapes of 2.82:1.81:1.00 or 2.79:1.78:1.00, respectively. The first of these solutions is shown in Figure

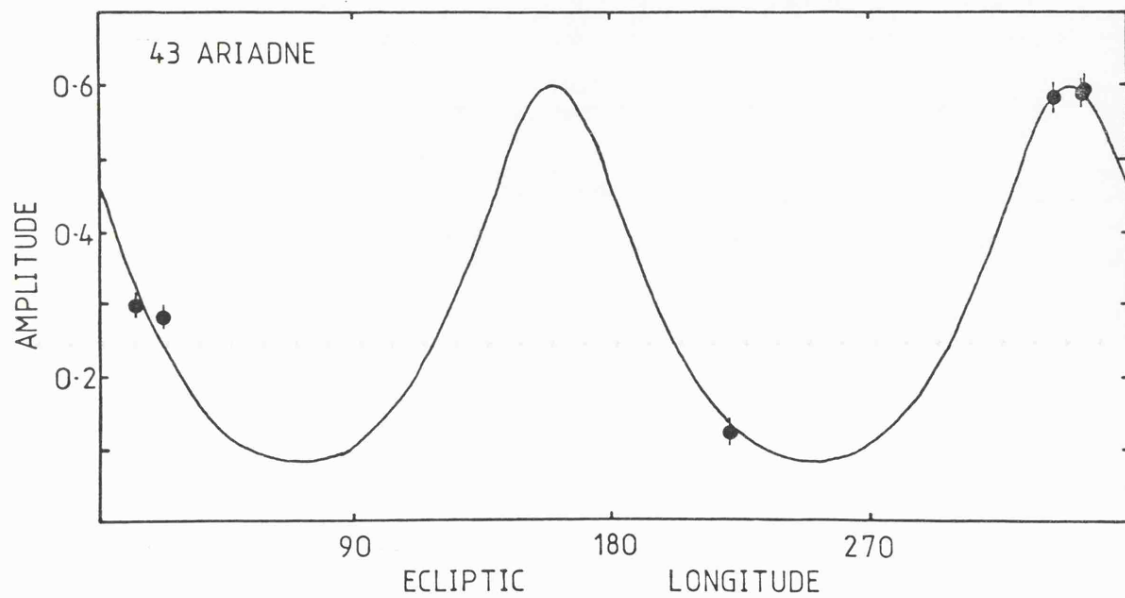


Figure 4.8 Amplitude vs. longitude for 43 Ariadne. The curve represents the expected amplitude for a given longitude with the pole at  $75^{\circ}, 38^{\circ}$  and a shape of 2.52:1.45:1.00. The data are plotted after correction to zero phase with  $\gamma=0.004$  mag/deg.

4.9a. From the lightcurves of the 1979 opposition, it can be calculated that  $\gamma=0.007$  mag/deg. However, from the 1983 lightcurves,  $\gamma$  is found to be 0.017 mag/deg. This larger value, if used to correct the data to zero phase angle, results in the lightcurves observed in 1954 having negative amplitudes, even though they are only  $20^\circ$  away in longitude (variations in  $\gamma$  might be expected in different regions of the sky, see discussion below). Using the first value of  $\gamma$  and applying it to all the data has a large effect on one of the solutions. The recalculated pole positions and shapes are:  $78^\circ, 76^\circ$  or  $290^\circ, 60^\circ$  with  $8.94:6.14:1.00$  or  $2.94:2.03:1.00$ . These solutions are shown in Figure 4.9b.

Calculating the pole position and shape from the complete data set gives the 1979 opposition relatively large weighting due to the large number of lightcurves obtained. This effect can be removed by making use of just one lightcurve from each opposition, selected to have the smallest phase angle of that opposition to reduce the errors introduced by the amplitude-phase relation. Recalculating the parameters gives  $96^\circ, 63^\circ$  or  $308^\circ, 75^\circ$  as the pole position with axial ratios of  $3.30:2.15:1.00$  or  $5.25:3.42:1.00$ . If the data are corrected to zero phase angle, then the solutions are  $69^\circ, 80^\circ$  or  $291^\circ, 65^\circ$  with corresponding shapes of  $15.00:10.25:1.00$  or  $3.51:2.40:1.00$ . Notice again that correcting the data to zero phase significantly alters the first solution. In fact, the derived shape is so extreme as to be physically unlikely. The ratio a:b has two slightly different values depending on whether the data has been corrected or not. These are a:b = 1.55 for the uncorrected

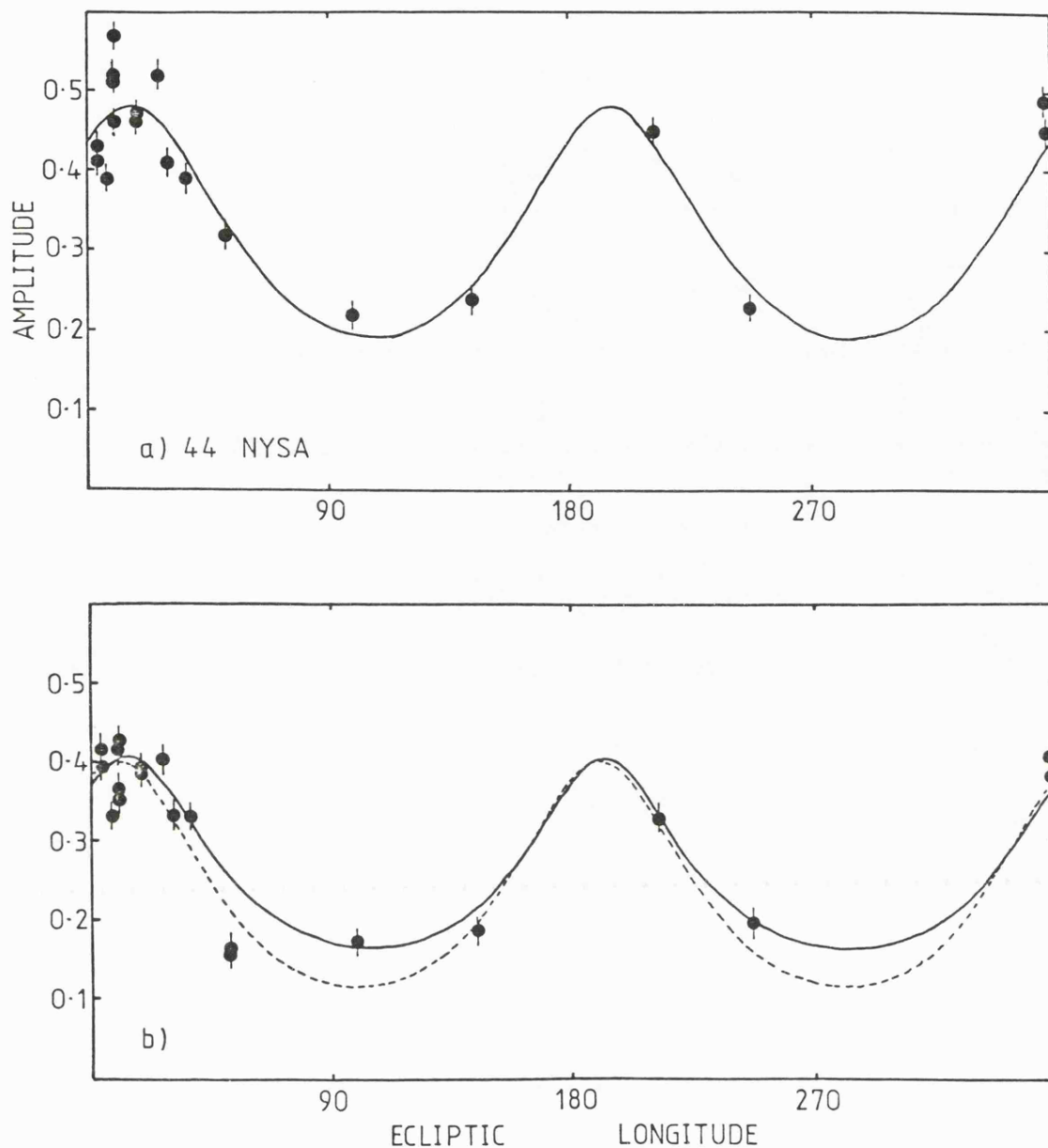


Figure 4.9 Amplitude vs. longitude for 44 Nysa. a) Shows the data uncorrected and the expected lightcurve amplitude with the pole at  $96^\circ, 58^\circ$  and a shape of 2.82:1.81:1.00. b) Shows the data corrected to zero phase angle with  $\gamma=0.007$  mag/deg. The solid curve was calculated with the pole at  $78^\circ, 76^\circ$  and a shape of 8.94:6.14:1.00 while the broken line has  $290^\circ, 60^\circ$  as the pole coordinates and 2.94:1.03:1.00 as the shape.

data and  $a:b = 1.46$ , if they have been reduced to zero phase. This difference occurs because the lightcurves with the maximum amplitude have large phase angles and thus change when corrected to zero phase. Both of these values agree reasonably well with the ratio of  $a:b = 1.51$  obtained by Zappalà and Knezevic (1984), although the shapes calculated here are more elongated. The pole positions around  $290^\circ, 65^\circ$  are reasonably constant and suggests that this is the more likely pole. This solution to the pole also agrees with the other solutions in this region.

#### DISCUSSION

None of the pole positions and axial ratios presented above have had errors quoted with them. This is because the errors cannot be calculated directly but have to be estimated. They thus merit a more detailed discussion. Generally, the larger the data set the more accurately the results can be determined. However, if a data set consists of a small number of lightcurves, all obtained at small solar phase angles, then the addition of another lightcurve with large phase angle could increase the errors of the result. The effect of the extra datum decreases as the number of lightcurves increases, since it represents a smaller proportion of the available data. The effect of the lightcurves having different phase angles can be considerably reduced if the value of  $\gamma$  can be determined for the asteroid, or if the asteroid exhibits a small or non-existent amplitude-phase relation (this may be the case with 29 Amphitrite).

It is possible that the amplitude-phase relation is caused by flat areas on the surface of the asteroid (Scaltriti and Zappalà, 1976) which, at non-zero phase angles, may be visible from the Earth without being illuminated by the Sun and thus reduce the amount of light reflected. This effect would be more prominent at minima in the lightcurve, the net result being an increase in the amplitude of the lightcurve. It is also possible that this effect depends on the material which forms the surface of the asteroid, but photometric lightcurves of models by Barucci and Fulchignoni (1983) showed amplitude-phase relations with the value of  $\gamma$  being independent of the material used to construct the model and of its shape. The approximate value of the amplitude-phase coefficient can be determined from a few lightcurves which have been obtained within a small range of ecliptic longitudes, but at widely different phase angles. If the effect is caused by surface macrostructure, then it is reasonable to assume that the value of  $\gamma$  will be dependent on the aspect angle and will thus vary with ecliptic longitude. Of the asteroids discussed above, three (4, 39 and 44) have sufficient data to allow  $\gamma$  to be determined at different points on the sky. The three values of  $\gamma$  for 4 Vesta do not show any significant differences, while the negative coefficient for 39 Laetitia is suggestive of erroneous data. 44 Nysa does have two different values of  $\gamma$ , 0.007 mag/deg. at  $0^\circ$  longitude and 0.017 mag/deg. at  $36^\circ$ . This later value gives rise to negative amplitudes when applied to the lightcurves at  $50^\circ$  longitude. Any variation in  $\gamma$  with longitude can reasonably be expected to be small and sinusoidal, similar to the variations of amplitude and

magnitude with longitude. From these asteroids it is not possible to deduce whether or not  $\gamma$  is a function of longitude.

Of the four parameters  $\lambda_0$ ,  $\beta_0$ , a and b, the longitude of the pole is the most consistent, varying only slightly with the various subsets of data used for a particular asteroid. The reason for this is that when the aspect angle is  $90^\circ$  and thus the asteroid is showing its maximum amplitude, the pole can lie anywhere on a great circle which approximately follows a line of longitude because most asteroids orbit close to the ecliptic plane. Thus the error in  $\lambda_0$  is probably  $\pm 10^\circ$  or less for asteroids with small orbital inclinations. The error in  $\beta_0$  is larger,  $\pm 10 - 15^\circ$ . Figure 4.10 shows the sum of the squares of the differences between the calculated and observed amplitudes for all possible pole positions for 39 laetitia assuming a fixed shape of 2.86:1.79:1.00. The four minima representing the ambiguous solutions are clearly visible.

The shape parameters a and b show the most fluctuation for small additions to, or changes in, the data used. If the lightcurves with the maximum amplitude were observed at small phase angles, or the corrections for the amplitude-phase effect are small, then the ratio a:b will remain constant for all solutions. This is because a:b can be determined directly from the maximum lightcurve amplitude using Equation 4.2 (compare 43 Ariadne and 44 Nysa). This can be seen in Figure 4.11 which is a contour plot of the goodness of fit for 39 Laetitia with the pole fixed at  $114^\circ, 47^\circ$  and allowing a

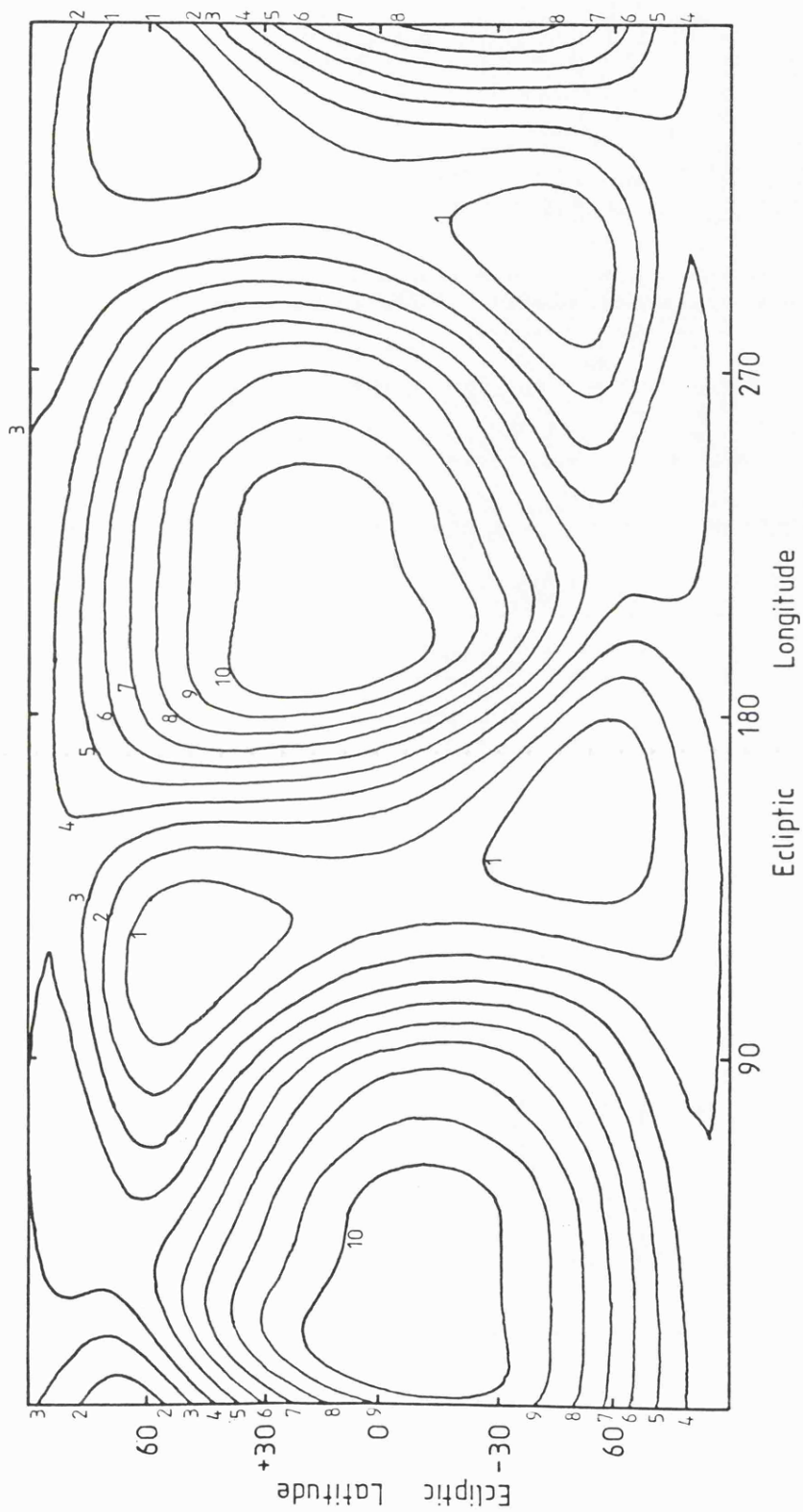


Figure 4.10 Shows the quality of fit of all possible pole positions for 39 Laetitia with the shape fixed at 2.86:1.79:1.00. The low numbered contours are the better fits. The minima corresponding to the four ambiguous solutions are clearly visible. The contours are calculated every 5°.

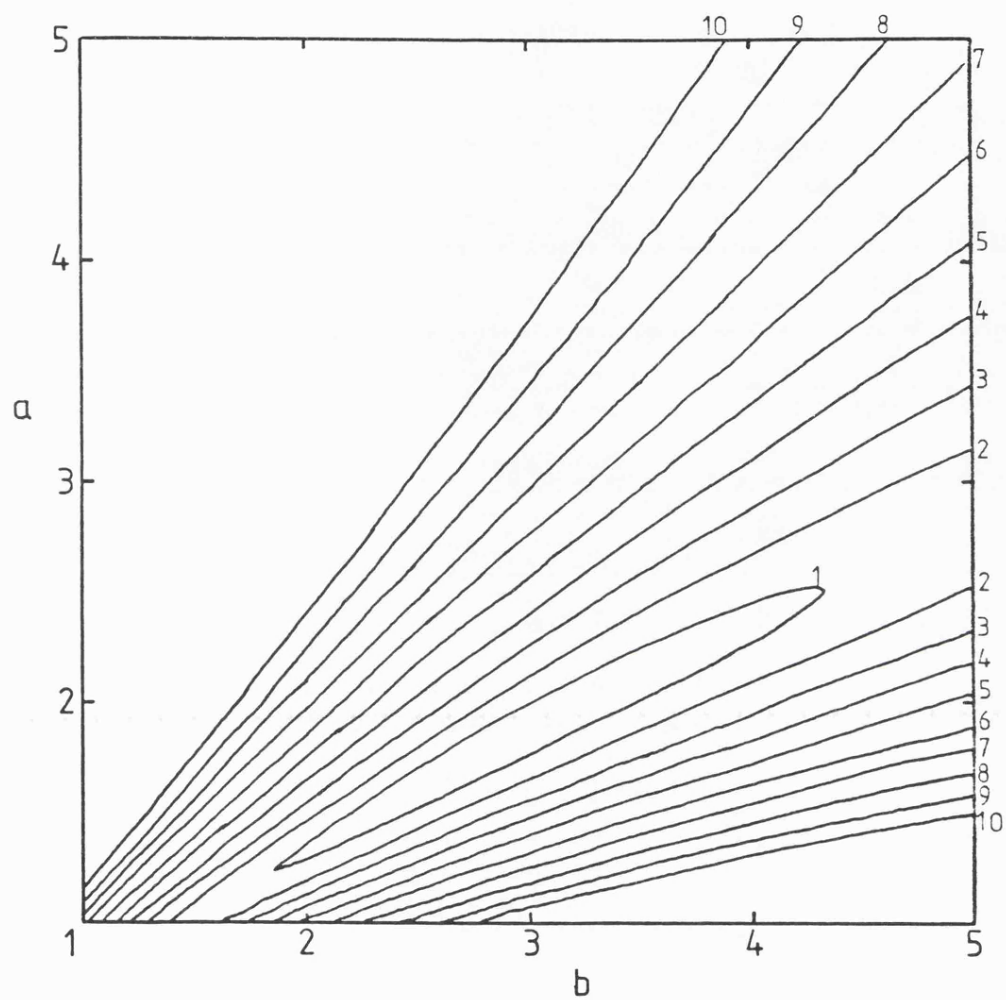


Figure 4.11 Shows the quality of fit of all possible shapes in the range 1 - 5 for 39 Laetitia with the pole fixed at  $114^{\circ}, 47^{\circ}$ . The contours are calculated at intervals of 0.05.

and  $b$  to vary from 1 to 5 independently. The "trough-like" nature of the contours indicate that there is little to choose between solutions which have the same ratio of  $a:b$ . Thus  $a$  and  $b$  cannot be accurately determined and have errors of  $\pm 1.0$  or more, but  $a:b$  only has errors of  $\pm 0.05 - 0.10$ . These values for the errors do not take into account the systematic over-estimation of the shape parameters by a factor of 1.25, or more, which have been observed in asteroid models (Barucci and Fulchignoni, 1983).

It is worth noting that four of the six asteroids which have had their shapes calculated in this Chapter are possible biaxial ellipsoids. This raises the question; does the method employed to determine the shape and pole position have a tendency to produce biaxial shapes? The alternative explanations are that the majority of asteroids are biaxial, or that these four asteroids just happen to be this shape. This latter possibility can only be dismissed on the ground that it is statistically unlikely. The other alternative cannot be tested until the shapes of many more asteroids have been derived. If true, however, it poses an important question which theories of the origin and evolution of the asteroids must answer. Despite these alternatives, the most plausible explanation is that the method does underestimate the value of  $b$ , producing more biaxial shapes. At this point it is worth remembering that the lower limit applied to both  $a$  and  $b$  was 1.00. Thus any asteroid which has  $b$  close to unity could, considering the errors, have  $b$  determined as 1.00. The probability of this occurring increases as the real value of  $b$  approaches 1.00 since it is not allowed to fall

Table 4.2. Summary of asteroid pole positions.

Ast.	$\lambda$	$\beta$	Reference.	Ast.	$\lambda$	$\beta$	Reference.
2	228	43	Tedesco (1979)	22	215	45	Tedesco (1979)
2	44	4	Zappala+ (1984)	22	212	46	Zappala+ (1982)
2	148	55	Zappala+ (1984)	22	11	19	Zappala+ (1982)
2	200	40	Binzel (1984)	22	212	46	Barucci+ (1983)
2	220	15	Binzel (1984)	22	11	19	Barucci+ (1983)
3	51	70	Chang+ (1962)	22	13	17	Zappala+ (1984)
3	101	29	Zappala+ (1984)	22	214	42	Zappala+ (1984)
3	321	57	Zappala+ (1984)	28	93	18	Zappala+ (1984)
4	310	77	Chang+ (1962)	28	285	37	Zappala+ (1984)
4	126	65	Gehrels (1967)	29	165	45	Tedesco+ (1981)
4	139	47	Tedesco (1979)	29	142	50	Zappala+ (1984)
4	333	39	Taylor (1979)	29	308	40	Zappala+ (1984)
4	151	49	Taylor (1979)	29	157	52	This thesis
4	350	40	Taylor (1979)	29	318	43	This thesis
5	148	9	Tedesco (1979)	31	178	72	This thesis
6	145	15	Gehrels+ (1962)	31	315	5	This thesis
6	5	50	Tedesco (1979)	39	117	24	van Hout-G+ (1958)
6	130	33	Zappala+ (1984)	39	112	31	van Hout-G+ (1958)
6	344	30	Zappala+ (1984)	39	185	86	Chang+ (1962)
7	193	15	Gehrels+ (1962)	39	130	10	Gehrels+ (1962)
7	212	47	Chang+ (1962)	39	121	37	Sather (1976)
7	19	41	Taylor (1977)	39	116	53	Zappala+ (1982)
7	11	41	Tedesco (1979)	39	340	62	Zappala+ (1982)
7	13	27	Zappala+ (1982)	39	116	49	Zappala+ (1984)
7	192	10	Zappala+(1982)	39	338	57	Zappala+ (1984)
8	157	10	Tedesco (1979)	39	114	47	This thesis
9	299	60	Chang+ (1962)	39	340	62	This thesis
9	156	15	Tedesco (1979)	39	111	56	This thesis
9	191	56	Zappala+ (1979)	39	5	70	This thesis
9	0	32	Zappala+ (1982)	41	157	28	Barucci (1983)
9	185	50	Zappala+ (1982)	41	15	36	Barucci (1983)
9	2	26	Zappala+ (1984)	43	68	31	This thesis
9	186	43	Zappala+ (1984)	43	243	25	This thesis
15	250	68	Chang+ (1962)	43	75	38	This thesis
16	222	4	Lupishko+ (1983)	43	246	31	This thesis
16	40	23	Zappala+ (1984)	43	74	42	This thesis
16	217	31	Zappala+ (1984)	43	248	43	This thesis
20	299	66	Chang+ (1962)	43	75	42	This thesis
20	30	54	This thesis	43	249	43	This thesis
20	205	79	This thesis	44	285	66	Chang+ (1962)
20	31	54	This thesis	44	105	30	Tedesco (1979)
20	206	77	This thesis	44	100	50	Zappala+ (1979)

Ast.	$\lambda$	$\beta$	Reference.	Ast.	$\lambda$	$\beta$	Reference.
44	101	47	Zappala+ (1982)	433	17	10	Taylor (1979)
44	288	53	Zappala+ (1982)	433	15	9	Taylor (1979)
44	94	59	Magnusson (1983)	433	18	27	Zappala+ (1982)
44	288	63	Magnusson (1983)	433	227	10	Zappala+ (1982)
44	99	49	Zappala+ (1984)	511	122	10	Tedesco (1979)
44	295	54	Zappala+ (1984)	511	92	28	Zappala+ (1982)
44	96	58	This thesis	511	304	31	Zappala+ (1982)
44	294	61	This thesis	624	324	10	Tedesco (1979)
44	78	76	This thesis	624	146	14	Zappala+ (1982)
44	290	60	This thesis	624	321	0	Zappala+ (1982)
44	96	63	This thesis	624	144	10	Magnusson (1983)
44	308	75	This thesis	624	322	-4	Magnusson (1983)
44	69	80	This thesis	624	152	29	Zappala+ (1984)
44	291	65	This thesis	624	314	15	Zappala+ (1984)
63	127	38	Zappala+ (1984)	1566	49	0	Tedesco (1979)
63	298	28	Zappala+ (1984)	1566	49	11	Zappala+ (1982)
216	71	21	Magnusson (1983)	1566	255	26	Zappala+ (1982)
216	234	38	Magnusson (1983)	1580	140	20	Tedesco (1979)
354	132	45	Zappala+ (1984)	1620	200	60	Tedesco (1979)
354	357	38	Zappala+ (1984)	1685	200	55	Tedesco (1979)
433	173	13	Gehrels+ (1962)	1685	209	34	Zappala+ (1982)
433	345	45	Chang+ (1962)	1685	249	14	Zappala+ (1982)
433	16	12	Tedesco (1979)				

below 1.00. It is also worth considering the assumption that the asteroid is rotating about the shortest axis. Although this is the case for most asteroids, it is almost certainly not the case for objects which have recently undergone collisions. Thus setting the rotation axis to a length of unity could mean that  $b$  and even  $a$  will have values of less than 1.00. Again the statistical probability of this event in such a small sample of asteroids is low. Finally, although four of the asteroids had biaxial shapes determined for them, two of these also had triaxial shapes as possible solutions. The errors in the axial ratios could be improved by incorporating the variation of the asteroids' absolute magnitude with ecliptic longitude (Zappalà et al. 1983).

Table 4.2 lists all the pole positions calculated in this Chapter and all those which were available in the literature. The distribution of these pole coordinates is shown in Figure 4.12. Most of these asteroids have poles which form two groups, one in each part of the diagram, corresponding to the ambiguous solutions at  $\lambda_0, \beta_0$  and  $\lambda_0 + 180^\circ, \beta_0$  (southern ecliptic pole positions have been ignored). The spread of each group gives a possible indication of the associated error of the solution. If the mean pole position of each group is considered, then there does not appear to be any significant clustering of the poles, nor areas of avoidance. (Note that, in fact, one pole for each asteroid is "spurious".) At present, the data set is too small to draw any meaningful conclusions, but the number of asteroids for which orientations are available has been increasing rapidly over the last ten years. Thus it should

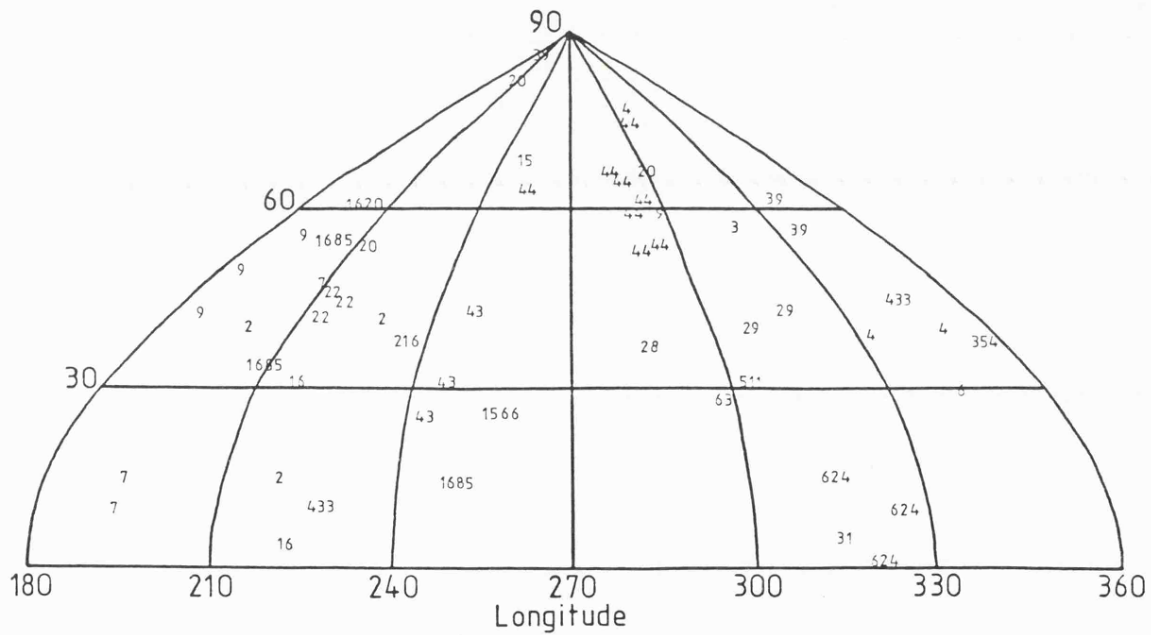
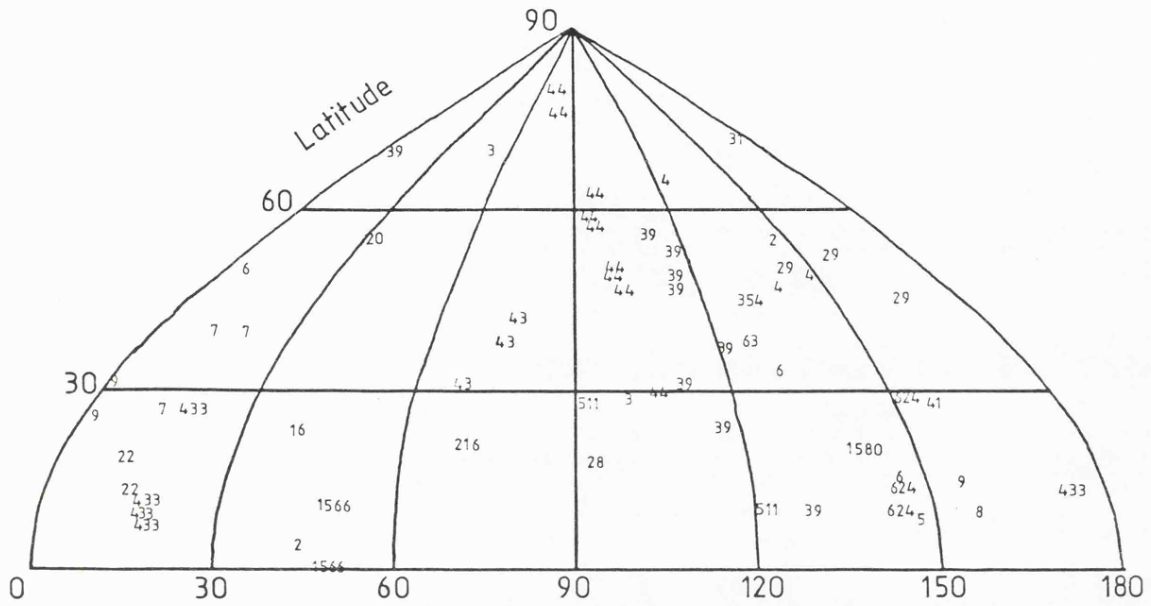


Figure 4.12 Shows the distribution of asteroid rotation axes. Only northern ecliptic pole positions are plotted. Data is listed in Table 4.2.

not be too long before significant results become possible  
and so provide clues to the evolution of the asteroid belt.

**CHAPTER 5**

**REFLECTION SPECTRA**

**AND**

**THERMAL EMISSION**

## INTRODUCTION

Asteroid spectra consist of two parts; a reflected solar component, modified by the reflectance spectrum of the asteroid and an emitted component. The reflected portion of the spectrum dominates below about  $5\mu\text{m}$ ; at longer wavelengths the emission spectrum is more important. This emission is the thermal re-radiation of the absorbed component of the incident solar flux. The wavelength at which the observed spectrum switches from being reflection-dominated to emission-dominated depends mainly on the distance of the asteroid from the Sun. The data discussed in Chapters 2, 3 and 4 have been obtained from the reflected portion of the spectrum. This final chapter relates to data from the cross-over region of the spectrum at  $3 - 4\mu\text{m}$  and from the thermal component. Data from additional observations (AO's) with the Infrared Astronomical Satellite (IRAS) are also presented.

The next section presents  $2.9 - 4.0\mu\text{m}$  spectra of 1 Ceres, 2 Pallas, 10 Hygeia, 15 Eunomia, 16 Psyche, 22 Kalliope, 83 Beatrix, 386 Siegena, 433 Eros and 471 Papagena. The reduction of these spectra illustrates the importance of accurate thermal modelling for separating the reflected and emitted portions of the spectra. The reflectance spectra also offer the possibility of extending the classification schemes already applied to asteroid data in the visible and near-infrared regions (as discussed in Chapter 2).

The model used to remove the thermal component from the 3 - 4 $\mu$ m spectra is then described and discussed. Following this, the AO data on 44 Nysa are presented and the observations compared with the predicted fluxes from the thermal model. The chapter concludes with a general discussion.

### 3 - 4 $\mu$ m SPECTRA

Compositional details of remote objects are obtained by observing their spectra and comparing these with laboratory spectra of known mineral samples. Early surveys of asteroid spectra generally only extend to 1.1 $\mu$ m (Chapman and Gaffey, 1979). These observations were extended into the infrared region by broadband (JHKL) photometry followed by narrow-band photometry and multiplex spectroscopy (Larson and Veeder, 1979). All of these data can be used in addition to the visible spectra to derive details of surface composition.

A broad absorption band at 3 $\mu$ m has been observed in some C-class asteroids (and in some U-class which are close to being C-class, such as 2 Pallas). Laboratory measurements have related this absorption feature to that produced by water of hydration in clay minerals or salts (Lebofsky, 1980; Feierberg et al., 1981; Lebofsky, et al., 1981; Larson et al., 1982). The presence of this feature has not previously been sought in asteroids of the S- and M-class.

The observations were made with the 3.8m UK Infrared telescope in Hawaii between January 11 and 24, 1982. The

spectra were measured with a circular variable filter in the UKT6 cryostat. Spectra were obtained from 2.9 to 4.0 $\mu$ m at intervals of 0.1 $\mu$ m with a resolution of 0.08 $\mu$ m. Each spectrum consisted of two 5-second integrations per wavelength point. The UKIRT CVF integrates point by point and thus fast-moving clouds, which were present on all nights except January 13, can contaminate the results. This effect can generally be removed by repeat measurements. The signal-to-noise ratio can be improved by adding spectra.

The first step in the reduction of the observed asteroid spectra was to remove the effects of atmospheric absorption. These were removed by dividing the asteroid spectra by that of a star with a spectral type around A0 which was as close to the asteroid in both time and airmass as possible. This ratio was then multiplied by a black-body spectrum of a temperature appropriate to the star's spectral type. The spectra of A0 stars in the 3 - 4 $\mu$ m region are featureless.

The spectra in Figure 5.1 are shown after the removal of the atmospheric absorption. Only two asteroids are shown, 15 Eunomia and 433 Eros, to illustrate the extremes of the spectra obtained at this stage. The increased flux at the longer wavelength relative to the shorter wavelength for 433 Eros is caused by the emitted thermal component of this asteroid's spectrum. The spectra in Figure 5.1 consist of three components: a reflected solar flux ( $\phi_s$ ), modified by the asteroid reflectance spectrum ( $\phi_r$ ), plus the thermal emission of the asteroid ( $\phi_t$ ). The total flux from the

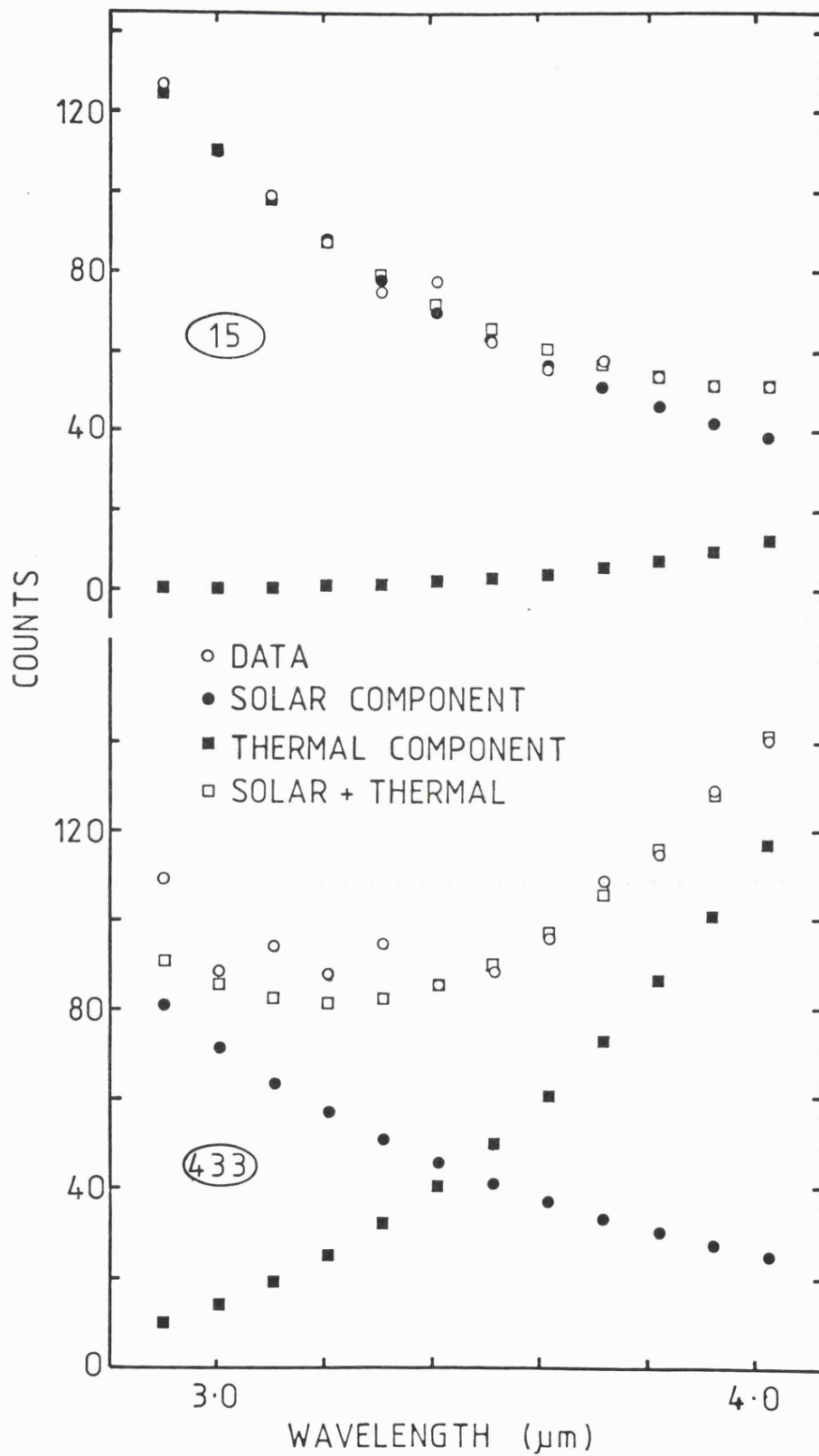


Figure 5.1 Observed spectra of two asteroids, 15 Eunomia and 433 Eros. Also shown are the thermal and reflected solar components of the spectra and their sum. These illustrate the different contributions made by the thermal emission of the asteroid.

asteroid is thus

$$\phi = (\phi_s \cdot \phi_r) + \phi_t \quad (5.1)$$

Before the asteroid's reflectance spectrum can be obtained, the thermal component must be removed. The contribution of the thermal emission to each asteroid's spectrum depends on the heliocentric distance of the asteroid, its diameter, albedo and the solar phase angle at the time of the observation. The contribution of the thermal emission can be calculated by use of a standard model (Morrison and Lebofsky, 1979) which utilizes the Bond albedo  $A=0.6p_v$  (the geometric albedo  $p_v$  is obtained from Morrison and Zellner, 1979). The model assumes that the asteroid is spherical, but takes into account the phase angle of the observations. In this model, the shape of the thermal spectrum depends on the heliocentric distance (which is known accurately) and the albedo. The flux is then dependent on the diameter of the asteroid. The absolute flux from the model could not be equated with the observed flux due to uncertainties in the diameter and because of lightcurve effects. Virtually all asteroids exhibit lightcurves due to a rotating non-spherical shape. In order for the model to predict accurately the thermal flux from an asteroid, the shape of the body and its orientation to the line of sight must be known. This enables the effective diameter of the asteroid to be estimated as it rotates.

A fitting procedure was employed to find the reflectance spectra. It was assumed that the reflectance spectrum was a sloping straight line over the last few wavelength points. The thermal model flux was varied (but

keeping the same shape) and the slope of the assumed reflectance spectrum was also varied, until the composite theoretical spectrum best fitted the observed spectrum. Once the best fit had been found, the thermal flux was subtracted from the observed spectrum which was then divided by the solar spectrum (Labs and Neckel, 1970) to give the reflectance spectrum. This was normalized to a relative reflectance of unity at the long wavelength end. Figure 5.1 shows the observed spectra of 15 Eunomia and 433 Eros together with the thermal and solar components and the calculated best-fitting spectrum. The thermal component of 433 Eros is considerably greater than for 15 Eunomia. This is because Eunomia was twice as far from the Sun as Eros and thus at a lower temperature. Table 5.1 gives the data for each asteroid observed. This Table also includes (i) the total integration time for each wavelength point for each asteroid, (ii) the star used to remove the atmospheric absorption and (iii) the black-body temperature assumed for that star.

The reflectance spectra for the eleven asteroids are shown in Figures 5.2 - 5.6. Of these asteroids, only 1 Ceres and 2 Pallas have previously been shown to have an absorption feature at  $3\mu\text{m}$  (Lebofsky, 1980). This result is confirmed by the spectra in Figure 5.2. However, there is a difference between the two results, since the data presented here show a much deeper absorption for Ceres than Lebofsy et al. (1981) found. They are, however, closer to the earlier results of Lebofsky (1978; 1980). If this discrepancy is not real, then the error must occur either in the removal of the thermal

Table 5.1 3 - 4 $\mu$ m Spectra data.

Ast.	Date	Class.	r	$\Delta$	$\alpha$	Int. time.	Star	Temp.
	1983		(AU)	(AU)	(deg)	(sec)		(K)
1	Jan 13	C	2.614	2.780	20.7	20	SAO139830	9850
2	Jan 13	U	2.282	1.983	25.4	20	SAO139830	9850
8	Jan 13	S	1.996	1.085	14.5	30	SAO094566	10600
10	Jan 11	C	3.296	2.331	3.9	20	BS4356	9850
10	Jan 12	C	3.296	2.327	3.5	40	SAO076126	12200
10	Jan 13	C	3.295	2.323	3.2	30	SAO097628	9120
15	Jan 12	S	2.326	1.462	14.6	20	SAO076126	12200
16	Jan 11	M	3.182	2.533	15.0	30	BS4356	9850
22	Jan 12	M	2.624	1.886	16.8	40	SAO076228	11300
83	Jan 13	C	2.366	1.396	5.0	60	SAO080113	10600
386	Jan 13	C	2.754	1.838	9.1	60	SAO134330	9850
433	Jan 14	S	1.150	0.313	51.1	20	SAO076126	12200
471	Jan 13	S	2.393	1.530	14.1	40	SAO076126	12200

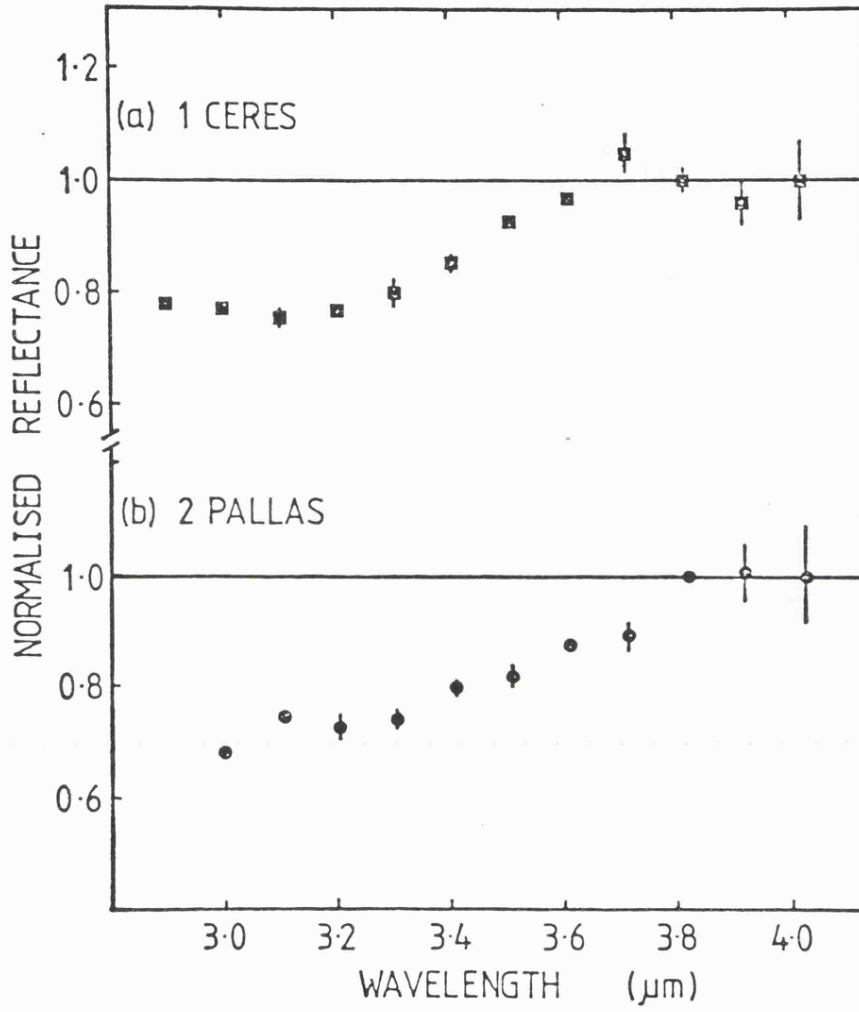


Figure 5.2 The 2.9 - 4.0μm reflectance spectra of a) 1 Ceres and b) 2 Pallas. The normalization procedure is described in the text. Error bars are standard error of the mean.

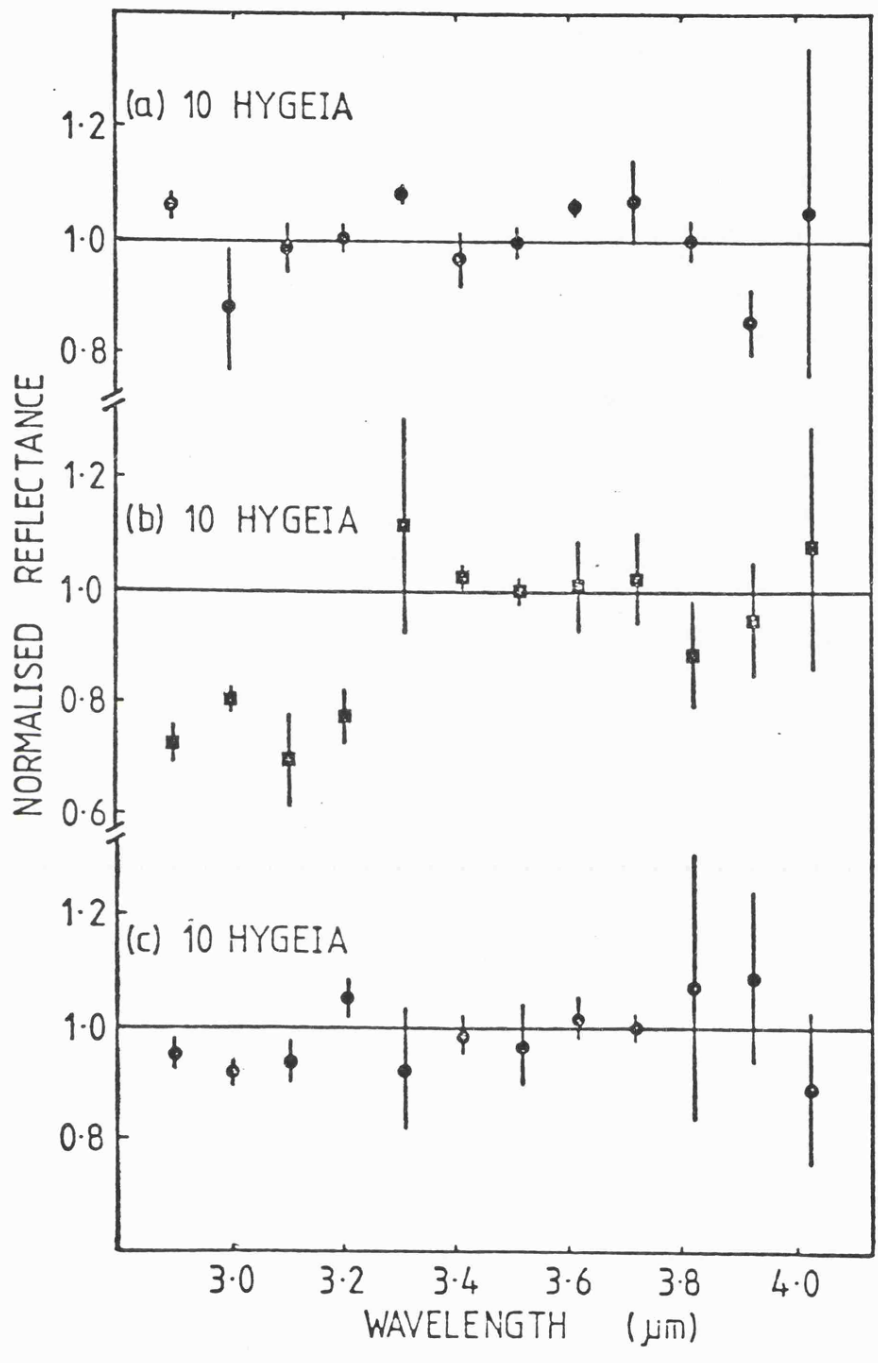


Figure 5.3 Same as Figure 5.2 but for the C-class asteroid 10 Hygeia. The observations were obtained on three separate nights.

component, or in the temperature assigned to the star used to eliminate the atmospheric absorption. The former possibility is more likely, since observations were made at large phase angles which may affect the accuracy of the standard model. None of the other three C-class asteroids (Figure 5.3) show any definite absorption features, although the data for 386 Siegena do not rule out the possibility of a small feature. One of the three spectra of 10 Hygeia (Figure 5.4) shows an apparent absorption feature, but this may be due to cirrus cloud.

Neither of the M-class asteroids (16 Psyche and 22 Kalliope) shown in Figure 5.5 exhibit an absorption feature. The spectrum of 8 Flora (Figure 5.6) does not resemble the featureless spectra of the other S-class asteroids and is superficially similar to those of Ceres and Pallas. However, the spectrum of 8 Flora is probably best explained as a continuation of the reddening which is seen in its 2.0 - 2.5 $\mu$ m spectrum (Feierberg et al., 1982), rather than due to the 3.0 $\mu$ m absorption band of water of hydration. Feierberg et al. (1982) subclassified S-class asteroids into nine groups (a-i). Flora was placed in the small f-group, which was described as "rather red". Of the other asteroids observed, 15 Eunomia is listed as belonging to group h and 433 Eros to group i; 471 Papagena was not listed, but falls into one of the groups a, c or i. Thus a sloping spectrum in the 2.9 - 4.0 $\mu$ m region may be a characteristic of the f group and could be used to identify other asteroids of this group.

The spectra of all the S- and M-class asteroids

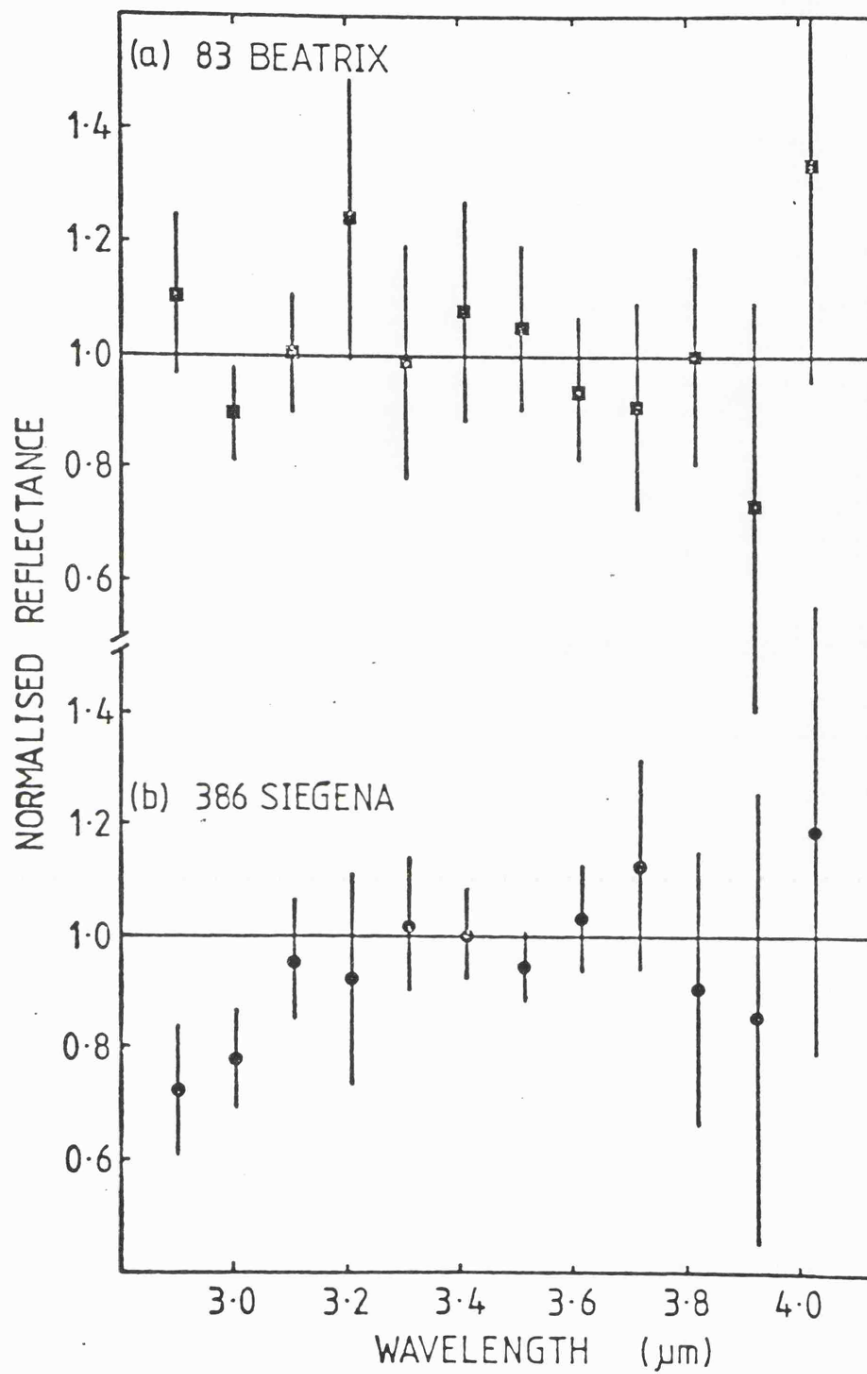


Figure 5.4 Same as Figure 5.2 but for the C-class asteroids  
 a) 83 Beatrix and b) 386 Siegena.

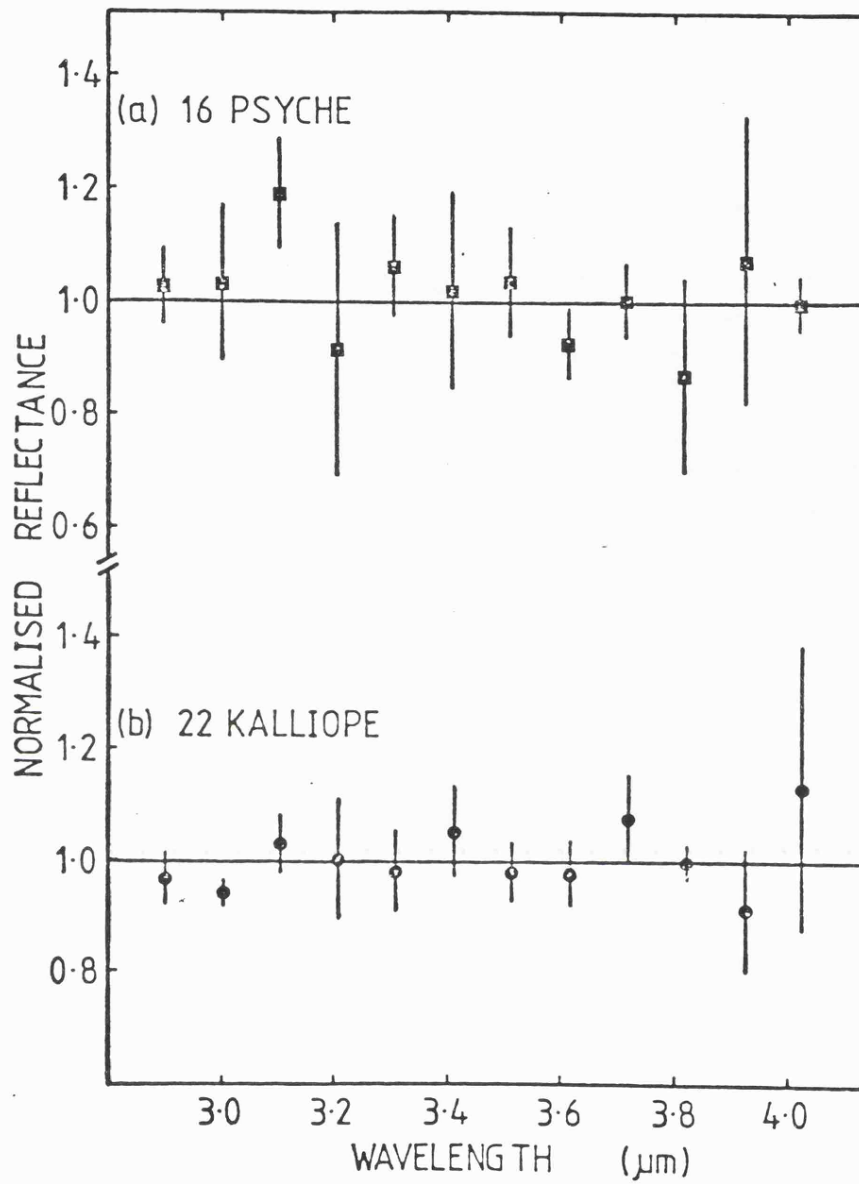


Figure 5.5 Same as Figure 5.2 but for the M-class asteroids  
 a) 16 Psyche and b) 22 Kalliope.

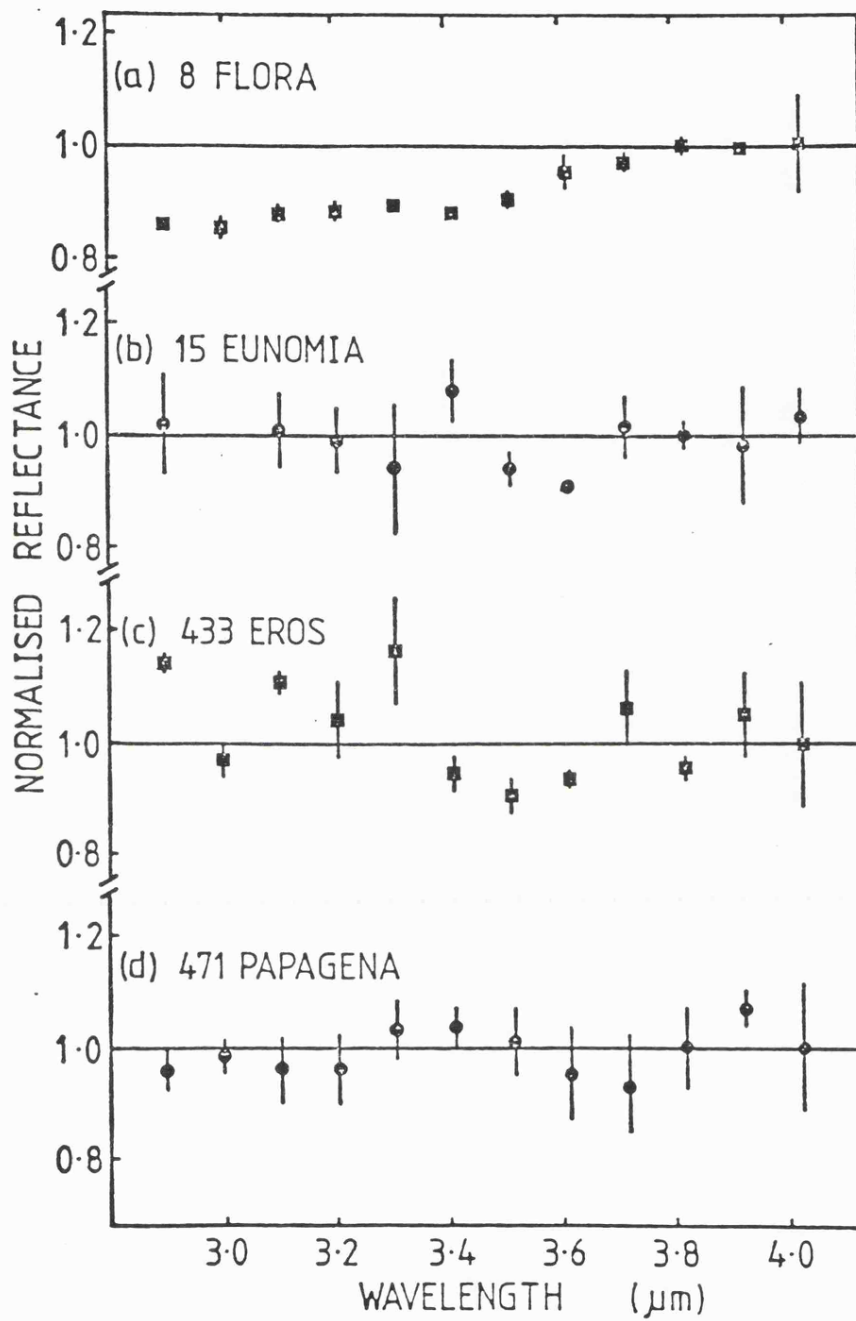


Figure 5.6 Same as Figure 5.2 but for the S-class asteroids  
 a) 8 Flora, b) 15 Eunomia, c) 433 Eros and  
 d) 471 Papagena.

observed are featureless in the region 2.9 - 4.0 $\mu$ m. 8 Flora appears to be different from the other S-class asteroids since its spectrum has a red slope of  $\sim 18\%$ . (None of the calibration stars had slopes differing more than 7% from that of BS1140, which has a spectral class of B7IV.) Of the three C-class objects which have not previously been observed in this region, none showed definite evidence of an absorption feature. Only 1 Ceres and 2 Pallas definitely exhibited the 3 $\mu$ m absorption of water of hydration seen previously by Lebofsky (1980). The 3 - 4 $\mu$ m spectra of asteroids offer the possibility of subclassifying the major divisions of asteroids, since it is apparent that not all C-class asteroids have the 3 $\mu$ m absorption band and that there are differences between the S-class asteroids observed. Possible targets for further observations could be asteroids which fall close to 8 Flora in the dendrograms of Chapter 2. Asteroids which are linked closely to Ceres and Pallas in the dendrograms may also have an 3 $\mu$ m absorption feature in their spectra. If the exact depth and width of the absorption band are to be precisely determined, then it is necessary to calculate accurately the thermal component of the asteroid's spectrum. This necessitates knowing the albedo, shape and, ideally, the position of the asteroid's rotation axis, all of which affect the nature of the thermal emission.

#### THE STANDARD THERMAL MODEL

Accurate calculation of the emitted thermal spectrum necessitates knowledge of the asteroid's diameter and the temperature variation across its surface. The temperature

distribution is dependent on many factors: distance from the Sun, bolometric Bond albedo, rotation period, emissivity and conductivity of the surface, shape of the asteroid and the orientation of the rotation axis. The thermal flux observed is also dependent on the Earth-asteroid distance and the phase angle at which the asteroid is observed. Of all these parameters, only the distances and phase angle are accurately known (with the exception of the rotation period for some asteroids). Thus it is necessary to adopt a model of the thermal emission from an asteroid in order to calculate the observed thermal flux. The model used to remove the thermal component from the 3 - 4 $\mu$ m spectra above was the standard thermal model (Morrison and Lebofsky, 1979). This model is also used as a comparison for the IRAS AO data of 44 Nysa (see below).

The standard thermal model assumes that the asteroid is spherical and that each element of its surface is in instantaneous equilibrium with its surroundings. Thus, for a given surface element of area  $dE$  the energy absorbed is equal to the energy emitted:

$$(1-A) S dE \cos\theta \cos\varphi r^{-2} = \epsilon \sigma T^4 dE \quad (5.2)$$

where  $A$  = bolometric Bond albedo

$S$  = solar constant at 1AU = 1360  $Wm^{-2}$

$r$  = Sun-asteroid distance in AU.

$\epsilon$  = emissivity of asteroid surface

$\sigma$  = Stefan-Boltzmann constant

$T$  = surface temperature of an element of area

( $\theta, \varphi$ ) are introduced as the astero-centric longitude and latitude of the surface element. This coordinate system has sub-solar and sub-Earth points at  $0^\circ, 0^\circ$  on the equator, ie. at zero phase angle. The maximum temperature on the surface is at the sub-solar point and is given by

$$T_{\max}^{\dagger} = \frac{(1-A) S}{\epsilon \sigma r^2} \quad (5.3)$$

and the temperature of any surface element is

$$T^{\dagger} = T_{\max}^{\dagger} \cos\theta \cos\varphi \quad (5.4)$$

The assumption that an element is in instantaneous equilibrium implies that the surface has a low thermal inertia, ie. (i) the material heats up and cools down rapidly, and (ii) no energy is conducted to adjacent elements, nor into the interior of the asteroid. It also implies that there is no internal heat source. Equation 5.4 is only valid for elements on the illuminated hemisphere. For an element on the dark side of the asteroid, the incoming solar radiation is zero and thus its temperature is also zero. Thus the model assumes that there is no radiation from the dark side. In reality, the temperature of the dark side will be lower than the illuminated side, but it will not be zero and will thus contribute to the observed flux. The contribution will be most evident at long wavelengths due to the lower temperatures involved. Several factors affect the temperature of the dark side. As has already been mentioned, the thermal inertia affects the dark-side contribution; in

addition, the period of rotation and the positioning of the rotation axis also affect the contribution. If the asteroid is a slow rotator, then the surface element crossing the terminator into the dark side will cool (by radiation) within a small fraction of a rotation; whereas on a rapidly rotating body the element will only have a short time to cool before emerging onto the illuminated hemisphere again. This is modified by the orientation of the rotation axis. If, for example, the axis points towards the Sun, then the dark side is never illuminated (until the asteroid moves around its orbit). Thus the dark-side temperature will be much lower than if the pole had been at  $90^\circ$  to Sun-asteroid direction. The final factor affecting the amount of radiation observed from the dark side is the phase angle. If  $\alpha=0^\circ$ , then there is no contribution, since the dark side cannot be seen. If  $\alpha \neq 0^\circ$ , then there are two possibilities: either the surface has just entered the unilluminated hemisphere (evening), or it is just about to leave it (morning). The temperature of the surface in the evening will be higher and thus give a higher contribution than the morning side. However, the difference between the morning and evening side of an asteroid are small, and usually lost in the noise of the signal.

The bolometric Bond albedo,  $A$ , is the ratio of the total incident radiation to the total reflected radiation integrated over all wavelengths and over the entire surface of the object. The Bond albedo is related to the geometric albedo,  $p$ , by the phase integral,  $q$ .

$$A = \overline{q(\lambda)p(\lambda)} \quad (5.5)$$

The phase integral is unknown, but the model assumes that  $q=0.6$ . For low-albedo objects, the emitted radiation is insensitive to the value of  $q$  chosen. The emissivity of asteroid surfaces is also unknown. However, the emissivity of natural dielectric materials at infrared wavelengths is  $\approx 0.9$ ; this is the value adopted in the standard model.

Integrating Equation 5.2 over the whole asteroid gives

$$\pi R^2 (1-A) S r^{-2} = \beta \epsilon \sigma R^2 \int_0^{2\pi} \int_{-\pi/2}^{\pi/2} T^4(\theta, \varphi) \cos \varphi d\theta d\varphi \quad (5.6)$$

where  $R$  is the diameter of the asteroid and  $\beta$  is a modelling constant. This constant allows for the enhanced emission at small phase angles (as seen for the Moon) and for departures from the adopted temperature distribution. Morrison adopted  $\beta \approx 0.9$  to calculate the diameters of the larger asteroids; his results were in agreement with the diameters found by stellar occultations. This value is used in the model. Since asteroids are rarely observed at zero phase, it is necessary to reduce the infrared flux, assuming a phase coefficient of 0.01 mag/deg. Finally, deviations from a spherical body will affect the total flux emitted, since the effective diameter of the asteroid is larger when it is observed at a maximum in its lightcurve. Thus allowances must be made for the level of the theoretical thermal spectrum when comparing it with an observed flux. This is especially true for asteroids which exhibit large lightcurve amplitudes. The shape of the body may also affect the shape of the

spectrum, since an ellipsoid at maximum brightness will have a greater proportion of its surface at a higher temperature, when compared to a sphere.

If the surface element radiates as a black body, then the flux observed for a given asteroid is

$$F(\lambda) = \frac{2\pi r^2 \epsilon}{\Delta^2} \int_0^{\pi/2} B(\lambda, T(\zeta)) \sin\zeta \cos\zeta d\zeta P \quad (5.7)$$

$$2.5 \log P = 0.01\alpha$$

where  $\zeta$  is half the angle subtended by an elemental ring, centred on the sub-solar point, as viewed from the centre of the asteroid.  $P$  is the correction due to non-zero phase angle,  $\alpha$ .  $\Delta$  is the Earth-asteroid distance.

#### IRAS OBSERVATIONS OF 44 NYSA

A total of seven observations of 44 Nysa were made over a period of two days under the UK Guest Observer programme using IRAS. The IRAS satellite has been described by Neugebauer et al. (1984). The observations were obtained with the satellite in deep sky mapping mode and the results were processed at the Jet Propulsion Laboratory. The observations have been calibrated using the June 1984 IRAS absolute calibration. This incorporates a correction for the non-linear load resistor. The calibration is probably accurate to 5% at 12 and 25 $\mu$ m and 10% at 60 and 100 $\mu$ m.

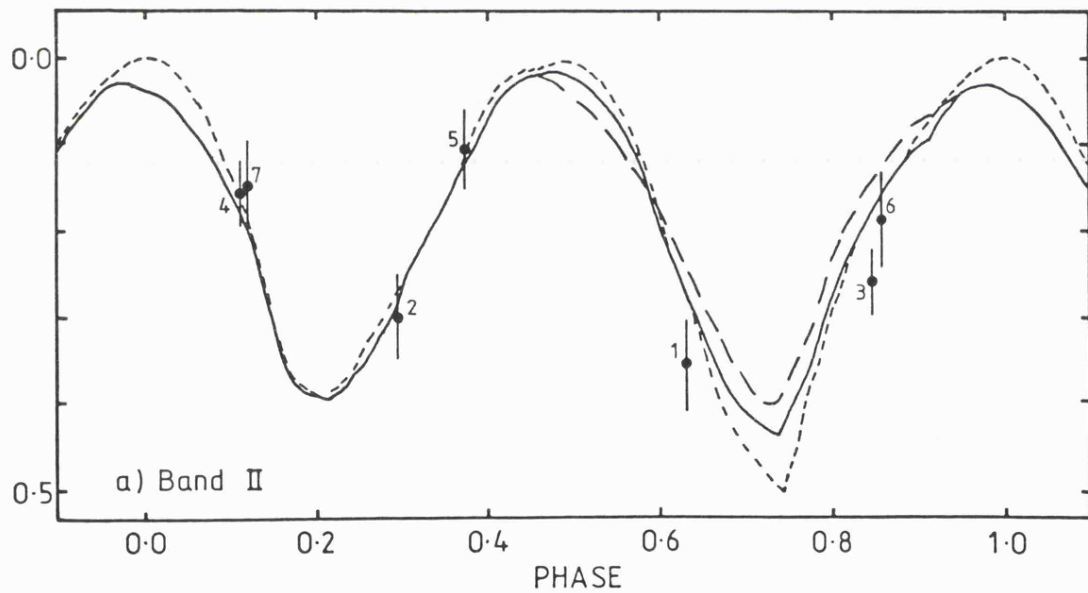
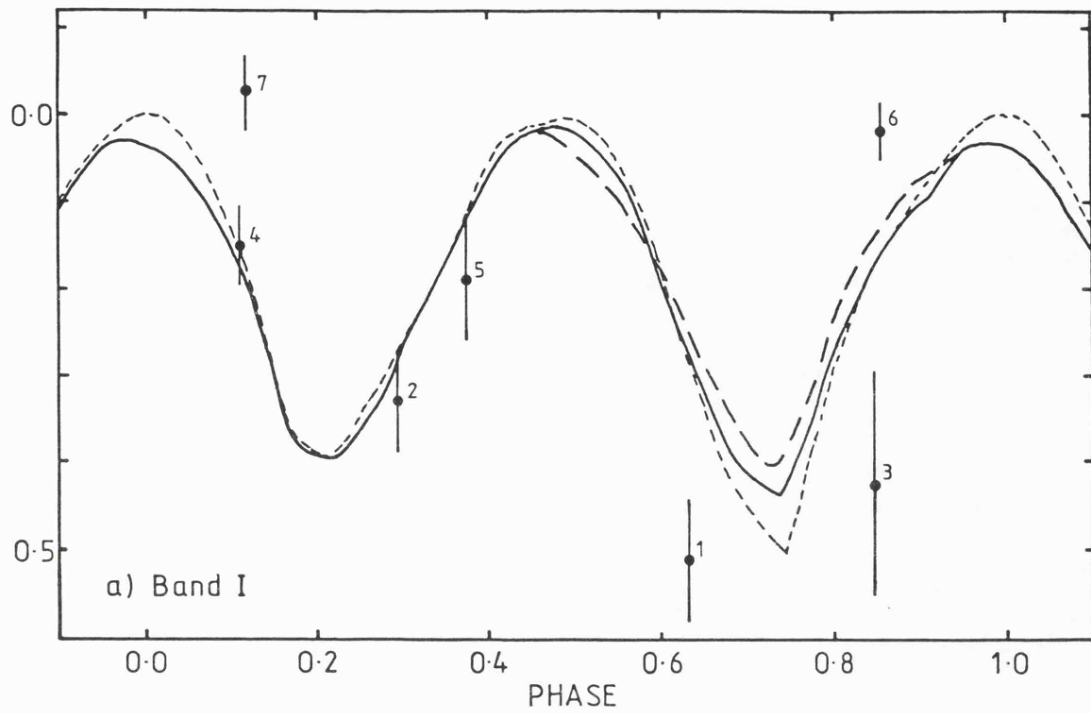


Figure 5.7 Points are IRAS data for a) band I,  $12\mu\text{m}$  and b) band II,  $25\mu\text{m}$ . The numbers indicate the time sequence of the observations. The solid curve is a V lightcurve obtained from SAAO, short broken curve was obtained from Tenerife and the long broken curve is from Di Martino.

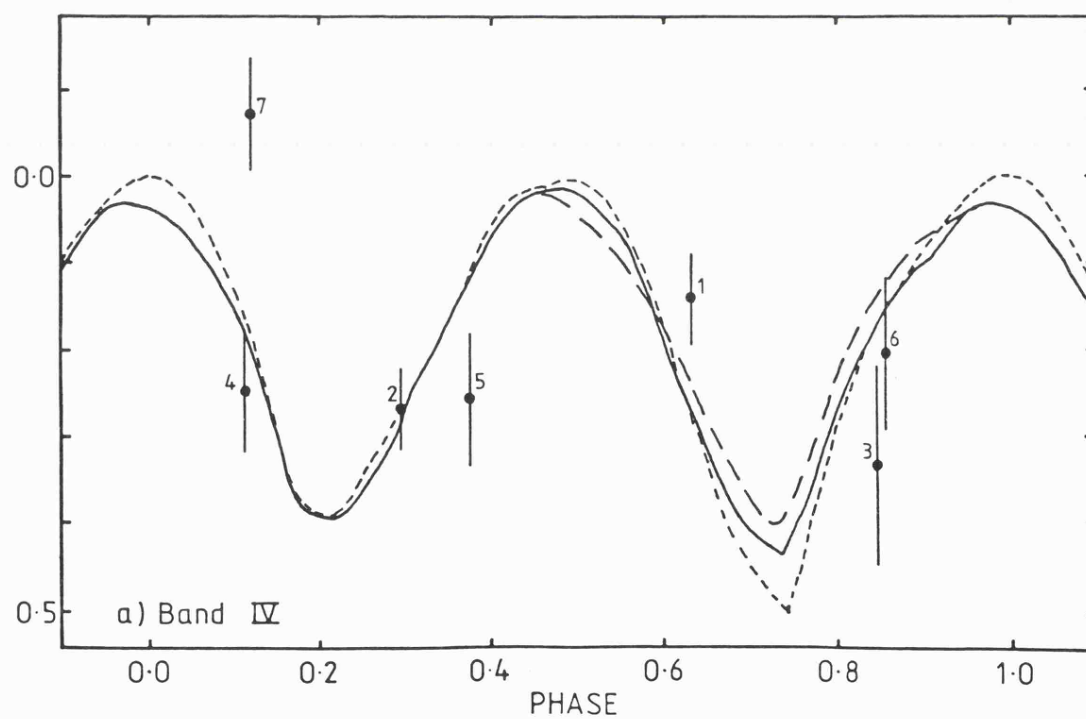
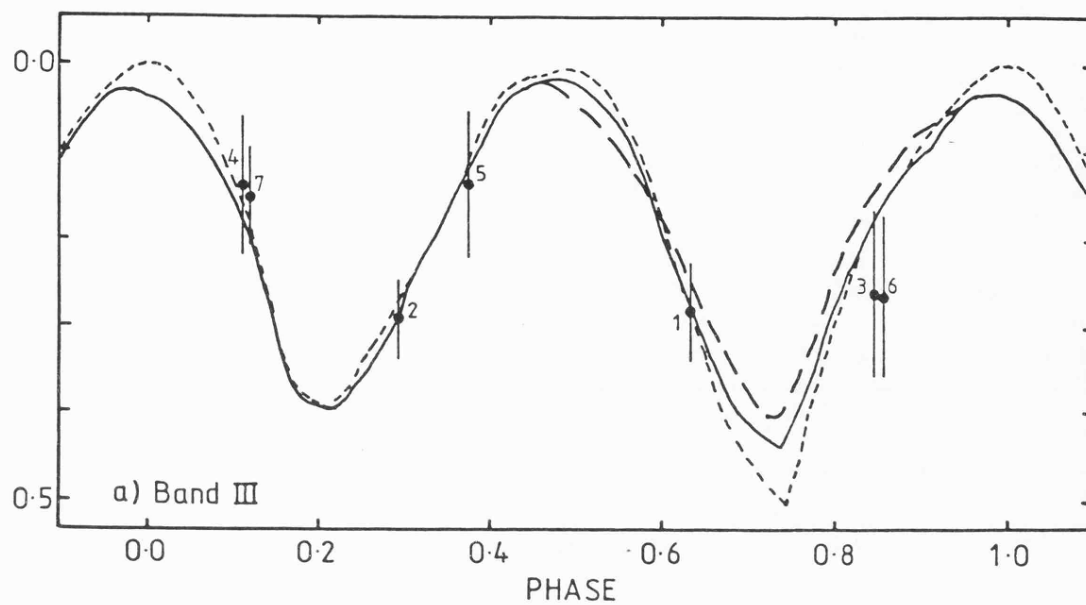


Figure 5.8 Same as for Figure 5.7 but for a) band III, 60μm and b) band IV, 100μm.

The folded IRAS data points are shown in Figures 5.7 and 5.8 as the solid symbols with error bars. The curves drawn through the infrared data represent three visible lightcurves which were obtained at the 1983 opposition. (Two are presented in Chapter 3, the third is from Di Martino, private communication.) Calculating the phase of observations separated by many weeks is not the simple matter of counting sidereal periods as used for the lightcurves of Chapter 3. The observed synodic rotational period of the asteroid is dependent on its motion across the sky. For 44 Nysa the relation is linear with a slope of  $0.00012\text{day}^2/\text{deg}$ . (Taylor and Tedesco, 1983). The synodic period is equal to the sidereal period when the observed motion is zero. When counting periods over intervals exceeding several weeks, it is necessary to calculate the mean synodic period from the mean motion. The dates in Table 5.2 are convenient zero points ( $0^h$  on the date given) from which to fold each set of data and to calculate the motions and, hence, synodic periods. Note that the four sets of data (IRAS plus three visible lightcurves) are individually folded with the sidereal period of 0.267581 days, (Taylor and Tedesco, 1983). It is necessary to correct for the change in light-travel time (Earth-asteroid distance), since it changes by  $\sim 0.01$  of a period between the IRAS observations and the visible lightcurves.

The band II and III data follow the optical lightcurves most accurately, with good agreement between data obtained at the same rotational phase. Bands I and IV show considerable scatter about the lightcurve and poor consistency. This is

Table 5.2 Lightcurve data

Lightcurve	Date	R.A.	Dec.	r	$\Delta$	$\alpha$	$\lambda$	$\beta$
	1983	(1950)		AU	AU	deg	deg	deg
IRAS	14 Aug	2 23 45	10 03 21	2.427	1.990	23.8	37.0	-4.0
SAAO	4 Oct	2 30 39	8 31 00	2.343	1.405	11.0	38.1	-6.0
Di Martino	11 Oct	2 26 35	7 59 25	2.332	1.368	8.3	37.0	-6.2
Tenerife	28 Nov	1 46 57	4 41 40	2.247	1.407	16.8	26.5	-5.9
	$\delta$ days	$\delta\lambda$	Motion	$P_{syn}$	$\delta\Delta$	Travel time		
		deg	deg/day	days	AU	(phase)		
SAAO	51	1.1	0.0220	0.267584	0.5855	0.0126		
Di Martino	58	0.0	0.0000	0.267581	0.6214	0.0134		
Tenerife	106	-10.5	-0.0986	0.267569	0.5826	0.0126		

due, in one case, to the low signal at 100 $\mu\text{m}$  and, in the other, to the noisy band I detectors. A more desirable distribution of the infrared data would have been with points close to the maxima and minima of the visible lightcurve. However, the timing of the observations is strictly limited by the satellite, which can only observe a particular object for a small fraction of each orbit. Thus an object can be observed once per orbit ( $\sim 100$  minutes). A better distribution would have enabled differing effective diameters to be calculated via radiometry, which could then have been compared with the shape derived in Chapter 4.

Table 5.3 Monochromatic corrections and thermal model fluxes

Band	$\lambda$ $\mu\text{m}$	$\Delta\lambda$ $\mu\text{m}$	$\Delta f$	$\Delta\lambda/\Delta f$	Model flux $\times 10^{-15} \text{ Wm}^{-2} \mu\text{m}^{-1}$
I	12	6.1	1.08	0.177	67.25
II	25	12.5	1.07	0.086	29.64
III	60	34.9	1.02	0.029	2.382
IV	100	35.2	1.01	0.029	0.3967

$\Delta f$  is a colour correction between 300K and the effective temperature of the asteroid.

Before the IRAS observations can be compared with the fluxes predicted by the thermal model, it is necessary to correct the broadband fluxes to monochromatic fluxes. To calculate these corrections requires knowledge of the asteroid spectrum. This was approximated by a black-body

spectrum with an effective temperature  $0.9T_{\text{max}}$ . The difference between these corrections and those given for a 300K black body by Neugebauer et al. (1984) are small and are not very sensitive to the temperature chosen for the black body. The thermal model fluxes have been calculated using an observing geometry for 44 Nysa corresponding to that encountered at the midpoint of the IRAS observations. This geometry corresponds to: R.A. =  $2^{\text{h}}24^{\text{m}}53^{\text{s}}.27$ ; Dec. =  $10^{\circ}5'46''.7$ ;  $r = 2.42802\text{AU}$ ;  $\Delta = 1.96959\text{AU}$ ; phase =  $23^{\circ}.448$ ;  $\lambda = 36^{\circ}.95$ ;  $\beta = -4^{\circ}.01$ . The monochromatic corrections and the thermal model fluxes are given in Table 5.3. The albedo of Nysa was taken as 0.48 (Morrison and Zellner, 1979) and its diameter as 69km (Bowell et al., 1979). The corrected fluxes and the ratios with the predicted fluxes are given in Table 5.4.

Inspection of the ratios of observed to predicted fluxes shows that band I has the lowest ratio. This increases to a highest value at band IV for all seven observations. The majority of the ratios are greater than unity, indicating that IRAS observed more flux than expected. This excess flux cannot be explained by an incorrect diameter for 44 Nysa, since this would affect all wavelengths equally. A possible source of the extra radiation is emission from the dark side of the asteroid. An estimate of the amount of radiation emitted from the unilluminated portion of the disc can be made by assuming it to radiate as a black body with a temperature of 100K. The effect of this radiation is to reduce the ratios in Table 5.4 by 0.03, 0.14 and 0.21 at 25, 60 and  $100\mu\text{m}$ , respectively. (Note that there is now an imbalance in the energy absorbed and emitted.) Thus it is

Table 5.4 IRAS fluxes

JD	Phase	Band I		Band II		Band III		Band IV					
		Flux $\times 10^{-15}$ $\text{Wm}^{-2} \mu\text{m}^{-1}$	Error %	Ratio	Flux $\times 10^{-15}$ $\text{Wm}^{-2} \mu\text{m}^{-1}$	Error %	Ratio	Flux $\times 10^{-15}$ $\text{Wm}^{-2} \mu\text{m}^{-1}$	Error %	Ratio			
2445000+		48.8	6.7	0.73	30.3	5.1	1.02	2.96	5.5	1.24	0.791	5.2	1.99
1 560.9361	1.623	48.8	6.7	0.73	30.3	5.1	1.02	2.96	5.5	1.24	0.791	5.2	1.99
2 561.6490	4.294	58.0	5.7	0.86	31.9	4.8	1.08	2.93	4.2	1.23	0.701	4.6	1.77
3 561.7963	4.845	52.8	13.1	0.78	33.2	3.7	1.12	3.02	9.4	1.27	0.659	11.5	1.66
4 561.8675	5.111	68.6	4.3	1.02	36.5	3.8	1.23	3.38	7.8	1.42	0.716	7.1	1.80
5 561.9379	5.374	66.1	6.8	0.98	38.3	4.3	1.29	3.39	8.2	1.42	0.708	7.5	1.78
6 562.8695	8.856	77.4	3.3	1.15	35.5	5.4	1.20	3.01	9.0	1.26	0.744	8.6	1.87
7 562.9398	9.119	81.1	4.3	1.21	36.8	5.1	1.24	3.34	5.5	1.40	0.967	6.5	2.44

apparent that dark side radiation cannot explain the discrepancy between the observed and predicted fluxes. Another possibility for the extra long wavelength radiation is that the emissivity of the surface is a function of wavelength. By varying the emissivity, the shape of the spectrum can be changed to fit the observations.

## DISCUSSION

It appears from the IRAS data that the thermal emission from asteroids is not in agreement with the standard model, even at 12 and 25 $\mu$ m. This is in contrast to results obtained from ground-based observations, which support the validity of the standard model at 10 and 20 $\mu$ m (Morrison and Lebofsky, 1979). Recent work by LeVan and Price (1984) at 85 $\mu$ m suggested that the observed flux, for the asteroids 2, 15, 27 and 45, was a factor 2 or 3 lower than that predicted by the model: this is the opposite to the results obtained by IRAS. Unfortunately, the processing of the IRAS data presented above is not uniform. AOs after Satellite Operation Program (SOP) 404 have better calibration than those obtained on previous SOPs, in particular, band I has not had a 10% correction applied to pre-SOP 404 data. Examination of the last two AOs (SOP 405) shows that the data for bands I, II and III fit the standard model, if a contribution is included from the dark-side. However, band IV continues to be in excess of model predictions. The ratio of band II to band III fluxes is reasonably constant, given the errors. Thus the standard model plus dark-side emissions appears on this analysis to agree with observations out to 60 $\mu$ m. This will

need to be checked when the final processed data is available.

The 3 - 4 $\mu$ m reflectance spectra show the importance of accurate thermal modelling if the spectra are to be used to determine the composition of the surface. Theoretically, the shape of the emission spectrum is dependent on factors not taken into account by the simple model, such as rotation and pole orientation. However, these only significantly affect the long wavelength emissions. Measurements beyond  $\sim$ 20 $\mu$ m are, at present, not of a sufficient accuracy to detect the differences between the standard model and a more realistic model (except in the case of dark-side emissions). This situation may improve with the intended launch of the Infrared Satellite Observatory by the European Space Agency. This does not prevent the reflectance spectra from being used to extend the classification schemes already in use, since the standard model is quite accurate in producing the shape of the thermal spectrum at the shorter wavelengths.

## *REFERENCES*

## REFERENCES.

- Allen, C. W. (1973). Astrophysical quantities. pp162. Athlone Press, Univ. of London.
- Allen, D. A. and T. A. Cragg (1983) The AAO JHKL' photometric standards. MNRAS 203, 777-783.
- Baier, G. and G. Weigelt (1983). Speckle interferometry observations of the asteroids Juno and Amphitrite. Astron. Astrophys. 121, 137-141.
- Barucci, M. A. (1983). Estimate of the shape and pole coordinates for the asteroid 41 Daphne. Astron. Astrophys. Suppl. 54, 471-473.
- Barucci, M. A., and A. Dipaoloantonio (1983). A check for the pole coordinate of asteroid 22 Kalliope. Astron. Astrophys. 117, 1-2.
- Barucci, M. A. and M. Fulchignoni (1982). The dependence of asteroid lightcurves on the orientation parameters and the shapes of asteroids. Moon and Planets 24, 47-57.
- Barucci, M. A. and M. Fulchignoni (1983). On the inversion of asteroidal lightcurve functions. In Asteroids, comets, meteors (C. I. Lagerkvist and H. Rickman, eds.) pp.101-105. Uppsala Universitat Reprocentralen HSC, Uppsala.
- Binzel, R. P. (1984). 2 Pallas: 1982 and 1983 lightcurves and a new pole solution. Icarus 59, 456-461.

- Birch, P. V., E. F. Tedesco, R. C. Taylor, R. P. Binzel, C. Blanco, S. Catalano, P. Hartigan, F. Scaltriti, D. J. Tholen and V. Zappalà (1983). Lightcurves and phase function of asteroid 44 Nysa during its 1979 apparition. *Icarus* 54, 1-12.
- Blanco, C. and S. Catalano (1979). UBV photometry of Vesta. *Icarus* 40, 359-363.
- Bowell, E. and K. Lumme (1979). Colorimetry and magnitudes of asteroids. In *Asteroids* (T. Gehrels ed.) pp.132-169. Univ. of Arizona Press, Tucson.
- Bowell, E., C. R. Chapman, J. C. Gradie, D. Morrison and B. Zellner (1978). Taxonomy of asteroids. *Icarus* 35, 313-335.
- Bowell, E., T. Gehrels and B. Zellner (1979). Magnitudes, colors, types and adopted diameters of the asteroids. In *Asteroids* (T. Gehrels ed.) pp.1108-1129. Univ. of Arizona Press, Tucson.
- Burchi, R. and L. Milano (1974). Photoelectric lightcurves of the minor planet 43 Ariadne during the 1972 opposition. *Astron. Astrophys. Suppl.* 15, 173-180.
- Burns, J. A. and E. F. Tedesco (1979). Asteroid lightcurves: Results for rotations and shapes. In *Asteroids* (T. Gehrels ed.) pp.494-527. Univ. of Arizona Press, Tucson.
- Chang, Y. C. and C. S. Chang (1962). Photometric investigations of seven variable asteroids. *Acta Astron. Sin.* 10, 101-111.
- Chang, Y. C. and C. S. Chang (1963). Photometric observations of variable asteroids, II. *Acta Astron. Sin.* 11, 139-149.

- Chang, Y. C., X. Y. Yang, Y. Y. Zhang, X. Q. Li and Z. X. Wu (1981). Lightcurves of variable asteroids, IV. Acta Astron. Sin. 22, 169-173.
- Chapman, C. R. (1971). Surface properties of asteroids. Ph.D. Thesis, Massachusetts Institute of Technology.
- Chapman, C. R. and M. J. Gaffey (1979). Reflectance spectra of 277 asteroids. In Asteroids (T. Gehrels ed.) pp.655-687. Univ. of Arizona Press, Tucson.
- Chapman, C. R., T. B. McCord and T. V. Johnson (1973). Asteroid spectral reflectivities. Astron.J. 78, 126-140.
- Chapman, C. R., D. Morrison and B. Zellner (1975). Surface properties of asteroids: A synthesis of polarimetry, radiometry and spectrophotometry. Icarus 25, 104-130.
- Chapman, C. R., J. G. Williams and W. K. Hartmann (1978). The asteroids. Ann. Rev. Astron. Asrtophys. 16, 33-75.
- Degewij, J. and C. J. van Houten (1979). Distant asteroids and outer Jovian satellites. In Asteroids (T. Gehrels ed.) pp.417-435. Univ. of Arizona Press, Tucson.
- Degewij, J., E. F. Tedesco and B. Zellner (1979). Albedo and color contrasts on asteroid surfaces. Icarus 40, 364-374.
- Di Martino, M. and S. Caccatori (1984). Photoelectric photometry of 15 asteroids. Submitted for publication.
- Elias, J. H., J. A. Frogel, K. Matthews and G. Neugebauer (1982). Infrared standard stars. Astron. J. 87, 1029-1034.
- Feierberg, M. A., L. A. Lebofsky and H. P. Larson (1981). Spectroscopic evidence for aqueous alteration products on the surface of low albedo asteroids. Geochim. Cosmochim. Acta 45, 971-981.

- Feierberg, M. A., H. P. Larson and C. R. Chapman (1982). Spectroscopic evidence for undifferentiated S-type asteroids. *Astrophys. J.* 257, 361-372.
- Gaffey, M. J. (1976). Spectral reflectance characteristics of the meteorite classes. *J. Geo. Res.* 81, 905-920.
- Gaffey, M. J. (1983). First "map" of Vesta. *Sky and Telescope* 66, 502.
- Gaffey, M. J. and T. B. McCord (1977). Asteroid surface materials - mineralogical characterizations from reflectance spectra. *Space Science Review* 21, 555-628.
- Gehrels, T. (1956). Photometric studies of asteroids V. The lightcurve and phase function of 20 Massalia. *Astrophys. J.* 123, 331-338.
- Gehrels, T. (1967). Minor planets I. The rotation of Vesta. *Astron. J.* 72, 929-938.
- Gehrels, T. and D. Owings (1962). Photometric studies of asteroids IX. Additional lightcurves. *Astrophys. J.* 135, 906-924.
- Gradie, J. and E. Tedesco (1982). Compositional structure of the asteroid belt. *Science* 216, 1405-1407.
- Groeneveld, I. and G. P. Kuiper (1954a). Photometric studies of asteroids I. *Astrophys. J.* 120, 200-220.
- Groeneveld, I. and G. P. Kuiper (1954b). Photometric studies of asteroids II. *Astrophys. J.* 120, 529-546.
- Hapke, B. W. (1971). Inferences from optical properties concerning the surface texture and compositions of asteroids. In *Physical Studies of Minor Planets* (T. Gehrels ed.) pp.67-80. NASA SP-267, US Government Printing Office, Washington, USA.

- Haupt, H. (1980). Photoelektrische beobachtungen der kleinen planeten (83) Beatrix, (139) Juewa, (349) Dembowska und (389) Industria. Sitzungsberichte der Math. Nat. Klasse der Osterr. Akad. d. Wiss. Abt. II 189, 429-436.
- Johnson, H. L., R. I. Mitchell, B. Irate and W. Z. Wisniewski (1966). UBVRIJKL photometry of the bright stars. Lun. Plan. Lab. Com. 4, 99-110.
- Johnson, T. V., D. C. Matson, G. J. Veeder and S. J. Loer (1975). Asteroids: Infrared photometry at 1.25, 1.65 and 2.2 microns. Astron. J. 197, 527-531.
- Labs, D. and H. Neckel (1970). Transformation of the absolute solar radiation data into the "International Practical Temperature Scale of 1968". Sol. Phys. 15, 79-87.
- Lagerkvist, C. I. (1978). Photographic photometry of 110 main belt asteroids. Astron. Astrophys. Suppl. 31, 361-381.
- Larson, H. P. and G. J. Veeder (1979). Infrared spectral reflectances of asteroid surfaces. In Asteroids (T. Gehrels ed.) pp.724-744. Univ. of Arizona Press, Tucson.
- Larson, H. P., M. A. Feierberg and L.A. Lebofsky (1983). The composition of asteroid 2 Pallas and its relation to primitive meteorites. Icarus 56, 398-408.
- Lebofsky, L. A. (1978). Asteroid 1 Ceres: Evidence for water of hydration. MNRAS 182, 17-21.
- Lebofsky, L. A. (1980). Infrared reflectance spectra of asteroids: A search for water of hydration. Astron. J. 85, 537-585.
- Lebofsky, L. A., M. A. Feierberg, A. T. Tokunaga, H. P. Larson and J. R. Johnson (1981). The 1.7- to 4.2- $\mu$ m spectrum of asteroid 1 Ceres: Evidence for structural water in clay minerals. Icarus 48, 453-459.

- LeVan, P. D. and S. D. Price (1984). 85- $\mu$ m fluxes from asteroids: 2 Pallas, & Iris, 15 Eunomia and 45 Eugenia. *Icarus* 57, 35-41.
- Lupishko, D. F., and I. N. Belskaya (1983). Surface, shape and rotation of the M-type asteroid 16 Psyche from UBV photometry in 1978 and 1979. In *Asteroids, comets, meteors* (C. I. Lagerkvist and H. Rickman eds.) pp.55-61, Uppsala Univesitat Repocentralen HSC, Uppsala.
- Magnusson, P. (1983). Determination of spin axis orientation for asteroids 44 Nysa, 216 Kleopatra and 624 Hektor. In *Asteroids, comets, meteors* (C. I. Lagerkvist and H. Rickman eds.) pp.77-85, Uppsala Univesitat Repocentralen HSC, Uppsala.
- McCord, T. B. and C. R. Chapman (1975). Asteroids: Spectral reflectance and colour characteristics. *Astrophys.J.* 195, 553-562.
- McCord, T. B., T. V. Johnson and J. B. Adams (1970). Asteroid Vesta: Spectral reflectivity and compositional implications. *Science* 168, 1445-1447.
- Morrison, D. (1974). Diameters and albedos of 40 asteroids. *Astrophys.J.* 194, 203-212.
- Morrison, D. and L. A. Lebofsky (1979). Radiometry of asteroids. In *Asteroids* (T. Gehrels ed.) pp.184-205. Univ. of Arizona Press, Tucson.
- Morrison, D. and B. Zellner (1979). Polarimetry and radiometry of the asteroids. In *Asteroids* (T. Gehrels ed.) pp.1090-1097. Univ. of Arizona Press, Tucson.
- Neckel, T. and R. Chini (1980). Sixty faint UBVRi standards. *Astron. Astrophys. Suppl.* 39, 411-414.

- Neugebauer, G., H. J. Harbing, R. van Dainen, H. H. Aumann, B. Baud, C. A. Beichman, D. A. Bentema, N. Bogges, P. E. Clegg, T. de Jong, J. P. Emerson, T. N. Gautier, F. C. Gillett, S. Harris, M. G. Hauser, J. R. Houck, R. E. Jennings, F. J. Low, P. L. Marsden, G. Miley, F. M. Olnon, S. R. Pottasch, E. Raimond, M. Rowan-Robinson, B. T. Soifer, R. G. Walker, P. R. Wesselius and E. Young (1984). The infrared astronomical satellite (IRAS) mission. *Astrophys. J. Let.* 278, L1-L6.
- Sather, R. E. (1976). Minor planets and related objects XIX. Shape and pole orientation of (39) Laetitia. *Astron. J.* 81, 67-73.
- Scaltriti, F. and V. Zappalà (1976). A photometric study of the minor planets 192 Nausikaa and 79 Eurynome. *Astron. Astrophys. Suppl.* 23, 167-179.
- Scaltriti, F. and V. Zappalà (1981). Photometric lightcurves and rotation periods of the asteroids 46 Hestia and 115 Thyra. *Icarus* 46, 275-280.
- Schober, H. J. and A. Scholl (1982). Surface properties of asteroids. In *Sun and planetary system* (W. Fricke and G. Teleki eds.) pp.285-286. D. Reidel Publishing Company.
- Schober, H. J., F. Scaltriti, V. Zappalà and A. W. Harris (1980). The remaining large minor planets with unknown rotation properties: 31 Euphrosyne and 65 Cybele. *Astron. Astrophys.* 91, 1-6.
- Shatzel, A. V. (1954). Photometric studies of asteroids III. The lightcure of 44 Nysa. *Astrophys. J.* 120, 547-550.
- Sherrington, M. S. (1980). Infrared and optical observations of cataclysmic variables. Ph.D. Thesis, Leicester University.

- Sneath, P. H. A. and R. Johnson (1972). The influence on numerical taxonomic similarities of errors in microbiological tests. *J. General Microbiology* 72, 377-392.
- Sokal, R. R. and P. H. A. Sneath (1963). Principles of numerical taxonomy. Freeman, London.
- Stephenson, C. B. (1951). The lightcurve and colour of Vesta. *Astrophys. J.* 114, 500-504.
- Taylor, R. C. (1973). Minor planets and related objects XIV. asteroid 4 Vesta. *Astron. J.* 78, 1131-1139.
- Taylor, R. C. (1977). Minor planets and related objects XXI. Photometry of asteroid 7 Iris. *Astron. J.* 82, 441-444.
- Taylor, R. C. (1979). Pole orientations of asteroids. In *Asteroids* (T. Gehrels ed.) pp.480-493. Univ. of Arizona Press, Tucson.
- Taylor, R. C. and E. F. Tedesco (1983). Pole orientation of the asteroid 44 Nysa via photometric astrometry, including a discussion of the methods application and its limitations. *Icarus* 54, 13-22.
- Tedesco, E. F. and R. E. Sather (1981). Minor planets and related objects: XXIX. Asteroid 29 Amphitrite. *Astron. J.* 86, 1553-1558.
- TRIAD. Zellner, B. (1979). Tucson revised index of asteroid data. In *Asteroids* (T. Gehrels ed.) pp.1011-1013. Univ. of Arizona Press, Tucson.
- Van Houten-Groeneveld, I. and C. J. van Houten (1958). Photometric studies of asteroids VIII. *Astrophys. J.* 127, 253-273.

- Van Houten-Groeneveld, I., C. J. van Houten and V. Zappalà (1979). Photoelectric photometry of seven asteroids. *Astron. Astrophys. Suppl.* 35, 223-232.
- Veeder, G. J., D. L. Matson, C. Kowal and G. Hoover (1982). Infrared (JHK) photometry of asteroids - II. *Astron.J.* 87, 843-839.
- Veeder, G. J., D. L. Matson and J. C. Smith (1978). Visual and infrared photometry of asteroids. *Astron.J.* 83, 651-663.
- Veeder, G. J., D. L. Matson and E. F. Tedesco (1983). The R asteroids reconsidered. *Icarus* 55, 177-180.
- Vesely, C. D. (1971). Summary on orientations of rotation axes. In *Physical studies of minor planets* (T. Gehrels ed.) pp.133-140. NASA SP-267, Washington, D.C., U.S. Government Printing Office, Washington, USA.
- Vogt, N., H. S. Geisse and S. Rojas (1981). Up-to-date UBVRI values for the E-region standard stars. *Astron. Astrophys. Suppl.* 46, 7-11.
- Wamsteker, W. and R. E. Sather (1974). Minor planets and related objects XVII. Five colour photometry of four asteroids. *Astron. J.* 79, 1465-1470.
- Yang, X. Y., Y. Y. Zhang and X. Q. Li (1965). Photometric observations of variable asteroids III. *Acta Astron. Sin.* 13, 66-74.
- Zappalà, V. (1981). A Semi-analytical method for pole determination of asteroids. *Moon and Planets* 24, 319-325.
- Zappalà, V. and Z. Knezevic (1984). Rotation axes of asteroids: Results for 14 asteroids. *Icarus* 59, 476-485.

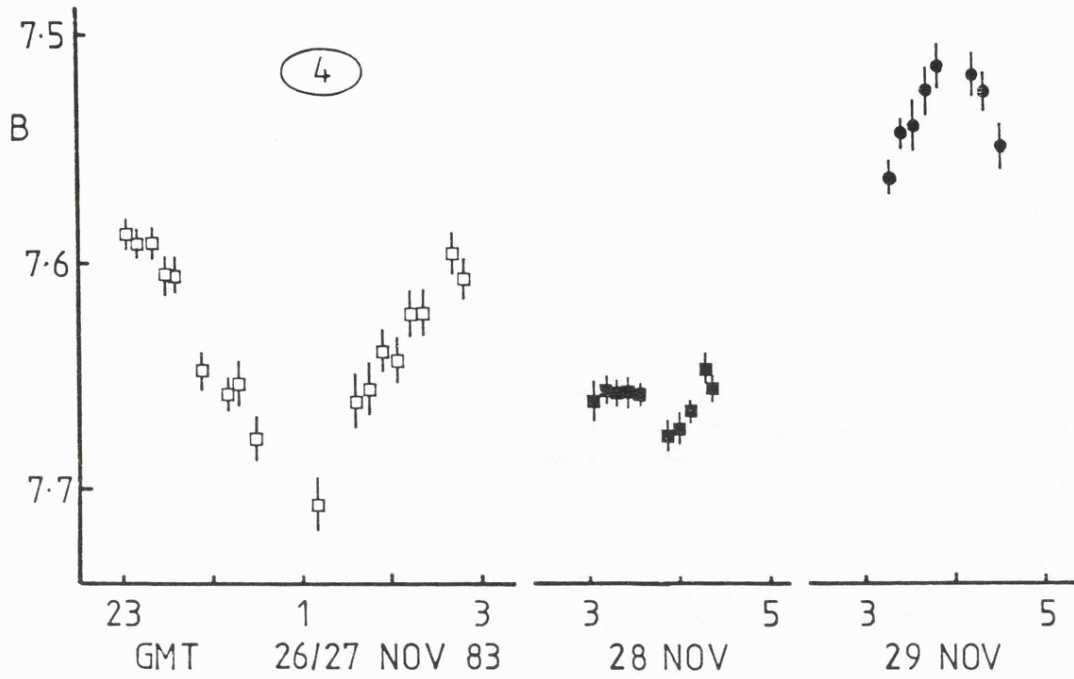
- Zappalà, V., and F. Scaltriti (1982). A coordinated program for pole determination of asteroids. In Sun and planetary systems (W. Fricke and G. Teleki eds.) pp.303-304. D. Reidel Publishing Company.
- Zappalà, V. and I. van Houten-Groeneveld (1979). Pole coordinates of the asteroids 9 Metis, 22 Kalliope, and 44 Nysa. Icarus 40, 289-296.
- Zappalà, V., M. Di Martino, P. Farinella and P. Paolicchi (1983). An analytical method for the determination of the rotational directions of asteroids. In Asteroids, comets, meteors (C. I. Lagerkvist and H. Rickman eds.) pp.73-76. Uppsala Univesitat Repocentralen HSC, Uppsala.
- Zappalà, V., I. van Houten-Groeneveld and C. J. van Houten (1979). Rotation period and phase curve of the asteroids 349 Dembowska and 354 Eleonora. Astron. Astrophys. Suppl. 35, 213-221.
- Zappalà, V., M. Di Martino, P. Farinella and P. Paolicchi (1983). An analytical method for the determination of the rotational directions of asteroids. In Asteroids, comets, meteors (C. I. Lagerkvist and H. Rickman, eds.) pp.73-76. Uppsala Univesitat Repocentralen HSC, Uppsala.
- Zellner, B. (1973). Photometric albedos of asteroids. Bull. Amer. Astron. Soc. 5, 388.
- Zellner, B. (1979). Tucson revised index of asteroid data. In Asteroids (T. Gehrels ed.) pp.1011-1013. Univ. of Arizona Press, Tucson.

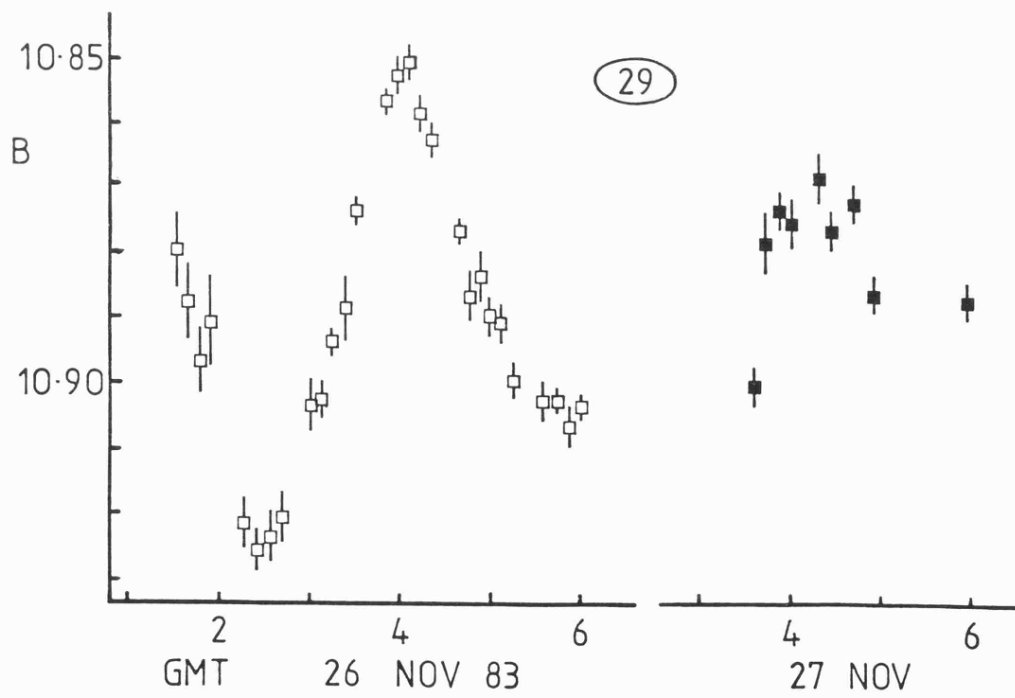
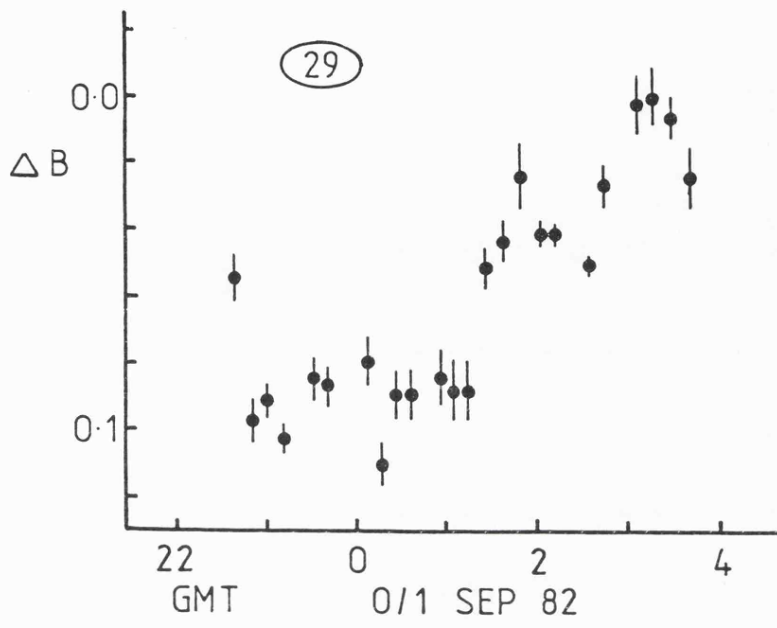
- Zellner, B. and E. Bowell (1977). Asteroid compositional types and their distributions. In Comets, Asteroids and Meteorites (A. H. Delsemme ed.) pp.185-197. Univ. of Toledo, USA.
- Zellner, B., T. Gehrels and J. Gradie (1974). Minor planets and related objects - XVII: Polarmetric diameters. Astron. J. 79, 1100-1110.
- Zellner, B. and J. Gradie (1976). Minor planets and related objects - XX: Polarmetric evidence for the albedos and compositions of 94 asteroids. Astron. J. 81, 262-280.
- Zellner, B., W. Z. Wisniewski and L. Andersson (1975). Minor planets and related objects - XVIII: UBV photometry and surface composition. Astron. J. 80, 986-995.
- Zhou, X. H., X. Y. Yang and Z. X. Wu (1983). Lightcurves of asteroids. Paper IV. Chin. Astron. Astrophys 7, 129-131.

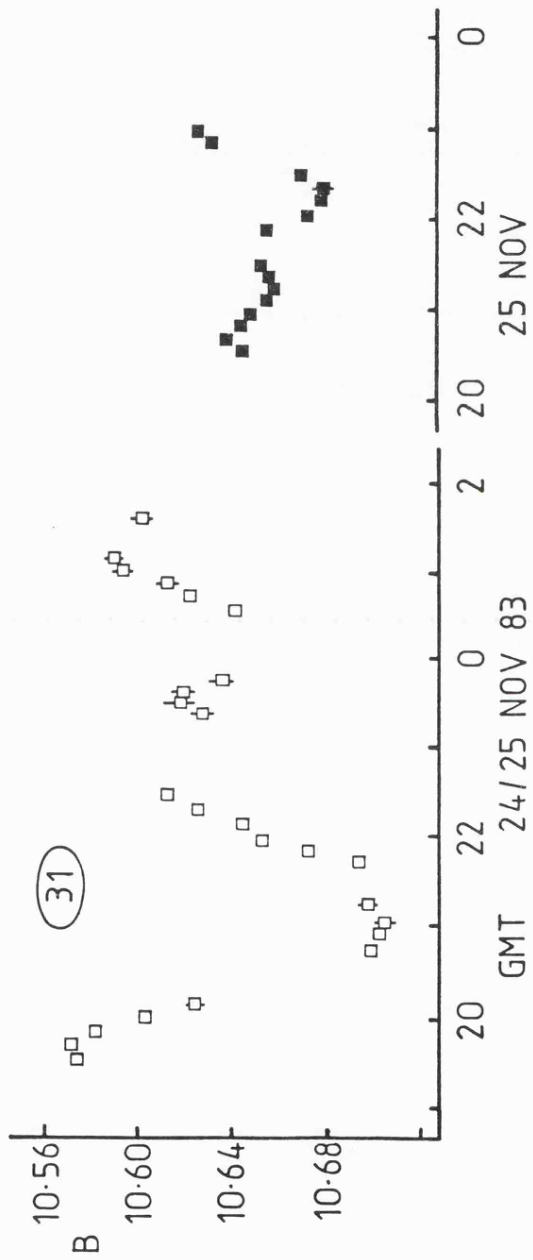
***APPENDIX***

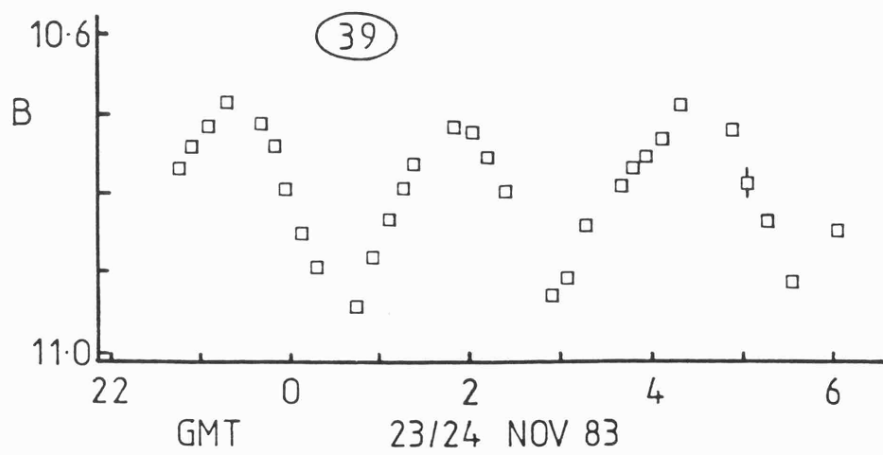
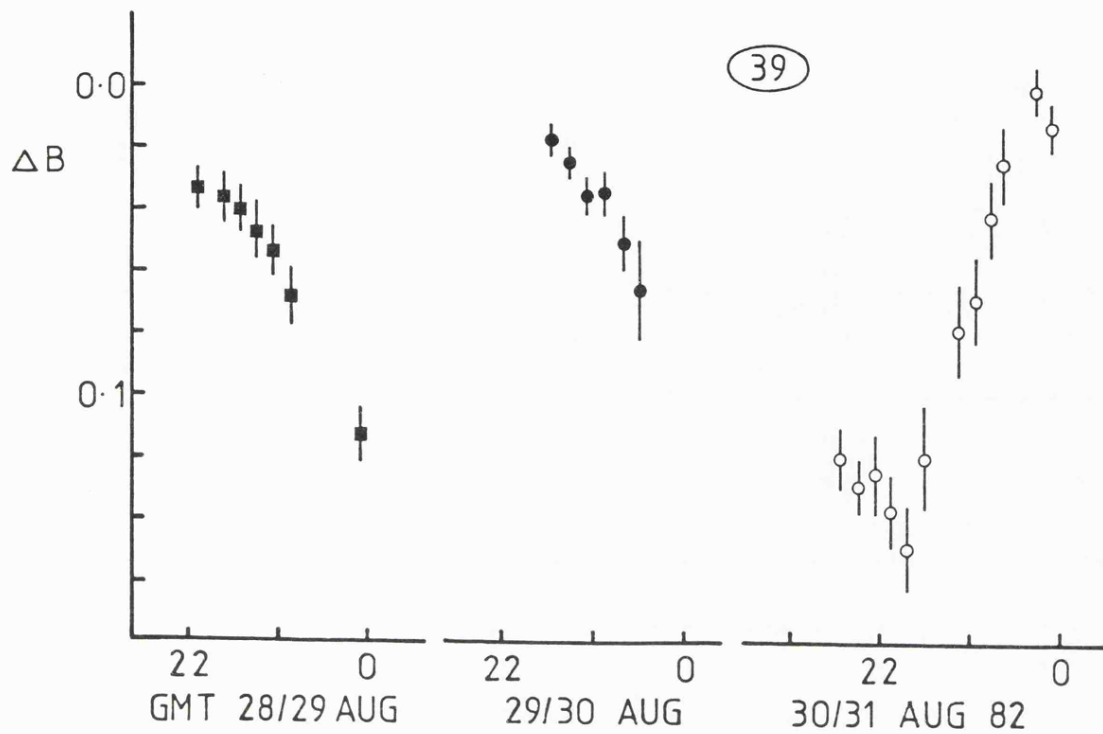
***LIGHTCURVES***

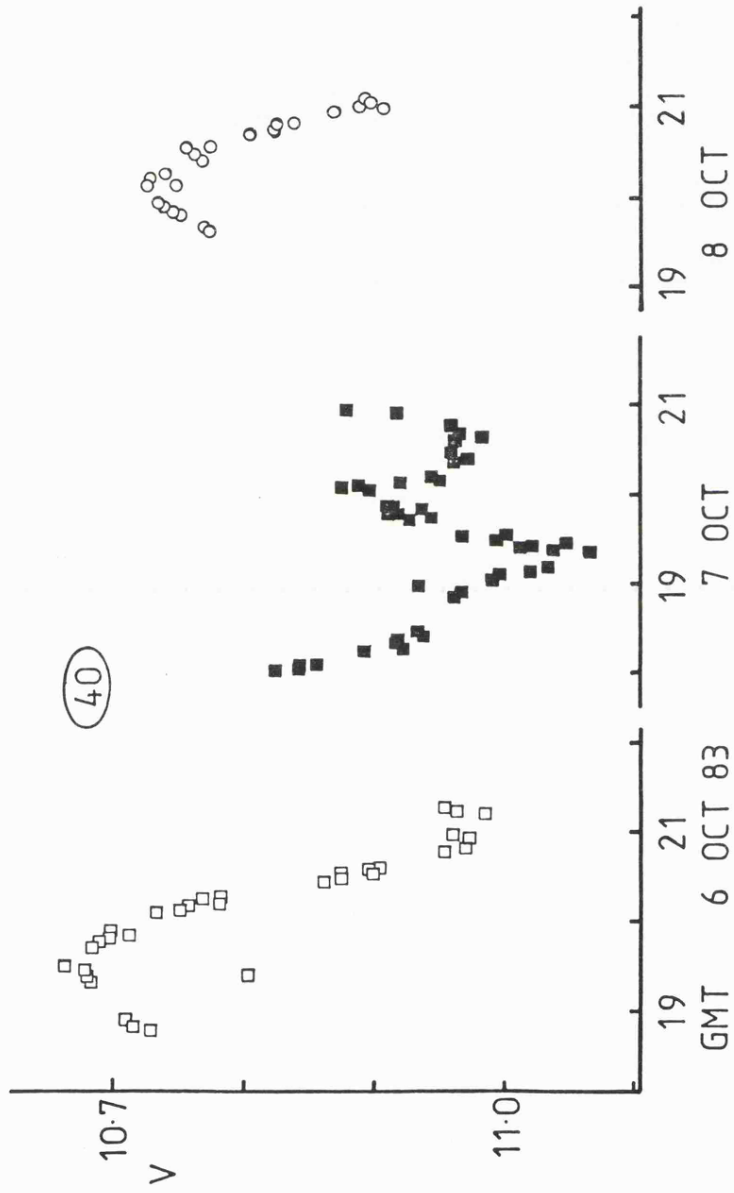
This appendix contains the lightcurves from Chapter 3. The data are presented as a time sequence (ie. not folded with the rotation period of the asteroid) and without any magnitude corrections for changing phase angle or Sun-asteroid or Earth-asteroid distances. Abscissa are in GMT hours for the date indicated. The ordinates are either B, V or  $\Delta B$  magnitudes. The B and V calibration is accurate to  $\pm 0.01$  magnitudes. Asteroids for which no calibration was obtained have the vertical axis labelled as  $\Delta B$ , which shows the magnitude relative to the maximum observed light. Calibration of a poorer quality was achieved for 349 Dembowska, the zero point on the scale is  $10.76 \pm 0.05$  mag. The number of the asteroid is contained in the ellipse.

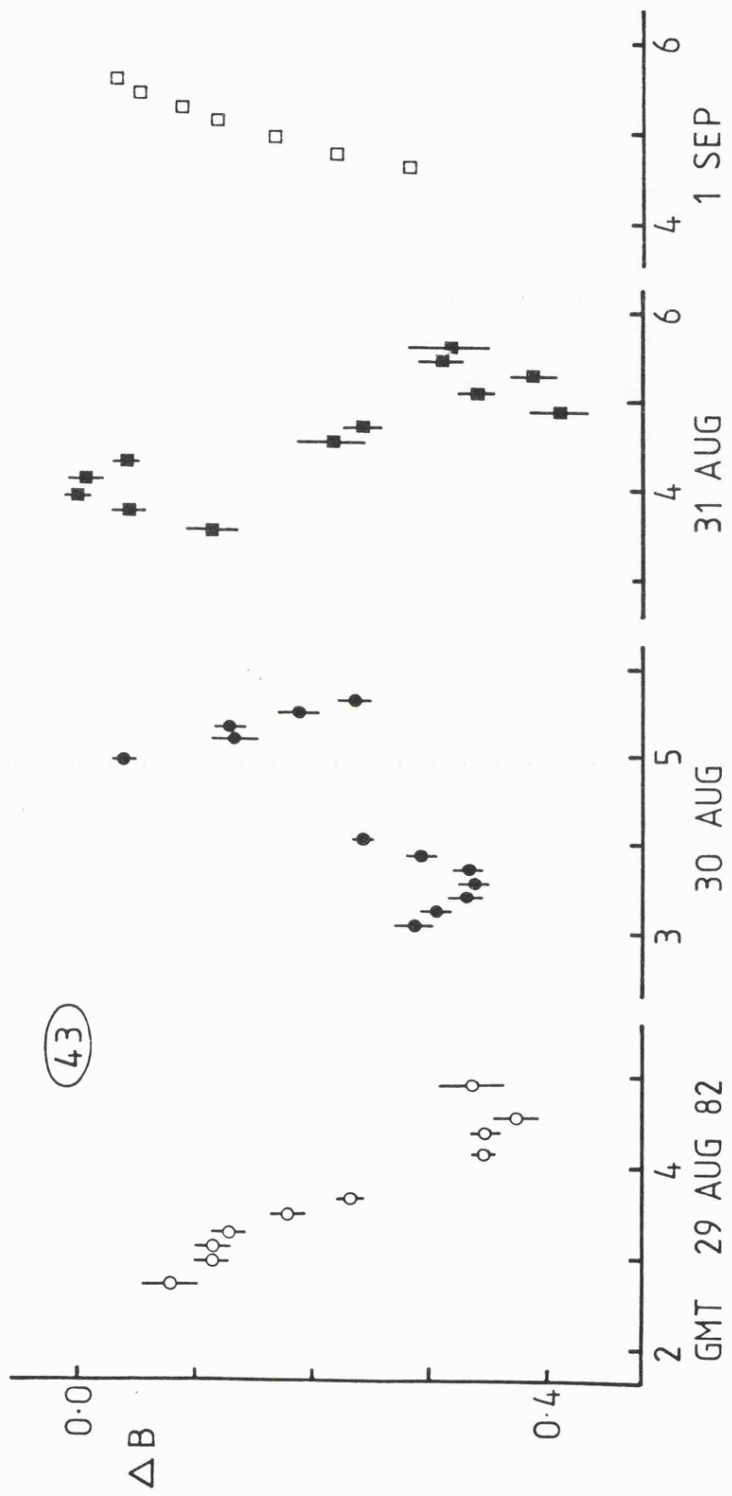


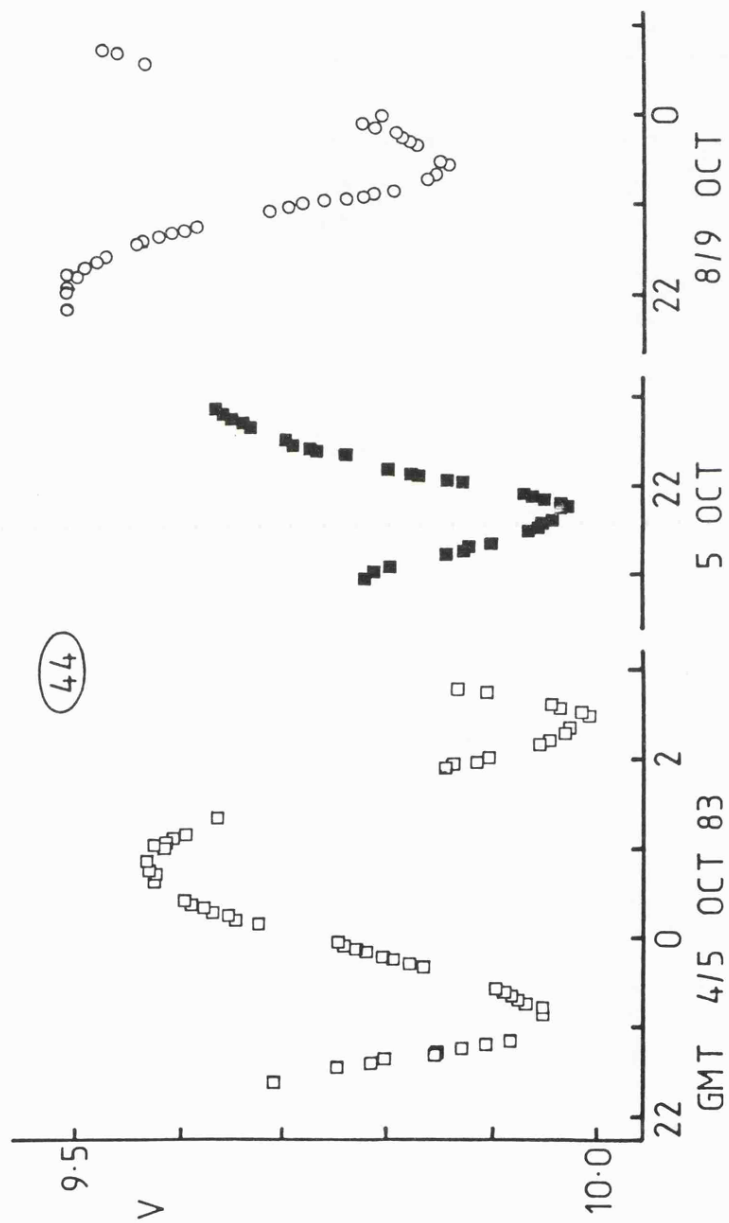


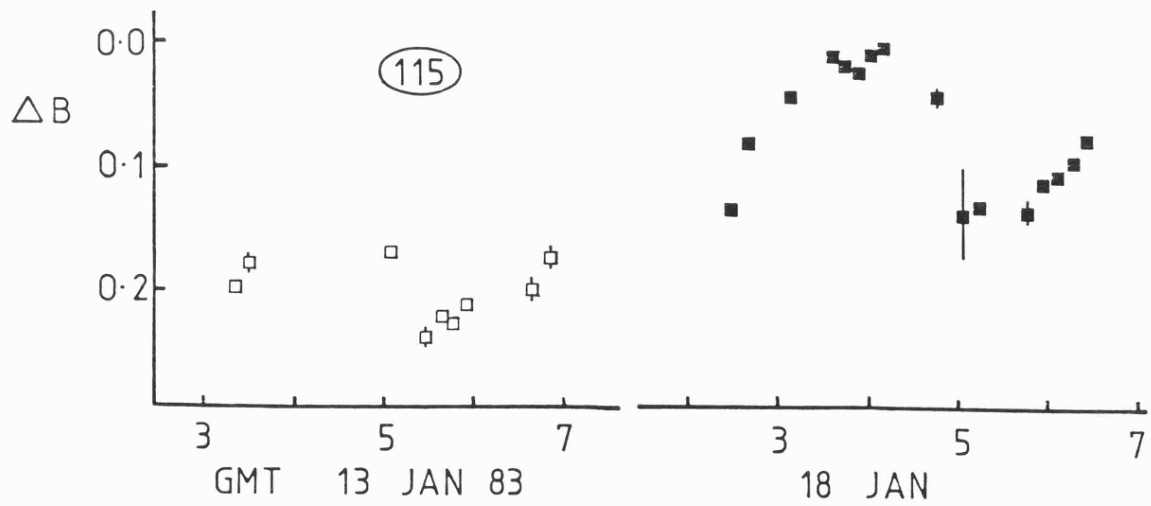
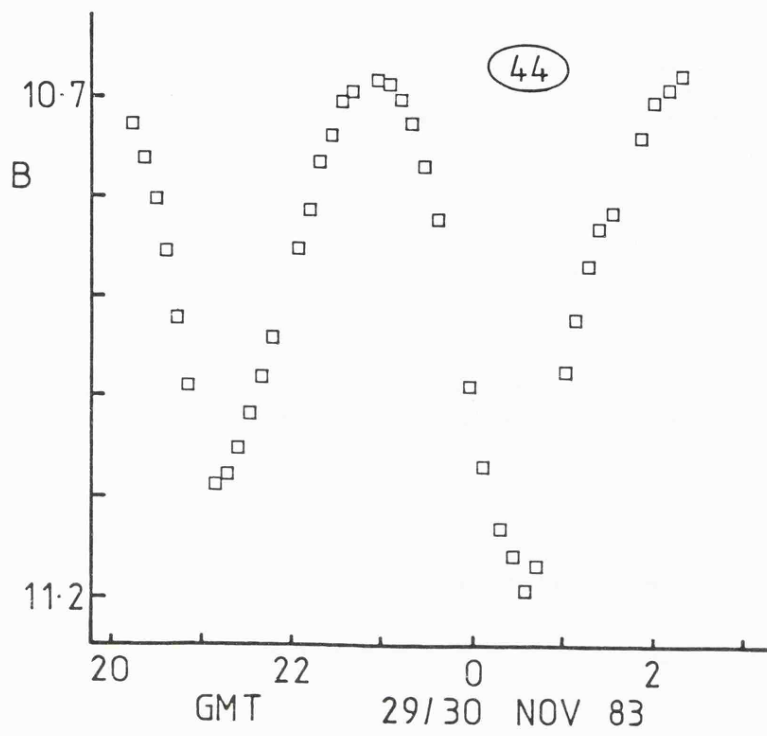


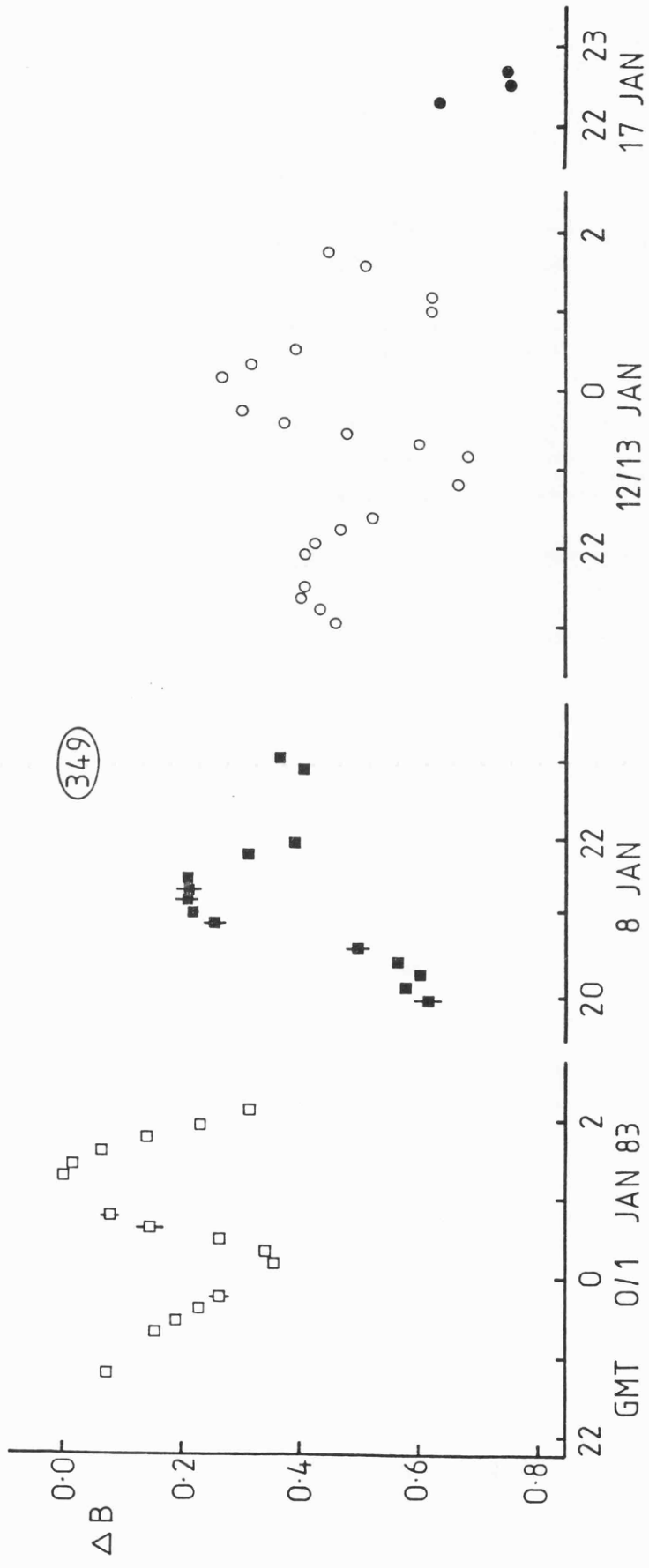












***PUBLICATIONS***

The following are publications resulting from the work presented in this thesis:

Davies, J. K., N. Eaton, S. F. Green, R. S. McCheyne and A. J. Meadows (1982). The classification of asteroids. *Vistas in Astronomy* 26, 243-251.

Eaton, N., S. F. Green, R. S. McCheyne, A. J. Meadows and G. J. Veeder (1983). Observations of asteroids in the 3- to 4- $\mu$ m region. *Icarus* 55, 245-249.

McCheyne, R. S., N. Eaton, S. F. Green and A. J. Meadows (1984). B and V lightcurves and pole positions of three S-class asteroids. *Icarus* 59, 286-295.

McCheyne, R. S., N. Eaton and A. J. Meadows (1984). Visible and infrared lightcurves of eight asteroids. *Icarus* in press.

The results have also been presented at two conferences: the 46th Meteoritical Society Meeting, Mainz, W. Germany and the 8th United Kingdom Geophysical Assembly, Newcastle. The following are published abstracts of these presentations (the speaker is underlined).

Green, S. F., N. Eaton, R. S. McCheyne and A. J. Meadows  
(1983). Spectrophotometry of asteroids in the infrared.  
Meteoritics 18, 306.

McCheyne, R. S., N. Eaton, S. F. Green and A. J. Meadows  
(1983). Asteroid lightcurves and surface properties.  
Meteoritics 18, 350.

McCheyne, R. S. (1984). Asteroidal shapes and spin axis  
orientation. Geophys. J. Roy. Astr. Soc. 77, 324-325.

## ABSTRACT

This thesis presents optical and infrared data of asteroids. The basis of the classification of asteroids by numerical taxonomy is data which are contained in the TRIAD file (Zellner, 1979). The resulting dendrograms are compared with existing classes of asteroids.

Simultaneous visible and near-infrared lightcurves of several asteroids are plotted as colour curves which, in some cases, show variations indicative of an inhomogeneous surface composition. The colour curves of 4 Vesta are explained in terms of eucrite and diogenite mineralogies. Some of these lightcurves, together with published data from previous oppositions, are used to calculate the overall shape of the asteroid and the orientation of the spin axis. These are calculated using a lightcurve amplitude-longitude relation.

Reflectance spectra in the 3 - 4 $\mu$ m region are presented, Two of which show evidence of water of hydration. These spectra highlight the importance of accurate thermal modelling. Data from IRAS is compared with the expected flux from the standard asteroid thermal model and the discrepancies examined in terms of emission from the unilluminated hemisphere.